SEMMELWEIS EGYETEM

DOKTORI ISKOLA

Ph.D. értekezések

2390.

RUPPERT MIHÁLY

Szív- és érrendszeri betegségek élettana és klinikuma

című program

Programvezető: Dr. Merkely Béla, egyetemi tanár

Témavezető: Dr. Radovits Tamás, egyetemi docens

The effect of pressure overload and pressure unloading of the left ventricle on cardiac structure and function

PhD thesis

Mihály Ruppert, M.D.

Doctoral School of Basic and Translational Medicine

Semmelweis University

Supervisor: Tamás Radovits M.D., Ph.D

Official reviewers: József Kaszaki M.D., Ph.D.
Anikó Görbe M.D., Ph.D.

Head of the Complex Examination Committee:
Tivadar Tulassay, M.D., D.Sc.

Members of the Complex Examination Committee:
Attila Patócs, M.D., D.Sc.
Péter Andréka, M.D., Ph.D.

Budapest
2020

Table of contents

1. List of abbreviations

AB: aortic banding

AH: arterial hypertension

ANP: atrial natriuretic peptide

ANOVA: analysis of variance

AVR: aortic valve repair

AS: aortic stenosis

AWT_d: anterior wall thickness in diastole

BNP: B-type natriuretic peptide

CD: cardiomyocyte diameter

CHF: chronic heart failure

CMR: cardiovascular magnetic resonance

cGMP: cyclic guanosine monophosphate

CO: cardiac output

CTGF: connective tissue growth factor

DBP: diastolic blood pressure

dP/dt_{max}: maximal systolic pressure increment

dP/dt_{min}: maximal diastolic pressure decrement

dP/dt_{max}-EDV: slope of the maximal systolic pressure increment-end diastolic volume relationship

E_a: arterial elastance

ECM: extracellular matrix

EDPVR: slope of the end-diastolic pressure-volume relationship

ER-β: estrogen receptor-β

ESPVR: slope of the end-systolic pressure-volume relationship

GAPDH: glyceraldehyde 3-phosphate dehydrogenase

HF: heart failure

HW/TL: heart weight-to-tibial length

IHD: ischemic heart disease

LGE: late gadolinium enhancement

LV: left ventricle

LVEDD: left ventricular end-diastolic diameter

LVEDP: left ventricular end-diastolic pressure

LVEDV: left ventricular end-diastolic volume

LVH: left ventricular hypertrophy

LVESD: left ventricular end-systolic diameter

LVESP: left ventricular end-systolic pressure

LVESV: left ventricular end-systolic volume

LW/TL: lung weight-to-tibial length

MAP: mean arterial pressure

MMP: matrix metalloproteinase

MHC: myosin heavy chain

mRNA: messenger ribonucleic acid

NP: natriuretic peptide

PCR: polymerase chain reaction

pGC: particulate guanylate cyclase

PO: pressure overload

PRSW: preload recruitable stroke work

P-V: pressure-volume

SBP: systolic blood pressure

SHR: spontaneous hypertensive rat

SV: stroke volume

SW: stroke work

TAC: transverse aortic constriction

TAVI: transcatheter aortic valve implantation

Tau: active relaxation time constant

TL: tibial length

VAC: ventriculo-arterial coupling

2. Introduction

In the twenty-first century, heart failure (HF) represents the most rapidly growing cardiovascular condition worldwide (1). Per definitionem, the term of HF defines a clinical syndrome when characteristic symptoms (e.g. breathlessness, ankle swelling and fatigue) are present, and the development of these typical symptoms are related to the structural and/or functional abnormalities of the heart (2). According to the current reports, the estimated prevalence of HF reaches 26 million (3). The projections for 2030 are even more alarming due to the aging trend of the human population (4). Besides the high patient prevalence, chronic HF (CHF) is associated with significant patient morbidity and mortality, with the 5-year mortality rate approaching 50% (5). Patients with CHF have a substantially worse quality of life when compared to both healthy individuals and patients suffering from other chronic health conditions (4). Finally, the financial cost of HF-associated medical treatment is substantial. In 2010, the estimated cumulative cost of HF was 39.2 billion American dollars in the United States (5). Therefore, despite the advances in CHF management, the continuing high prevalence of this condition coupled with high mortality rate, poor quality of life and severe financial burden for the health care system warrants further therapeutical improvements.

A wide range of pathological conditions can lead to the development of CHF. Among them, myocardial ischemia, primary cardiomyopathies (due to genetic background) and secondary cardiomyopathies (due to toxic, infectious or immunological reasons) are responsible for the majority of HF cases (1). It is noteworthy that most forms of ischemic heart disease ([IHD] e.g. following an extensive myocardial infarction) and primary/secondary cardiomyopathies are associated with irreversible myocardial insult. Therefore, in this patient population heart transplantation often remains the only curative medical therapy.

Besides the above-mentioned etiologies, chronic hemodynamic overload (pressure overload [PO] in case of arterial hypertension [AH], aortic stenosis [AS] and volume overload [VO] in case of aortic/mitral regurgitation) remains one of the main contributors to HF development (1). Of particular interest, a great body of scientific evidence supports the notion that termination of hemodynamic overload could result in a state of reverse remodeling with substantial improvement in cardiac structure and function (6). Furthermore, due to the recent technical advances in the field of interventional cardiology,

patients with AS (via transcatheter aortic valve implantation [TAVI]) can receive definitive medical therapy without undergoing open heart surgery (7). Thus, the unique opportunity for successful medical interventions has brought hemodynamic overload-induced HF into the focus of interest.

Parallel to the clinical investigations, substantial efforts have been made in the field of experimental research to better understand the (patho)physiology of hemodynamic overload-induced remodeling and unloading-evoked reverse remodeling. Due to the extremely high prevalence of AH and AS in Western societies, the majority of preclinical studies has focused on PO-induced HF and pressure unloading-evoked myocardial reverse remodeling. These investigations have revealed important findings which might serve as a basis for the optimization of current medical therapies. However, there is still a considerable number of unsolved questions, which warrants further preclinical experimentations.

2.1. Clinical conditions associated with pressure overload of the left ventricle

In case of PO, the afterload (load that the heart has to pump against during systole) of the left ventricle (LV) is increased. The two most common clinical conditions, which are associated with increased afterload of the LV are AH and AS.

Arterial hypertension. AH is generally defined as a sustained systolic blood pressure (SBP) at least 140 mmHg and/or diastolic blood pressure (DBP) at least 90 mmHg (8). Based on the latest surveys, the estimated global prevalence of AH was 1.13 billion in 2015 (9). Another terrifying fact that the prevalence of AH is exponentially increasing by age (10). Therefore, due to the aging trend of the Western population, the epidemiological burden of AH is expected to progress in the following years.

Aortic stenosis. AS refers to the pathophysiological state when the outflow tract of the LV is narrowed. AS can be divided into the following subcategorizes: supravalvular, valvular and subvalvular. In the present thesis, AS will refer to valvular AS. Data from the Euro Heart Survey has revealed that AS is the most common single native valvular left-sided heart disease in Europe (11, 12). Besides its high prevalence, the significance of AS is given by the fact that approximately 67,500 aortic valve replacement (AVR) surgeries are performed every year in the USA alone (13). Similar to AH, degenerative

AS also typically affects the elderly. Correspondingly, the prevalence of AS increases by age, reaching almost 10% in people over 80 years (14).

2.2. Pressure overload-induced pathological myocardial remodeling

Under sustained PO the heart undergoes extensive remodeling, which affects both the myocardium, the extracellular matrix (ECM), and the intramyocardial coronary arteries (15, 16). The remodeling process has some initial advantageous components that promotes the early adaptation of the ventricles to the increased hemodynamic loading conditions. However, in the long term the PO-associated molecular, cellular and histological alterations become maladaptive and contribute to the progression of HF. It is also important to point out that the remodeling process which can be observed in physiological states (e.g. regular exercise-induced or pregnancy-evoked myocardial remodeling) is characteristically different from chronic PO-induced remodeling (17). Therefore, the terminology of pathological remodeling is used to distinguish hemodynamic overload-induced maladaptive alterations from other physiological processes.

2.2.1. Increased systolic wall stress: the main driving force of pressure overload-induced pathological remodeling

In case of PO, the primary stimulus of pathological remodeling is increased wall tension (mechanical load) on the level of the individual cardiac cells (18). Traditionally, Laplace's law has been used to describe wall tension. According to Laplace's equation ($T=P*r/2h$), wall tension (T) is directly related to ventricular pressure (P) and ventricular radius (r) and inversely related to ventricular wall thickness (h) (19). In case of PO (AS, AH), systolic ventricular pressure is elevated leading to increased wall stress. Of particular interest, cardiac cells possess specific sensors (the so called mechano-sensors), which make them able to convert the mechanical stimulus (increased systolic wall tension) into specific biochemical signals (20). These initial biochemical signals further activate distinct intracellular signal transduction pathways that eventually lead to pathological remodeling. The main characteristics of PO-induced pathological remodeling on the structural, molecular and functional level is summarized in the following sections.

2.2.2. Pressure overload-induced structural alterations

2.2.2.1. Myocardial hypertrophy

The most fundamental structural finding in case of chronic LV PO is myocardial hypertrophy. Cardiac hypertrophy is broadly defined as an increase in heart mass (21). Since cardiomyocytes are terminally differentiated cells with very low ability for proliferation, cardiomyocyte hypertrophy rather than cardiomyocyte hyperplasia underpins the increase in heart mass (22).

It is noteworthy to mention that cardiomyocyte hypertrophy manifests promptly after induction of PO. Accordingly, the development of myocardial hypertrophy can be already detected 2 days after PO induction under standard laboratory conditions (23). These findings call attention to the fact that cardiomyocytes are extremely sensitive to an increase in afterload.

According to the conventional interpretation of Laplace's law, the increase in cardiomyocyte size is a compensatory reaction as it reduces systolic wall tension through the thickening of the LV wall. However, this long-standing hypothesis has been reconsidered, as it was demonstrated that normalization of wall stress may not be necessary for the adaptation to sustained hemodynamic overload (24). On the contrary, the Framingham Heart study has yielded unequivocal evidence that LV myocardial hypertrophy (LVH) increases the risk for cardiovascular morbidity and mortality (25). Hence, to date, PO-induced LVH is generally considered to be deleterious.

On the subcellular level, the hypertrophic response of the cardiomyocytes consist of altered gene expression, intensified rate of protein synthesis and organization of the synthesized contractile proteins into sarcomeres (21). In case of PO-evoked remodeling, the freshly created sarcomeric units are placed parallel within the cells, which subcellular localization mostly increases the width of the cardiomyocytes (21). Consistent with this ultrastructural pattern, clinical and experimental investigations have reported that PO-induced remodeling is predominantly associated with thickening of the ventricular walls with no or only moderate chamber dilatation (26, 27). Consequently, concentric LVH is most often observed during PO-evoked pathological remodeling.

2.2.2.2. Myocardial fibrosis

Another hallmark of PO-induced structural remodeling is myocardial fibrosis (28). Myocardial fibrosis generally manifests later than cardiomyocyte hypertrophy, representing a maladaptive structural milestone in the progression of PO-induced LVH to decompensated HF. Importantly, myocardial fibrosis can be subcategorized into replacement and reactive fibrosis (including interstitial and perivascular fibrosis) (29). Chronic PO-induced remodeling is predominantly associated with reactive fibrosis. Nevertheless, at advanced stages of PO-induced LVH, replacement fibrosis also manifests (30).

Replacement fibrosis. Replacement (or reparative) fibrosis occurs following macroscopic (the most typical pathophysiological situation is that takes place after myocardial infarction) or microscopic myocardial injury and aims to replace the irreversibly damaged cardiac tissue (31). At severe stages of PO-induced HF, different forms of cell death become activated (e.g. apoptosis (32)), which collectively result in substantial loss of myocardial tissue. Hence, at advanced stages of PO-induced HF, replacement fibrosis is often observed (33).

Reactive interstitial fibrosis. In contrast to replacement fibrosis, reactive fibrosis is the consequence of direct stimulation of fibroblasts without cellular injury (31). Fibroblast stimulation in PO involves complex pathomechanisms. Increased mechanical stress (enhanced systolic wall stress) has been implicated as one of the main pathological stimuli (34). Importantly, fibroblasts have mechano-sensors embedded in their extracellular membrane similar to cardiomyocytes (35). Therefore, fibroblasts are also capable to directly sense the physical stimuli of increased wall stress, converting it to pro-fibrotic biochemical signals. Furthermore, increased wall stress also determines fibroblast function indirectly via cardiomyocyte-fibroblast cross-talk. In addition inflammation, oxidative stress and mast cell infiltration/degranulation have been also suggested to contribute to the development of interstitial fibrosis in PO-induced HF (29). All of these mechanisms eventually promote the transformation of fibroblasts into myofibroblasts (36). These transformed cells are mainly responsible for the excessive synthesis of different ECM components (e.g. distinct types of collagens, fibronectin) (29). However, it must be noted that PO-induced ECM remodeling does not simply implicate the accumulation of distinct matrix proteins in the extracellular space, but includes

simultaneous degradation of important scaffold proteins. Of particular interest, these pathological degrading processes disrupt the integrity of the cellular-ECM network, leading to substantial alterations in LV geometry. The molecular background for the degradation process is supported by a group of distinct enzymes, the so-called matrix metalloproteinases (MMP). Under physiological conditions, the biological action of MMPs is tightly regulated on the transcriptional, translational and posttranslational levels (37). In contrast, in advanced stages of PO-induced HF, both the expression, the activation and the inhibition of MMPs become disturbed, leading to an uncontrolled breakdown of important ECM components and consequently LV dilatation (38).

Reactive perivascular fibrosis. Perivascular fibrosis is also an important pathogenic feature of PO-induced LVH and HF (39). This is underpinned by the fact that in certain clinical (e.g. in AH) and experimental (e.g. abdominal aortic banding [AB]) forms of PO, hypertension is also present in the coronary artery system. In these cases, the elevated blood pressure in the small intramyocardial arteries induces inflammation in the arterial walls (40). This inflammatory reaction evokes the transmigration of macrophages into the perivascular space. The accumulated macrophages subsequently activate fibroblasts located around the arteries, eventually inducing reactive perivascular fibrosis.

2.2.3. Molecular markers of pressure overload-induced pathological remodeling: reactivation of the fetal gene program

During fetal development the LV is associated with a specific gene expression profile termed as the “fetal gene program” (41). Importantly, under physiological conditions, this characteristic gene expression pattern cannot be observed after birth. However, in case of PO-induced pathological LVH the gene expression profile of the postnatal heart resembles that of the fetal gene program (42, 43). The most widely known features of the fetal gene program are the switch of the myosin heavy chain (MHC) isoforms and the increased ventricular expression of the atrial natriuretic peptide (ANP).

MHC isoform switch. Myosin II is a motor protein that is required for muscle contraction in myocytes. Myosin II is a hexameric enzyme, consisting of two MHCs and four myosin light chains (44). The MHC has an actin-binding site and an ATP hydrolysis site. Based on the enzymatic activity of the ATP hydrolysis site, two isoforms of MHC can be distinguished. The α-MHC isoform has the higher, while the β-MHC isoform has

the lower actomyosin ATPase activity (44). During fetal development the ratio of β/α-MHC expression is relatively high in the ventricles. However, this ratio substantially decreases after birth. It is noteworthy that the isoform switch occurs to a different extent in rodents and humans. Accordingly, α-MHC makes up 90% of the total MHC in the postnatal rodent ventricles (45). On the contrary, β-MHC remains the dominant isoform in "adult" human ventricles. The discrepancy between humans and rodents might be explained by the robust differences in heart rate (HR), with rats on average demonstrating 6-7 times higher HR than humans (46). Despite the inter-species differences, the relative ratio of β/α-MHC has been found to increase in both humans and rodents in PO-induced pathological LVH and HF. Due to the high baseline expression of β-MHC, the increment of β/α-MHC is mainly the consequence of the reduction of α-MHC in humans (44, 45). On the contrary, intensified expression of β-MHC and decreased expression of α-MHC equally contribute to the altered β/α-MHC ratio among rodents (47).

Ventricular ANP expression. Natriuretic peptides (NPs) are endocrine factors with natriuretic, diuretic and vasorelaxant effects on the cardiovascular system (42, 48). Three main types of NPs exist, including ANP, B-type NP (BNP) and C-type NP. ANP gene expression is observed in the fetal LV (49). However, the expression of ANP is restricted to the atria in the postnatal heart under physiological conditions. In contrast, during the development of congestive CHF, robust elevations in mRNA levels of ANP have been documented in ventricular samples (49, 50). Of particular interest, recent experimental studies have discovered that NPs mediate anti-hypertrophic paracrine/autocrine signaling in the myocardium. In more details, cardiomyocytes have NP receptors that are coupled with the particulate guanylate cyclase (pGC) enzyme. In case of ANP/BNP binding, the pGC enzyme catalyzes the formation of the second messenger cyclic guanosine monophosphate (cGMP) (42). The elevated cytoplasmic cGMP content potentiates the activity of the enzyme protein kinase G, which subsequently downregulates many pro-hypertrophic signaling pathways. Thus, although ANP is a member of the fetal gene program, its increased expression during chronic LV PO also represents an inbuilt break system of cardiac hypertrophy (51).

2.2.4. Pressure overload-induced functional alterations

The in vivo assessment of LV function under sustained PO is technically challenging. The difficulty arises due to the fact that the robust increment in afterload makes the conventional load-dependent parameters inappropriate to characterize in vivo LV function in pathological conditions associated with sustained PO. Hence, to adequately investigate alterations of LV function in PO-induced LVH and HF, the confounding effect of different loading conditions has to be eliminated. To date, invasive pressure-volume (P-V) analysis represents the "gold standard" technique to assess distinct aspects of in vivo LV function independently from loading conditions (52, 53). Therefore, our knowledge concerning the alterations in systolic and diastolic LV function during the development of PO-induced LVH and HF are mainly derived from P-V analysis data.

2.2.4.1. Left ventricular systolic function in chronic pressure overload

Numerous research groups have aimed at measuring systolic function in PO-induced LVH. These investigations have consistently reported that LV systolic function is maintained (ejection fraction [EF] is preserved) at a relatively early stage of PO-induced pathological remodeling but deteriorates at advanced stages (EF is reduced). Of particular interest, it has been demonstrated that the time point at which decompensation of systolic function takes place is dependent on the severity of the PO. Accordingly, in rodent models with extremely elevated LV PO (e.g. severe aortic banding [AB]), rapid deterioration of LV systolic function is frequently observed (54). In contrast, in animal models with relatively moderate LV PO (e.g. spontaneous hypertensive rat [SHR] strain), a substantially longer "compensated" phase precedes the development of systolic HF (55). In clinical practice, the majority of patients with AH and AS demonstrate preservation of LV global systolic function for a relatively long period of time.

Previous clinical and experimental studies using P-V analysis have noted that the load-independent indices of LV contractility are markedly increased at the early stage of PO-induced LVH (47, 56, 57). Based on these findings, it has been postulated that augmentation of LV contractility represents an early compensatory reaction that enables the LV to counterbalance the increased arterial afterload. To describe the interaction between the contractile state of the LV and the afterload of the connecting arterial system, ventriculo-arterial coupling (VAC) is traditionally assessed by P-V analysis. VAC can be

defined as the ratio of arterial elastance ([E_a], an integrative parameter of arterial afterload) and LV contractility (measured by the slope [E_{es}] of the end-systolic pressure-volume relationship [ESPVR]) (58, 59). In case of PO, E_a is increased. However, the increment in LV contractility (E_{es}) is proportional to the elevation of afterload (E_a) during the early stage of PO-induced LVH. As a result, VAC is maintained and systolic function (EF) is preserved (57).

In contrast, during the transition of compensated LVH to systolic HF, a mismatch develops between LV contractility and the afterload of the connecting arterial system (impaired VAC). Previous experiments have yielded controversial findings, whether decrement in LV contractility or increment in arterial elastance underlies the contractility-afterload mismatch during the progression of PO-induced LVH to systolic HF (60-62). As such, further studies utilizing P-V analysis are warranted to better understand the decompensation of systolic function in PO-induced LVH.

2.2.4.2. Left ventricular diastolic function in chronic pressure overload

Diastolic dysfunction is a characteristic feature of PO-induced HF. Of particular interest is the observation that impairment of diastolic function frequently precedes the deterioration of systolic function in case of PO-induced LVH. Hence, many HF patients with long-lasting PO exhibits diastolic dysfunction but preserved systolic performance (63). Importantly, data from invasive P-V analysis has revealed that both the active and the passive components of diastolic function are impaired in PO-induced HF.

In order to describe ventricular relaxation independently from loading conditions, the active relaxation time constant (Tau) is often calculated by the use of P-V analysis data (52). In patients with AS, marked prolongation of Tau has been repeatedly observed, indicating severely impaired active relaxation (64, 65). These findings have been precisely replicated by numerous animal models of PO-induced HF (47, 57, 66, 67).

Evaluation of the passive diastolic properties of the LV by P-V analysis relies on the calculation of LV end-diastolic pressure (LVEDP) and the slope of the end-diastolic P-V relationship (EDPVR) (52). Both of these indices have been found to be greatly increased in patients with AS as well as in a wide range of different animal models with sustained LV PO (56, 64, 65, 68).

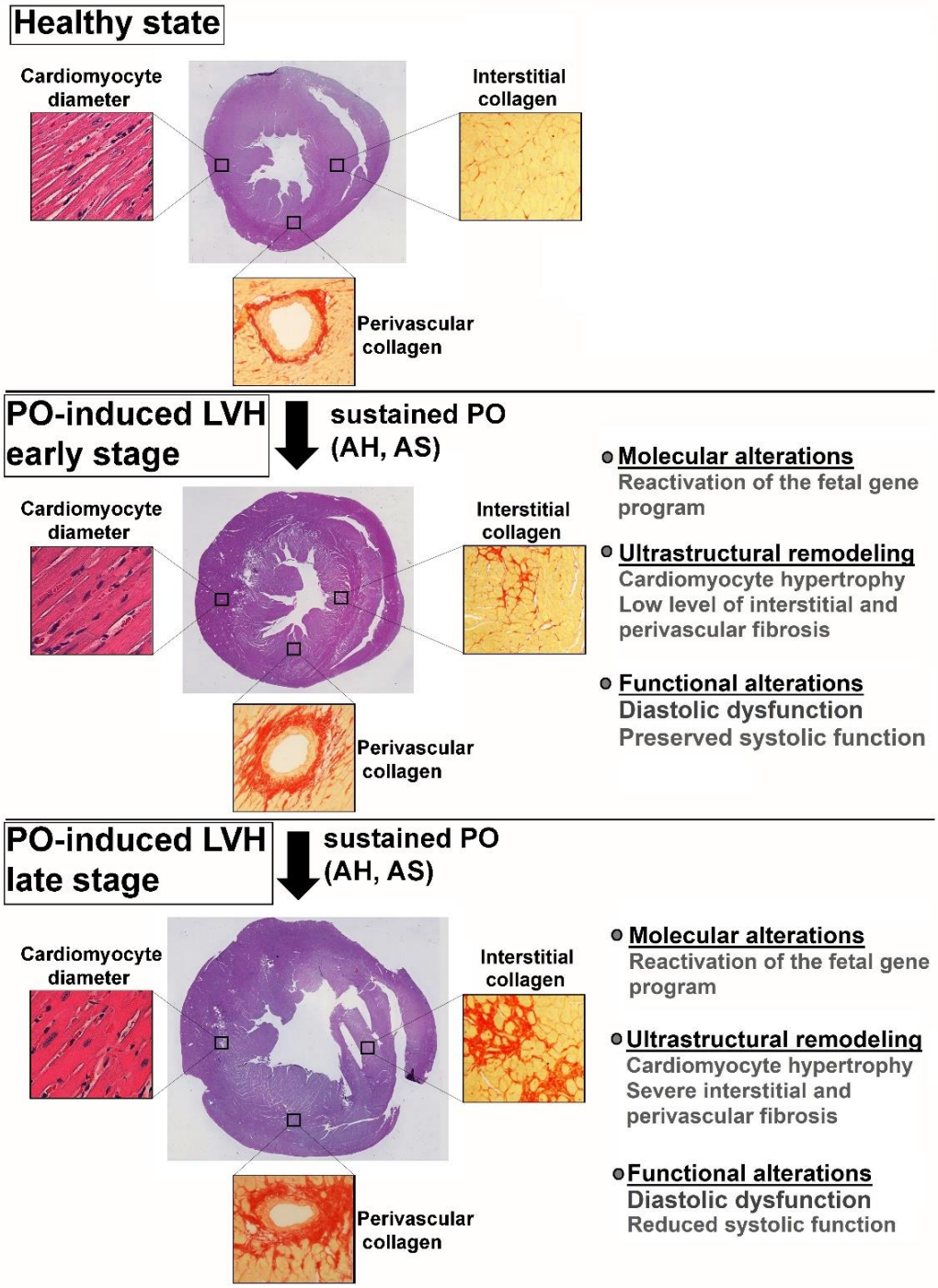

Figure 1. Summary of pressure overload-induced pathological myocardial remodeling. The early stage of pressure overload (PO)-induced left ventricular myocardial hypertrophy (LVH) is associated with cardiomyocyte hypertrophy and low level of interstitial and perivascular fibrosis on the ultrastructural level. At this stage, diastolic dysfunction is often present, however systolic function is preserved. At later stages, further accumulation of interstitial and perivascular collagen occurs. In addition, systolic function also deteriorates. AH: arterial hypertension, AS: aortic stenosis, PO: pressure overload. Cross sectional whole heart pictures are adapted from Ruppert et al. (2018) Front Physiol, 9:1869.(68)

2.3. Pressure unloading-induced myocardial reverse remodeling

In recent years, a growing body of clinical data has provided evidence that termination of the pathological insult of sustained PO (e.g. by AVR/TAVI in case of AS or by antihypertensive medications in case of AH) induces the regression of LVH. This process is termed myocardial reverse remodeling and involves the restoration of the physiological LV phenotype on the molecular, ultrastructural, geometrical as well as functional level (69). In the following sections, different aspects of pressure unloading-induced myocardial reverse remodeling are summarized.

2.3.1. Pressure unloading-induced structural alterations

2.3.1.1. Regression of myocardial hypertrophy

Clinical and experimental studies have shown that myocardial hypertrophy remains reversible even after a long period of sustained PO (70, 71). Correspondingly, substantial reduction in LV mass has been documented after different types of pressure unloading therapies. Furthermore, the regression of myocardial hypertrophy after TAVI/AVR or antihypertensive therapy has been found to follow a characteristic time course. Based on these reports, termination of the pathological stimulus of sustained PO leads to a rapid regression of LVH (6, 72-78). Of particular interest is the observation that the majority of LV mass reduction (approximately two-thirds of the total mass regression) occurs during this early phase (within the first 18 months). The initial phase is subsequently followed by a second more chronic phase, which continues over several years after the correction of the primary hemodynamic abnormality (73, 79).

Beyond the clinical investigations, animal models have been also utilized to investigate the temporal regression of LVH under laboratory conditions. These preclinical studies have reported that decrement in myocardial hypertrophy takes place already within 3 days of PO termination (80, 81). Furthermore, data from animal experiments have confirmed that the prompt regression of LVH is followed by an additional chronic phase under standard laboratory circumstances as well (70).

Furthermore, numerous studies have sought to determine the extent to which the hypertrophied myocardium may recover after a successful pressure unloading therapy. These investigations have found that LV mass almost returns to the healthy controls' level

in case of a long follow-up period after AVR (72, 73). Nevertheless, it has to be noted that a “restitutio ad integrum” generally does not occur. One possible explanation for the incomplete regression of LVH is that pressure unloading therapies often fail to completely alleviate the increased PO. For example, in case of AVR, the prosthetic valve itself may create a slight stenosis compared to the absolutely healthy aortic valves (73). Therefore, a relatively low level of PO may persist even after successful surgical interventions. The residual increment in PO might impede the complete normalization of myocardial hypertrophy.

In addition to the macroscopic findings, ample amount of data has provided evidence that reduced cardiomyocyte size (assessed by myocardial fiber diameter or cross sectional area) is mainly responsible for the decrement of LV mass on the microscopic level. This observation is corroborated by the analysis of endomyocardial biopsies obtained from AS patients who underwent AVR (72). Moreover, the detailed histopathological analysis of the whole LV myocardium in different animal models has come to the same conclusion (82, 83).

2.3.1.2. Regression of myocardial fibrosis

Regression of myocardial fibrosis after pressure unloading is generally considered to be a less efficient process compared to the regression of cardiomyocyte hypertrophy. Importantly, as previously mentioned, myocardial fibrosis can be subcategorized into replacement and reactive (including perivascular and interstitial) fibrosis. Recent investigations have come to the conclusion that these two forms of myocardial fibrosis differ in their plasticity.

Replacement fibrosis. In vivo assessment of myocardial replacement fibrosis (also known as focal fibrosis) is carried out by late gadolinium enhancement (LGE) cardiovascular magnetic resonance imaging (CMR) (84). Thus, majority of the available clinical research data concerning the regression of replacement fibrosis after pressure unloading therapy is derived from LGE CMR reports. These studies have revealed that replacement fibrosis persists after AVR (6, 30, 85). The irreversible nature of replacement fibrosis stands in parallel with the current concept of its development. Accordingly, as also mentioned above, replacement fibrosis is believed to substitute for the place of dead

cardiac cells. Considering that cardiomyocytes have very low proliferative ability, the permanent nature of replacement fibrosis after pressure unloading is an expected finding.

Reactive interstitial fibrosis. The non-invasive, in vivo evaluation of interstitial fibrosis has not been feasible for a long period of time. Nevertheless, recent advances in CMR imaging technology has made the quantification of interstitial fibrosis possible (75, 86). Data from current CMR studies along with prior endomyocardial biopsies have revealed that interstitial fibrosis is plastic and able to regress on the long term (6, 85, 87). However, the time course of interstitial fibrosis regression has been reported to be much slower than that of cardiomyocyte hypertrophy. As a consequence, at a relatively early time point after pressure unloading, when a substantial reduction in cardiomyocyte size (diameter/cross sectional area) has already taken place, the amount of interstitial fibrotic tissue often remains unchanged (88, 89). Accordingly, the percent of interstitial fibrosis has been reported to even increase at an intermediate stage of myocardial reverse remodeling (64, 65). In contrast, at later stages (8-10 years after AVR) the amount of extracellular collagen decreases, and hence the percentage of interstitial fibrosis reduces as well (65). However, the extent to which interstitial fibrosis regresses after pressure unloading therapy is still under intense investigation. Results from experimental studies indicate that complete regression of pre-established interstitial fibrosis does not occur, even in the long term follow-up (90).

Reactive perivascular fibrosis. Currently, detection of perivascular fibrosis is only accomplished by histological analysis. However, the possibility for carrying out myocardial biopsies in AS patients after pressure unloading therapy is limited. Hence, our knowledge concerning the reversibility of perivascular fibrosis is mainly derived from animal studies. These investigations have revealed that perivascular fibrosis displays similar regression to interstitial fibrosis after pressure unloading (91).

2.3.2. Pressure unloading-induced molecular alterations

Due to the fact that LV mRNA/protein expression analysis requires myocardial tissue collection, molecular features of myocardial reverse remodeling has been mainly investigated in relevant animal models. These preclinical experiments have provided compelling evidence that the regression of LVH after pressure unloading therapy is accompanied by robustly reduced fetal gene expression (70, 80). Interestingly, prior

research has also indicated that normalization of the fetal gene program might even precede the structural and functional recovery of the hypertrophied and failing myocardium (92).

Furthermore, recent findings have called attention to the fact that those molecular alterations that occur during myocardial reverse remodeling are not merely the reverse of those that cause LVH and HF (92). Correspondingly, characteristically different gene expression profiles have been observed during PO-induced remodeling and pressure unloading-evoked reverse remodeling (93). Hence, it seems possible that from a molecular point of view the reverse-remodeled heart is not simply the halfway mark between PO-induced LVH and the healthy state, but it rather represents a distinct third category.

2.3.3. Pressure unloading-induced functional alterations

2.3.3.1. Recovery of left ventricular systolic function after pressure unloading

Most of the clinical studies have found that removal of the chronic PO induces a rapid improvement in systolic function (94-96). Correspondingly, it has been suggested that enhancement of LV systolic performance after pressure unloading therapy does not necessarily require a complete normalization of LV structural abnormalities (especially fibrosis) (70). These observations raise the possibility that the termination of the increased afterload might be sufficient to achieve a prompt improvement in LV systolic function without substantial changes in LV contractility. However, a common limiting factor for the above mentioned investigations is that LV systolic function has been assessed only by load-dependent methods. Hence, more sophisticated hemodynamic characterization by P-V analysis is warranted to gain a deeper insight into the rapid recovery of LV systolic function after pressure unloading.

2.3.3.2. Recovery of left ventricular diastolic function after pressure unloading

Contrary to systolic dysfunction, amelioration of PO-induced diastolic dysfunction occurs in a slow fashion and usually continues over several years following pressure unloading. Interestingly, clinical experience suggests that the two aspects of diastolic function, namely passive filling and active relaxation, differ in their reversibility after pressure unloading (65).

Passive filling. Villari et al. have found that myocardial stiffness follows very precisely the changes of interstitial fibrosis in patients with AS undergoing pressure unloading therapy (64). As previously mentioned, the percent of interstitial fibrosis may even be increased at a relatively early time point after AVR. At this particular stage, Villari et al. have observed that myocardial stiffness was also further impaired. In contrast, at later stages (8-10 years after AVR) the resorption of interstitial fibrosis implied the normalization of myocardial stiffness (64, 65).

Active relaxation. On the contrary, in the same investigations a significant improvement in the active relaxation time constant (Tau) was documented already at an intermediate time point after pressure unloading therapy (64). Furthermore, a rapid (2 weeks after surgery) recovery in active relaxation was also demonstrated by Ikonodimis et al. Of particular interest, in the later echocardiographic follow-up study, patients undergoing AVR had experienced a significant improvement in myocardial relaxation early after surgery, at a time point when regression of LV wall thicknesses has not yet occurred (79).

These clinical findings suggest that improvement of passive filling is immensely dependent on the regression of structural abnormalities (mainly fibrosis). On the other hand, clinical data indicate that normalization of active relaxation might require less structural reverse remodeling. However, experimental results are not available to support these phenomena since the effect of complete versus incomplete structural reverse remodeling on diastolic function has not yet been investigated under experimental conditions.

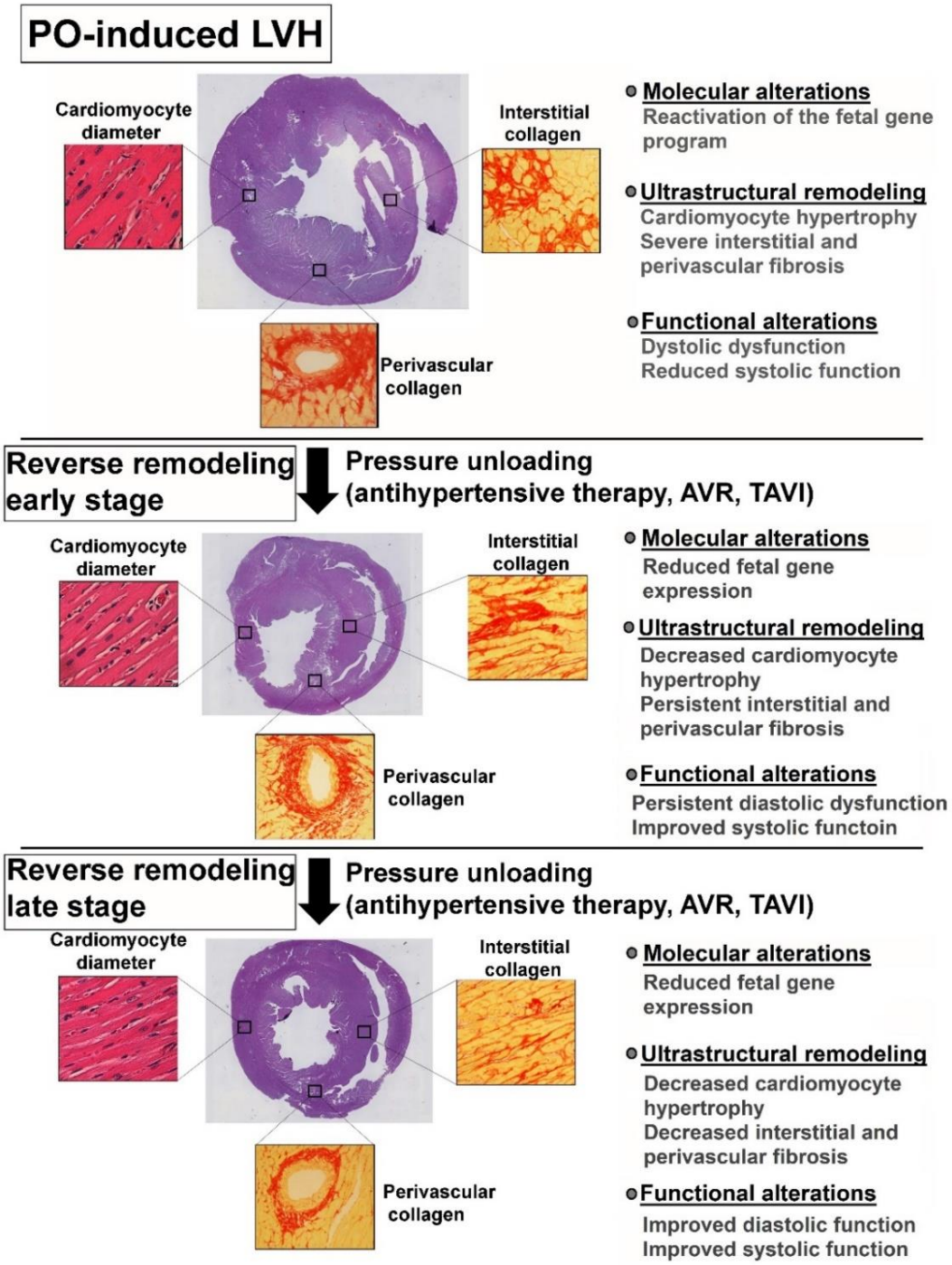

Figure 2. Summary of pressure unloading-induced myocardial reverse remodeling. Pressure unloading induces a rapid regression of cardiomyocyte hypertrophy leading to substantial reduction in left ventricular mass. However, reactive interstitial and perivascular myocardial fibrosis often persists at a relatively early stage after pressure unloading. From a functional point of view, the early phase of reverse remodeling is characterized by improved systolic function but impaired diastolic function. In contrast, at later stages, reactive myocardial fibrosis also regresses, resulting in the amelioration of diastolic function. AVR: aortic valve replacement, TAVI: transcatheter aortic valve implantation. Cross sectional whole heart pictures are adapted from Ruppert et al. (2018) Front Physiol, 9:1869.(68)

2.4. Sex differences in pressure overload-induced pathological remodeling and pressure unloading-induced reverse remodeling

Sex differences have been increasingly recognized in various frequent cardiovascular disorders, such as in IHD and hemodynamic overload-induced HF. Importantly, sex-related discrepancies have been found to affect both the pathophysiology, the clinical manifestation and the epidemiology of cardiovascular pathologies (97, 98). Recent investigations have shed light on the molecular basis, which might be responsible for the observed differences between men and women. These subcellular mechanisms involve sex chromosomes-derived genetic differences, diversity in epigenetic regulation (due to characteristic microRNA expression) and the effects of different sex steroid hormones (98). Although, all of the three proposed mechanisms may be involved, the majority of previous investigations have focused on the role of sex steroid hormones (mainly estrogen). The observation, which drew attention to the potential cardioprotective effects of estrogen was that differences associated with female sex disappear in women at the postmenopausal stage. In good agreement with the clinical findings, preclinical studies have reported that sex differences in hemodynamic overload-induced HF diminish in female rats after ovariectomy (99). In contrast, exogenous estrogen administration in ovariectomized female rats restores the characteristic sex-related differences in PO-induced HF (100). Further research has also identified that the regulatory effects of estrogen are mainly mediated via the nuclear estrogen receptor β (ER-β) in PO-evoked LVH (101-103). The interaction between estrogen and ER-β induces alterations in myocardial gene expression, which fundamentally affects the hypertrophied LV phenotypes in females. In the following sections, sex-related differences in PO-induced LVH are briefly summarized.

2.4.1. Effect of sex on structural alterations

2.4.1.1. Sex-associated differences in myocardial hypertrophy

Women with long-lasting AH or AS, as well as female rats with sustained PO are prone to develop thicker ventricular walls, smaller LV chamber dimensions and a more concentric form of LVH compared to male counterparts (104-109). Recent experiments have proposed that the characteristic morphological and geometrical differences might be the consequence of a set of pathological cellular processes which occur in males but not

in females during the progression of PO-induced LVH. Accordingly, relatively early after PO-induction, concentric LVH is observed in both genders. However, during the progression of chronic cardiovascular conditions, continuous cardiac cell loss and ECM remodeling takes place in males but not in females, resulting in chamber dilatation and eccentric geometry (110, 111). In contrast, female sex and estrogen-mediated signaling yield protection against apoptosis and MMP upregulation (111, 112), and prevents chamber dilation.

Recent clinical experiments also aimed at investigating potential sex-related discrepancies in the regression of LVH after pressure unloading therapy. Petrov and his colleagues found that LV end-diastolic diameter (LVEDD) decreased in female but not in male patients 3 days after AVR (111). In contrast, Dobson et al. have reported no sex-related differences in LV mass regression during a 6-month long follow-up period (76). Similarly, Stangl et al. have also observed that reduction of LV mass occurred to a similar extent in both genders 3 month after AVR/TAVI (113). In contrast, antihypertensive therapies have demonstrated a less efficient regression of LV mass in female patients compared to their male counterparts (108, 114). Unfortunately, no animal studies to date have been conducted on this field to confirm or contradict the mentioned clinical findings.

2.4.1.2. Sex-associated differences in myocardial fibrosis

Sex differences in myocardial fibrosis have been widely documented by numerous preclinical and clinical investigations during the development of PO-induced LVH. Accordingly, examination of endomyocardial biopsies from AS patients have consistently revealed more severe collagen accumulation in men compared to women (109, 115). The histological findings have been further supported by gene expressional analysis, reporting substantially higher mRNA levels of pro-fibrotic genes in LV speciments from male AS patients compared to their female counterparts (111). Besides the histological examinations, current CMR studies have reported considerable differences in myocardial fibrosis between men and women under sustained PO. Importantly, in these particular studies, the newly developed CMR imaging modalities have allowed investigators to differentiate between replacement and reactive fibrosis. The separate quantification of replacement and reactive interstitial fibrosis has revealed that both types of myocardial fibrosis are increased to a greater extent in men compared to women despite an equal

increment in afterload (116). Of particular interest, animal models of LV PO have also confirmed that male sex is associated with more maladaptive ECM remodeling under standard laboratory conditions (101, 102).

To date, only a few studies have analyzed the potential influential effect of sex on the regression of myocardial fibrosis following pressure unloading. Among them, Dobson et al. has reported that myocardial fibrosis regressed only in female but not in male patients after AVR during a 6 month long follow-up period (76). However, further preclinical research is warranted to test whether female sex is indeed associated with a more plastic form of myocardial fibrosis.

2.4.2. Effect of sex on molecular alterations

The adaptation of the LV to chronic PO seems to differ on the molecular level as well between the two genders. Accordingly, in a TAC-induced pathological LVH model, PO evoked more severe upregulation of the fetal gene program (β-MHC and ANP) in male rats compared to their female counterparts (117). Furthermore, detailed analysis of the LV transcriptome has identified specific sex-dependent regulation of gene expression. These investigations have revealed that the transcription of genes associated with mitochondrial function and fatty acid oxidation were more robustly suppressed in males compared to females. In contrast, genes encoded ribosomal proteins and ECM components were more intensely upregulated in male rodents compared to female ones (118).

2.4.3. Effect of sex on left ventricular function

2.4.3.1. Sex-associated differences in left ventricular systolic function

Sex is a major determinant of LV systolic function during the development of PO-induced LVH. Accordingly, better EF and fractional shortening have been consistently reported in female patients with chronic AH or AS compared to male patients (105, 106, 108, 109, 119). Furthermore, it has been also suggested that females might experience a greater improvement in EF after pressure unloading compared to their male counterparts (113). Besides the clinical findings, animal models of PO-induced LVH have confirmed that following a common compensated stage, deterioration of LV systolic function occurs in male but not in female rodents under standard laboratory conditions (104, 117).

However, a major limitation of the beforementioned clinical and preclinical investigations is that none have assessed in vivo LV contractility independently from loading conditions.

2.4.3.2. Sex-associated differences in left ventricular diastolic function

Besides the prominent sex-related differences in LV systolic function, hemodynamic characterization of male and female AS patients have indicated that distinct discrepancies might exist in diastolic function as well.

Active relaxation. Villari and his colleagues have observed the prolongation of the active relaxation time constant (Tau) in both genders with chronic PO (109). According to their findings, deterioration of active ventricular relaxation occurred to an equal extent in both men and women.

Passive filling. In contrast to active relaxation, major differences have been documented in passive filling between the two sexes. Correspondingly, impairment of myocardial stiffness was only detected in men but not in women patients with AS (109). Furthermore, LVEDP was found to be elevated in male rodents, while no significant alteration could be detected in LVEDP in their female counterparts (101, 104). Thus, clinical and experimental evidence suggests that male sex is associated with a more severe impairment of LV passive diastolic properties under sustained PO. This latter functional finding is in good agreement with the ultrastructural differences between the two genders, with more severe ECM remodeling having been reported in male patients and experimental animals.

2.5. Animal models of pressure overload-induced remodeling and pressure unloading-evoked reverse remodeling

In the past years, various animal models of PO-induced pathological remodeling have been introduced. Among them, aortic constriction-induced PO (by surgically constricting the ascending [AAC], the transverse [TAC] or the abdominal [AB] aorta), essential hypertension-induced PO (e.g. the SHR strain or the Dahl salt sensitive rat strain), renal hypertension-induced PO (e.g. 5/6 nephrectomy) and genetically modified rodent strains (e.g. rats overexpressing the mouse renin gene) are the most widely utilized (120-123).

All of these experimental approaches have proven to be valuable tools in studying the temporal development of PO-induced LVH and its progression to symptomatic HF. Nevertheless, surgical models have the advantage that the pathological trigger of PO (the aortic constriction) can be removed by a second minimal invasive operation. Therefore, these models provide a unique opportunity to study not only PO-induced remodeling but also pressure unloading-evoked reverse remodeling under standard laboratory conditions. Importantly, prior investigation utilizing AB and debanding rodent models have reported that these experimental approaches reliably recapitulate those alterations that occur in human patients after pressure unloading therapy (68, 70, 80, 83, 88, 89, 92, 124-128). Hence, these particular animal models could indeed serve as an adequate tool to address those scientific questions regarding myocardial reverse remodeling that cannot be investigated in a clinical scenario.

3. Objective

A considerable body of clinical evidence has accumulated to support the notion that in case of PO-induced HF, termination of the pathological stimulus (by antihypertensive medications in case of AH or AVR/TAVI in case of AS) could results in a state of reverse remodeling with substantial improvement in LV structure and function. Nevertheless, it has been also recognized that not all the patients experience the same extent of functional and structural improvement following pressure unloading therapy. Hence, efforts have been taken to identify factors which might influence the regression of LVH. These recent studies have raised the possibility that the time point of medical interventions (performing pressure unloading at early versus late stages of PO-induced LVH) and the sex of the patients might determine the success of the reverse remodeling process (70, 76, 92, 111). Considering that many confounding factors (differences in comorbidities, age and medications) can limit the overall impact of the clinical observations, further experimental studies utilizing animal models are warranted.

Based upon that, the aims of the present studies were:

1. To establish a rat model of mechanical PO-induced pathological remodeling and pressure unloading-evoked reverse remodeling with microsurgical techniques.

2. To explore timeline alterations in LV structure and function during the development of PO-induced LVH and its progression to HF in male rats.

3. To investigate the effects of myocardial reverse remodeling from early versus late stages of PO-induced LVH in male rats.

4. To study the effect of sex on different aspects of LV structure and function during the development of PO-induced LVH.

4. Methods

4.1. Animals

The investigation conformed to the EU Directive 2010/63/EU and the Guide for the Care and Use of Laboratory Animals used by the US National Institutes of Health (NIH Publication No.85–23, revised 1996). The experiments were approved by the ethics committee of the Land Baden-Württemberg for Animal Experimentation (G-94/15 and G-198/16). The studies were interpreted in accordance with the ARRIVE (Animals in Research: Reporting in Vivo Experiments) guidelines (129). The animals were kept under standard conditions (22±2ºC with 12h light/dark cycles) and were allowed access to laboratory rat diet and water ad libitum during the whole experimental period. Before performing any type of surgeries, the rats underwent a one-week long acclimatization period.

4.2. Animal models

4.2.1. Rat model of pressure overload-induced myocardial remodeling

In order to induce PO of the LV, the previously described method of AB was established in our laboratory with slight modifications (61). In brief, the surgery consisted of the following steps. General anesthesia was induced in male and female Sprague-Dawley rats (5-6 weeks-old; 160-180g; Janvier, France) with 5% of isoflurane gas in a chamber and maintained by inhalation from a connected tube with 1.5–2% of isoflurane in O_2. The animals were placed in a supine position on an automatic heating pad to maintain the core temperature at 37°C, measured via a rectal probe. The abdominal hair was removed and an antiseptic solution was applied to disinfect the skin on the surgical area. The surgery was performed in midline laparotomy under sterile conditions. After the intestinal tract was gently placed aside, the peritoneal layer was dissected in order to gain access to the retroperitoneal space. The abdominal aorta between the right renal artery and the superior mesenteric artery was carefully cleaned from the surrounding connective tissue. A blunted 22-gauge needle was utilized to constrict the aorta above the right renal artery. After AB was completed, the intestines were placed back to the abdominal cavity and the abdominal muscle layer was sutured in single interrupted fashion. Finally, the skin wound was closed by applying surgical clips. Following surgery,

analgesia was provided by subcutaneously administered buprenorphine in the dose of 0.05mg/kg. Furthermore, 1ml physiological saline was also applied subcutaneously to avoid post-operative hypovolemia. Sham-operated animals were subjected to the same surgical procedure, except the aortic constriction (n=28).

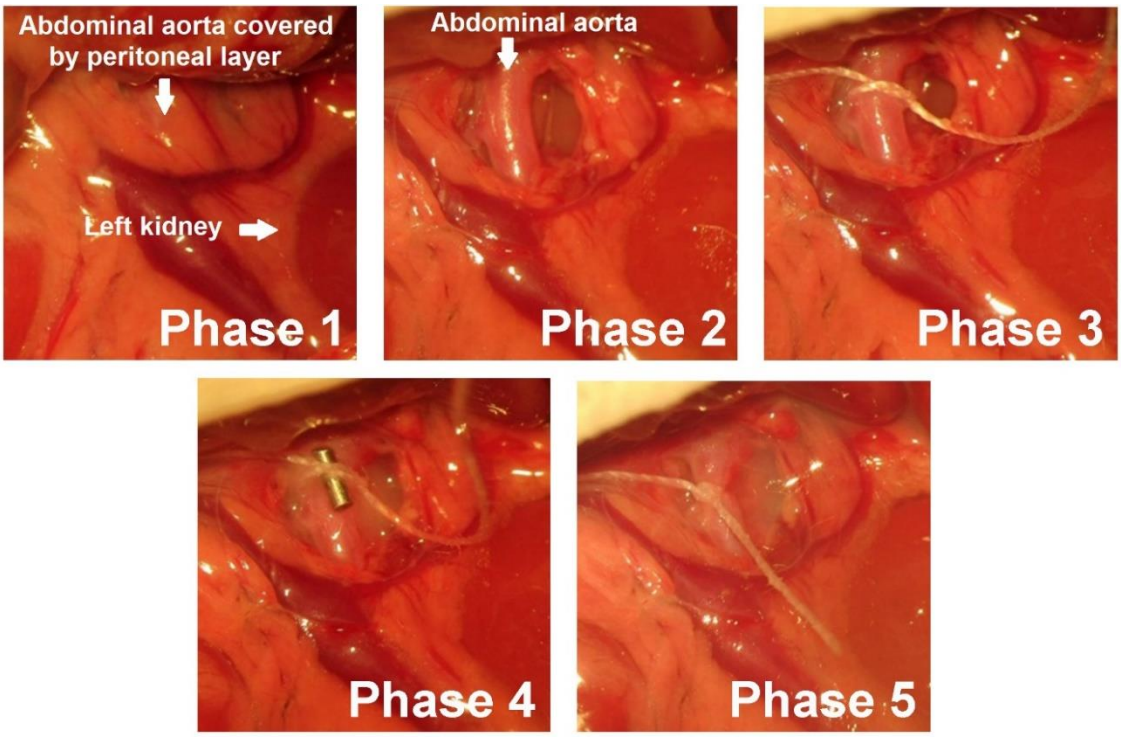

Figure 3. Abdominal aortic banding. Photos were taken at different phases during the surgical procedure of abdominal aortic banding. *Phase 1*: After a midline laparotomy, the intestines were taken aside and the peritoneal layer was visualized. *Phase 2*: By dissecting the peritoneal layer the abdominal aorta was identified. *Phase 3:* A 2.0 silk suture was placed around the abdominal aorta at the suprarenal level. *Phase 4*: A blunted 22-gauge needle was taken between the anterior surface of the aorta and the ligature. *Phase 5*: The ligature around both the needle and the aorta was tied. Finally, the needle was carefully removed, leaving a constriction on the abdominal aorta with a size of the external diameter of a 22-gauge needle.

4.2.2. Rat model of pressure unloading-induced reverse myocardial remodeling

After 6 weeks of AB (early debanding) or 12 weeks of AB (late debanding) a group of animals underwent a second minimal invasive surgery, when the aortic constriction was removed from the abdominal aorta (debanding). During this second surgery, general anesthesia was provided by isoflurane inhalation (5% for induction of anesthesia and 2-3% for maintenance of anesthesia). Rats were placed on a heating pad in a supine position. The surgical area was cleaned by removing the abdominal hair and disinfecting with an

antiseptic solution. A midline laparotomy was performed in the line of the scar from the previous surgery. The intestines were then localized in a way, that their position allowed us to visualize the abdominal aorta. The previously placed aortic constriction was identified and it was cleaned from the surrounding fibrotic tissue. The narrowing suture was carefully cut and removed from the abdominal aorta. The abdominal muscle and the skin layer were sutured in the single interrupted fashion. To prevent postoperative pain and dehydration, buprenorphine (in the dose of 0.05mg/kg) and physiological saline (1.5ml) was injected subcutaneously before the animals regained awareness.

4.3. Study protocols

The study protocols are summarized in *Figure 4, Figure 5 and Figure 6*.

4.3.1. Study 1: Longitudinal assessment of pressure overload-induced structural and functional alterations of the left ventricle in male rats

In the AB model, LV PO is evoked to a moderate level, which results in a relatively slow disease progression. Based on previous literature data, the time points of week 6, 12 and 18 were chosen to detect characteristic alterations at early and advanced stages of PO-induced HF. Accordingly, after AB or sham operations, the rats were randomized into the following 6 experimental groups:

Sham-wk6 group (n=9): after sham operation the rats were followed-up for 6 weeks;

AB-wk6 group (n=13): after AB the rats were followed-up for 6 weeks;

Sham-wk12 group (n=9): after sham operation the rats were followed-up for 12 weeks;

AB-wk12 group (n=13): after AB the rats were followed-up for 12 weeks;

Sham-wk18 group (n=10): after sham operation the rats were followed-up for 18 weeks;

AB-wk18 group (n=13): after AB the rats were followed-up for 18 weeks, respectively.

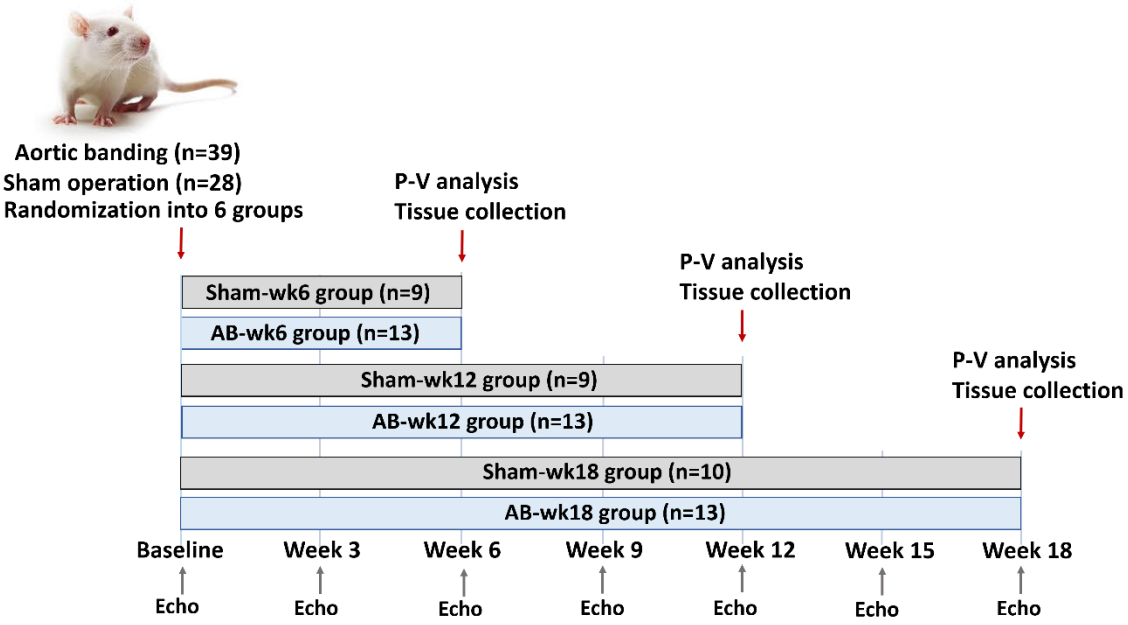

Figure 4. Schematic illustration of the experimental protocol of Study 1. At baseline, the rats underwent abdominal aortic banding ([AB]; n=39) or sham operation (n=28) and were subsequently randomized into 6 groups. In the *Sham-wk6* (n=9) and *AB-wk6* (n=13) groups, pressure-volume (P-V) analysis and tissue collection were performed 6 weeks after AB/sham operations. In the *Sham-wk12* (n=9) and *AB-w12* (n=13) groups, P-V analysis and tissue collection were performed 12 weeks after AB/sham operations. In the *Sham-wk18* (n=10) and *AB-w18* (n=13) groups, P-V analysis and tissue collection were performed 18 weeks after AB/sham operations. Furthermore, repetitive echocardiographic measurements at baseline, week 3, 6, 9, 12, 15 and 18 were also carried out in the Sham-wk18 and AB-wk18 groups.

4.3.2. Study 2: Investigating the effects of myocardial reverse remodeling from early- versus late-stage left ventricular hypertrophy in male rats

Similar to Study 1, the AB model was utilized to induce different stages of PO-induced LVH in Study 2 as well. However, in this investigation two additional groups were introduced to study the regression of LVH from early and late stages of LVH. In these experimental groups, a second minimal invasive surgery was performed to remove the aortic constriction at week 6 (early debanded) and week 12 (late debanded). Both debanded groups were followed up for 6 weeks. Accordingly, Study 2 consisted of the following 8 groups:

Sham-wk6 group (n=10): after sham operation the rats were followed-up for 6 weeks;

AB-wk6 group (n=10): after AB the rats were followed-up for 6 weeks;

Sham-wk12 group (n=10): after sham operation the rats were followed-up for 12 weeks;

AB-wk12 group (n=11): after AB the rats were followed-up for 12 weeks;

Sham-wk18 group (n=9): after sham operation the rats were followed-up for 18 weeks;

AB-wk18 group (n=13): after AB the rats were followed-up for 18 weeks, respectively.

Early debanded group (n=14); these rats underwent AB operation, after week 6 the banding suture was removed and the rats were followed up until week 12;

Late debanded group (n=15): these rats underwent AB operation, after week 12 the banding suture was removed and the rats were followed up until week 18.

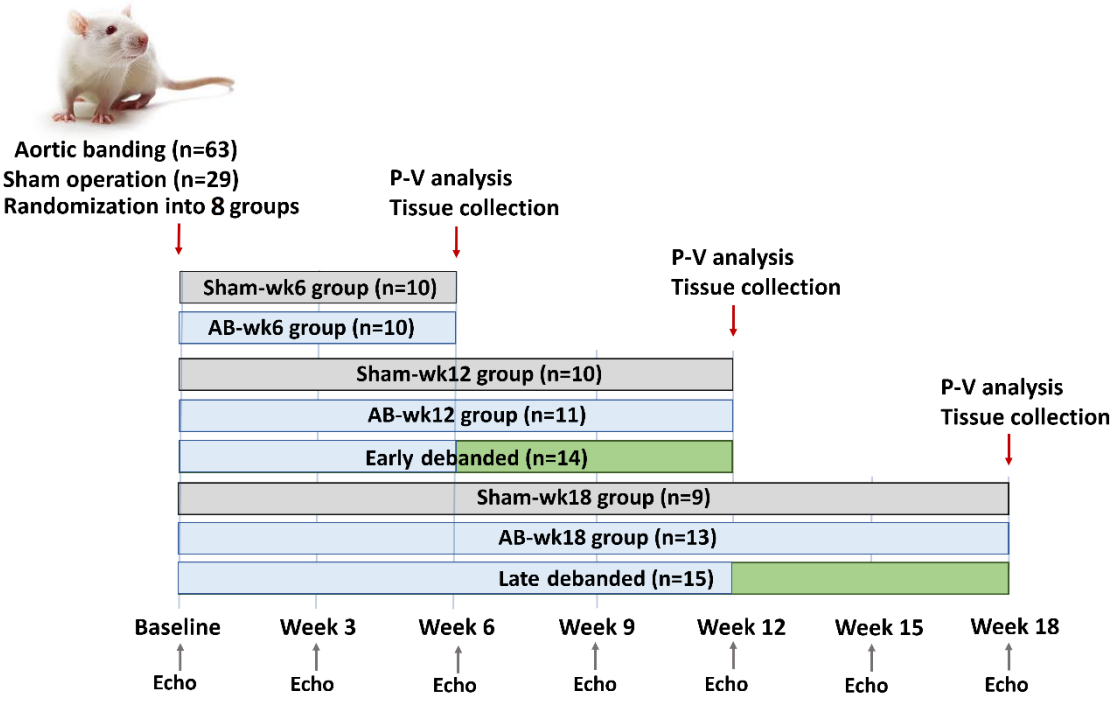

Figure 5. Schematic illustration of the experimental protocol of Study 2. At baseline, the rats underwent abdominal aortic banding ([AB]; n=63) or sham operation (n=29) and were subsequently randomized into 8 groups. The Sham-wk6 (n=10), AB-wk6 (n=10) groups were followed-up for 6 weeks. The Sham-wk12 (n=10), AB-wk12 (n=11) groups were followed-up for 12 weeks, while the Sham-wk18 (n=9), AB-wk18 (n=13) were followed-up for 18 weeks. In the early debanded group (n=14) the aortic constriction was removed after week 6, while in the late debanded group (n=15) the narrowing suture was removed after week 12.

4.3.3. Study 3: Investigation of sex differences during the development of pressure overload-induced left ventricular hypertrophy.

In this particular study, male and female rats underwent AB to investigate sex-related differences in the adaptation to chronic PO. Age- and sex-matched sham operated animals served as controls. Considering that sex differences were suggested to develop by time, functional and structural characterization of PO-induced LVH was carried out at a relatively early (week 6) and late (week 12) time points as well after PO induction. Accordingly, the following experimental groups were used in Study 3:

Male sham-week6 group (n=8): male rats underwent sham operation and were followed-up for 6 weeks

Male AB-week6 group (n=8): male rats underwent AB and were followed-up for 6 weeks;

Female sham-week 6 group: female rats underwent sham operation and were followed-up for 6 weeks

Female AB week 6 group (n=7): female rats underwent AB and were followed-up for 6 weeks;

Male sham week 12 group (n=8): male rats underwent sham operation and were followed-up for 12 weeks;

Male AB week 12 group (n=10): male rats underwent AB and were followed-up for 12 weeks;

Female sham week 12 group (n=8): female rats underwent sham operation and were followed-up for 12 weeks;

Female AB week 12 group (n=7): female rats underwent AB and were followed-up for 12 weeks.

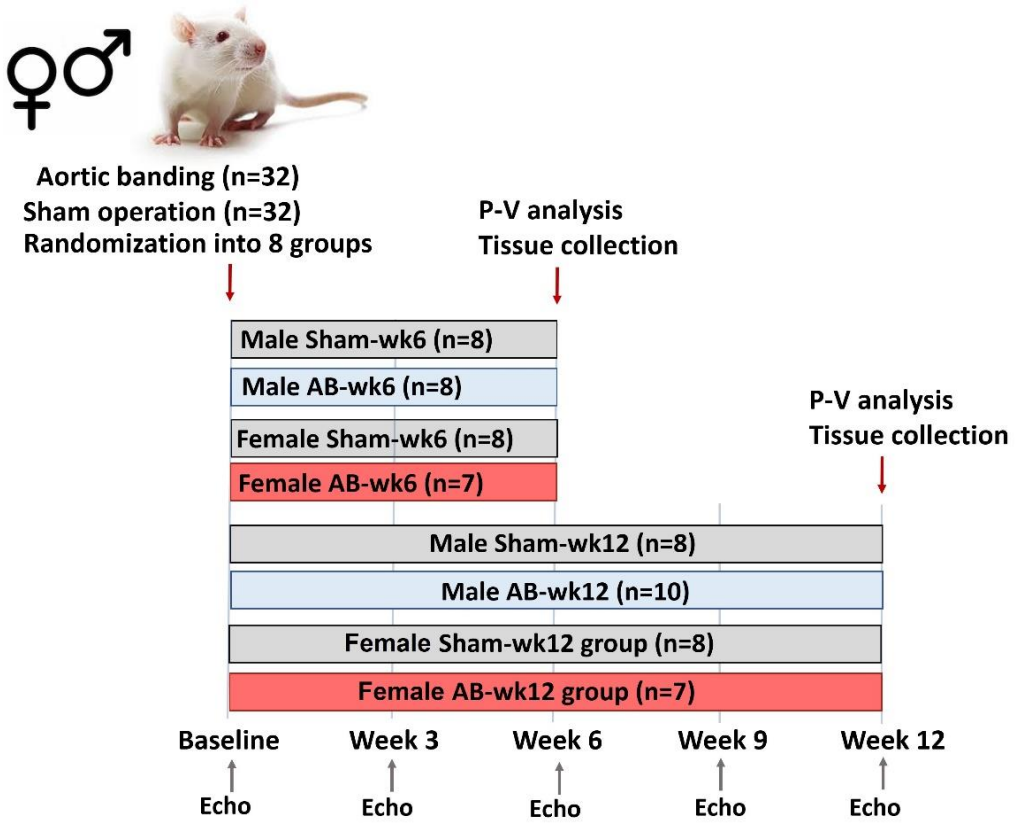

Figure 6. Schematic illustration of the experimental protocol of Study 3. At baseline, male and female rats underwent abdominal aortic banding ([AB]; n=32) or sham operation (n=32) and were subsequently randomized into 8 groups. In the male sham-wk6 (n=8) and AB-wk6 (n=8) groups and female sham-wk6 (n=8) and AB-wk6 (n=7) groups pressure-volume (P-V) analysis and tissue collection were performed at week 6. In the male sham-wk12 (n=8) and AB-wk12 (n=10) groups and female sham-wk12 (n=8) and AB-wk12 (n=7) groups pressure-volume (P-V) analysis and tissue collection were performed at week 12. Furthermore, repetitive echocardiographic measurements were performed in the male and female sham-wk12 and AB-wk12 groups.

4.4. Echocardiography

Echocardiography was carried out to characterize the morphological alterations during PO-induced pathological remodeling and pressure unloading-evoked reverse remodeling. For the sonographic measurements the Vevo® 2100 imaging system (Fujifilm Visual Sonics Inc., Toronto, Ontario, Canada) equipped with a 21-MHz linear probe was utilized. Repetitive measurements were performed at baseline and at week 3, 6, 9, 12, 15 and 18. During the echocardiographic measurements the following protocol was utilized. General anesthesia was induced by isoflurane. The rats were placed on an automatic heating pad in a supine position to maintain the body temperature of the animals at 37°C. The thorax of the animals was shaved to obtain an optimal acoustic window. Images in

two dimensional parasternal long-axis and short-axis views as well as M-mode recordings at the mid-papillary level were taken. Digital images were analyzed in a blinded fashion. LV end-diastolic diameter (LVEDD), LV end-systolic diameter (LVESD), anterior wall thickness (AWT) and posterior wall thickness (PWT) in diastole (d) and systole (s) were measured. All values were calculated as an average of three consecutive cardiac cycles. Furthermore, from the measured parameters, EF, relative wall thickness ([RWT]=[AWT_d+PWT_d]/LVEDD), LV mass (according to the Devereux formula) (130), and its index to the body weight (LV mass index) were calculated.

4.5. Pressure-volume analysis

At the end of the experimental period (at week 6, 12 or 18, respectively) the rats were anaesthetized by inhalation of 5% isoflurane gas in a chamber. After anesthesia was induced, the rats were placed in a supine position on an automatic heating pad to keep the core temperature at 37°C. To maintain anesthesia during the whole hemodynamic measurement, the rats were tracheotomized, intubated and artificially ventilated with 1-1.5% isoflurane gas in 100% O_2. Rocuronium bromide in the dose of 2mg/kg was administered intraperitoneal to induce muscle relaxation. A polyethylene catheter was inserted into the left external jugular vein for fluid administration. A 2F microtip pressure-conductance catheter (SPR-838, Millar Instruments, Houston, Texas, USA) was inserted into the right carotid artery and subsequently advanced into the ascending aorta. Following stabilization, arterial blood pressure was recorded. The catheter was then guided to the LV under pressure control. With the use of a special P-V analysis program (PVAN, Millar Instruments, Houston, TX, USA) systolic arterial blood pressure (SBP), diastolic arterial blood pressure (DBP), mean arterial pressure (MAP), heart rate (HR), LV end-systolic pressure (LVESP), LV end-diastolic pressure (LVEDP), maximal slope of systolic pressure increment (dP/dt_{max}) and diastolic pressure decrement (dP/dt_{min}), LV end-diastolic volume (LVEDV), LV end-systolic volume (LVESV), stroke volume (SV), cardiac output (CO), EF, arterial elastance (E_a; calculated by the following equation E_a=LVESP/SV (131)), and time constant of LV pressure decay (Tau; according to the Glanz method (132)) were computed and calculated.

In order to detect load-independent contractility parameters, P-V loops were also registered at transiently decreasing preload. This was achieved by transient occlusion of

the inferior caval vein. The slope of the end-systolic P-V relationship (ESPVR, according to the parabolic curvilinear model (133)) and preload recruitable stroke work (PRSW) and the slope of the dP/dt_{max}-end-diastolic volume relationship (dP/dt_{max}-EDV) were calculated as reliable indices of LV contractility.

To characterize myocardial compliance, the slope of the end-diastolic P-V relationship (EDPVR) was calculated.

Furthermore, ventriculo-arterial coupling (VAC) was also assessed as the ratio of E_a and ESPVR (VAC= E_a/ESPVR).

From the hemodynamic and echocardiographic measurements, LV meridional wall stress (σ) was estimated by the following equation σ= 0.334*LVESP*[LVDs/(1+PWTs/LVDs)] (104).

Parallel conductance was calculated and volume calibration of the conductance system was performed as previously described (52).

4.6. Morphometry and tissue conservation

Following P-V analysis, the infrarenal part of the abdominal aorta was cannulated and the blood of the animals was subsequently collected. To remove the residual blood cells from myocardial tissue, retrograde perfusion from the abdominal aorta was applied with 50ml oxygenated, physiological saline. After perfusion, the heart of the animals was removed from the thorax and their weights were quickly measured on a scale. This was followed by conservation of LV myocardial tissue. Accordingly, transverse segments (the middle third part) of the right and the left ventricles were fixed in buffered paraformaldehyde solution (4%; for 24 hours) followed by 70% alcohol. The fixed samples were than embedded in paraffin for histological analysis. Furthermore, the apex of the LV was cut into small pieces (40-50mg) and subsequently snap frozen in liquid nitrogen. The collected samples were stored at -80°C until molecular measurements (qRT-polymerase chain reaction [PCR] or Western blot) were performed. After tissue conservation was accomplished, tibial length (TL) was measured and the ratio of heart weight-to-tibial length (HW/TL) was calculated.

4.7. Left ventricular histology

Transverse, transmural, 5-μm thick slices of the paraffin-embedded heart samples were cut and placed on adhesive slides. These sections were subsequently stained with hematoxylin and eosin staining to determine cardiomyocyte diameter (CD) as a cellular marker of myocardial hypertrophy. In each sample, 100 longitudinally oriented cardiomyocytes from the LV were examined, and their diameters at transnuclear positions were defined with ImageJ software (National Institutes of Health, Bethesda, MD, USA). The mean value of 100 measurements represented one sample.

The extent of myocardial fibrosis was assessed on picrosirius-stained sections. ImageJ software was used to identify the picrosirius-red positive area. Six images (magnification 50X) were randomly taken from the free LV wall on each section. After background subtraction, eye controlled auto-threshold has been determined to detect positive areas. The collagen area (picrosirius red positive area-to-total area ratio) was determined on each image, and the mean value of six images represents each animal. Furthermore, perivascular fibrosis was assessed by the percentage of perivascular collagen area to total vascular area. The extent of perivascular fibrosis was also assessed by using ImageJ software.

The evaluation of the histological sections was performed by an independent observer who was blinded to the experimental design.

4.8. Left ventricular gene expression analysis

LV myocardial samples stored at -80°C were homogenized (Precellys Evolution tissue homogenizer, Bertin Instruments, Montigny-le-Bretonneux, France) in a lysis buffer (RLT buffer; Qiagen, Hilden, Germany). During tissue homogenization, the temperature of the samples was maintained at 0°C by using the Cryolis Evolution cooling system (Bertin Instruments). RNA was isolated using the RNeasy Fibrous Tissue Mini Kit (Qiagen), according to the manufacturer's instructions. The quality and concentration of the isolated RNA were assessed by the NanoDrop 2000 Spectrophotometer (Thermo Scientific, Waltham, MA, USA). Accordingly, optical density at 230, 260, and 280 nm was measured. The ratios of 230/260 and 230/280 nm were defined for quality control. Reverse transcription reaction (1μg total RNA of each sample) was completed using the QuantiTect Reverse Transcription Kit (Qiagen).

Quantitative real-time PCR was performed either with the StepOnePlus Real-Time PCR System (Applied Biosystems, Foster City, CA, USA) in duplicates (in Study 1) or with the LightCycler 480 System (Roche, Mannheim, Germany) in duplicates (in Study 2 and 3). The reaction mixture for the measurement with StepOnePlus Real-Time PCR System contained 1µl sample cDNA, 5µl TaqMan Universal PCR MasterMix (Applied Biosystems), 0.5µl TaqMan Gene Expression Assay (Applied Biosystems) (the assay identification numbers are shown in Table 1) and 3.5µl RNA-free water (Qiagen).The reaction mixture for the measurement with the LightCycler 480 System consisted of 2µl sample cDNA, 0.2µl forward primer (TIB Molbiol, Berlin, Germany), 0.2µl reverse primer (TIB Molbiol), 0.2µl Universal Probe Library (UPL) probe (Roche) (the sequences of forward and reverse primers and the identification numbers of the UPL probes are shown in Table 2), 10µl LightCycler 480 Probes Master (Roche) and 7.4µl RNA-free water (Qiagen).

Gene expression data was normalized to glyceraldehyde 3-phosphate dehydrogenase (GAPDH), and expression levels were calculated using the CT comparative method ($2^{-\Delta CT}$). All results are expressed as values normalized to a positive calibrator (a pool of cDNA from all samples of the Sham-wk6 group in Study 1 and 2 and the Male-Sham-wk6 group in Study 3 [$2^{-\Delta\Delta CT}$]).

Table 1. The full names and the abbreviations of the measured target genes and the identification numbers of TaqMan® Gene Expression Assays are shown.

	Target Gene (Full name)	**Target Gene (Abbreviation)**	**TaqMan® Gene Expression Assay ID**
Fetal gene program	myosin heavy chain-α	α-MHC	Rn00568304_m1
	myosin heavy chain-β	β-MHC	Rn00568328_m1
	atrial natriuretic peptide	ANP	Rn00664637_g1
Pro-fibrotic mediator	connective tissue growth factor	CTGF	Rn01537279_g1
House-keeping	glyceraldehyde 3-phosphate dehydrogenase	GAPDH	Rn01775763_g1

Table 2. The full names and the abbreviations of the measured target genes, the sequences for forward (F) and (R) reverse primers and the identification numbers of Universal Probe Library (UPL) probes are shown.

	Target Gene (Full name and abbreviation)	**Forward (F) and reverse (R) primers**	**UPL probes**
Fetal gene program	atrial natriuretic peptid (ANP)	**F:**5'-CAACACAgATCTgATggATTTCA-3'	65
		R:5'-CgCTTCATCggTCTgCTC-3'	
	myosin heavy chain-α (α-MHC)	**F:**5'-ggAggTggAgAAgCTggAA-3'	65
		R:5'-ATCTTgCCCTCCTCATgCT-3'	
	myosin heavy chain-β (β-MHC)	**F**:5'-gCTgCAgAAgAAgCTCAAAgA-3'	65
		R:5'-gCAgCTTCTCCACCTTgg-3'	
Pro-fibrotic mediator	connective tissue growth factor (CTGF)	**F:**5'-CCggTAggTCTTCACACTgg-3'	129
		R:5'-gCTgACCTAgAggAAAACATTAAgA-3'	
House-keeping	glyceraldehyde 3-phosphate dehydrogenase (GAPDH)	**F:** 5'-CTACCCACGGCAAGTTCAAT-3'	111
		R: 5'-ATTTGATGTTAGCGGGATCG-3'	

4.9. Left ventricular protein expression analysis

Western blot measurement was performed to detect alterations in the myocardial protein expression of CTGF. Fresh-frozen LV samples were homogenized in RIPA buffer (Sigma Aldrich, St. Louis, Missouri, USA) containing Complete Protease Inhibitor Cocktail (Roche) and PhosSTOP^{TM} phosphatase inhibitor coctail (Roche) at 0°C. Tissue homogenization was carried out by using Precellys Evolution homogenizer equipped with the Cryolis Evolution cooling system. The tissue lysates were agitated at 4°C for 1 hour. Subsequently, centrifugation was applied for 20 minutes with 12,000rpm at 4°C and the

supernatant was collected. Protein concentration was measured by Pierce BCA Protein Assay Kit (Thermo Fisher Scientific, Rockford, IL, USA). Samples were mixed with 2X Laemmli Sample Buffer (Sigma Aldrich) containing reducing agent and subsequently boiled at 95°C for 5min. An equal amount of protein (20μg) was loaded onto a commercially available precast 4–12% sodium dodecyl sulfate–polyacrylamide gel electrophoresis gel (NuPAGE® Novex® Bis-Tris Mini Gel, Invitrogen, Carlsbad, CA, USA) and separated by gel electrophoresis (using PowerEase 500 electrophoresis power supply [Invitrogen], and applying 90mV for 30min and 120mV for 60min). Transfer of the separated proteins to a polyvinylidene fluoride membrane was carried out under dry conditions by using an electroblotting system (iBlot™ Gel Transfer Device, Invitrogen). After transfer, the membranes were washed and blocked for 1h in 5% of BSA in Tris-buffered saline-Tween 20 at room temperature to reduce the nonspecific bindings of antibodies. The membranes were then incubated overnight at 4°C with the primary antibody. The blots were washed to remove excessive primary antibody binding and incubated with horseradish peroxidase-conjugated secondary antibodies for 1h at room temperature (anti-rabbit IgG, Cell Signaling Technology, Danvers, MA, USA). GAPDH housekeeping protein was used as loading control and protein normalization. Blots were developed by the enhanced chemiluminescence detection assay (SuperSignal™ West Pico PLUS Chemilumiescent Substrate, Thermo Fisher Scientific) and the intensity of the bands was measured by the ChemiDoc™ Touch Imaging system (Bio-Rad, Hercules, CA, USA).

Table 3. The full names and the abbreviations of the measured target proteins, the code of the primary antibody, the dilution of the primary antibody and the detected molecular weight are shown.

Target protein (Full name)	**Target protein (Abbreviation)**	**Primary antibody**	**Dilution**	**Molecular Weight**
connective tissue growth factor	CTGF	#6992 Abcam, Cambridge, UK	1:2000	38 kDa
glyceraldehyde 3-phosphate dehydrogenase	GAPDH	#5174 Cell Signaling	1:5000	37 kDa

4.10. Statistical analysis

4.10.1. Study 1

All values are expressed as mean±standard error of the mean. The distribution of the datasets was tested by D'Agostino-Pearson omnibus test (when number of measurements reached 8 in a group) or by Shapiro-Wilk normality test (when number of measurements failed to reach 8 in a group).

An unpaired two-sided Student's t-test in case of normal distribution or Mann-Whitney U test in case of non-normal distribution was used to compare the echocardiographic parameters between the Sham-wk18 and the AB-wk18 groups at baseline, and at week 3, 6, 9, 12, 15 and 18. Repeated-measures one-way analysis of variance (ANOVA) or Friedman test was performed for comparing data of the echocardiographic measurements at different time points (week 3, 6, 9, 12, 15 and 18) within a group. To examine intergroup differences, Holm-Sidak or Dunn post hoc test was carried out.

Two-way ANOVA with the factors "time" and "AB" were carried out to compare six independent groups in all the other measurements. Prior to two-way ANOVA, those datasets that failed to show normal distribution were logarithmically transformed. Tukey post hoc test was utilized to detect intergroup differences.

A P value of <0.05 was used as a criterion for statistical difference. Furthermore, two additional categories ($P<0.01$ and $P<0.001$) were introduced to indicate the strength of the observed statistical difference.

4.10.2. Study 2

All values are expressed as mean±standard error of the mean. The distribution of the datasets was tested by D'Agostino-Pearson omnibus test (when number of measurements reached 8 in a group) or by Kolmogorov-Smirnov test (in case of Western blot measurements, when number of samples were 6 per group).

An unpaired two-sided Student's t-test in case of normal distribution or Mann-Whitney U test in case of non-normal distribution was used to compare two independent groups. One-way ANOVA followed by Tukey's post hoc test or Kruskal-Wallis test followed by Dunn's post hoc test was carried out to compare three independent groups.

When data was available (in case of repeatable, non-invasive measurements: echocardiography) from the same animal at the time of the debanding surgery (*pre-*

debanding: week 6 in case of early debanded and week 12 in case of late debanded) and at the end of the experimental period (*post-debanding:* week 12 in case of early debanded and week 18 in case of late debanded) a ratio of *post-debanding/pre-debanding* values was calculated. These values were used to directly compare the extent of regression between the early and the late debanded groups.

When repetitive data was not available (in case of not repeatable measurements: postmortem organ measurements, P-V analysis, histology and PCR) from the same animal, individual data were normalized to the mean value of the corresponding sham groups. These normalized values were used to compare hypertrophy-associated alterations among the AB groups (AB-6wk, AB-12wk, AB-18wk groups) and between the debanded groups (early and late debanded), respectively.

A P value of <0.05 was used as a criterion for statistical difference.

4.10.3. Study 3

All values are expressed as mean±standard error of the mean. The distribution of the datasets was tested by Shapiro-Wilk normality test.

Two-way ANOVA with the factors “time” and “AB” was utilized to compare the four male (Sham/AB 6 week and Sham/AB 12 week groups) and the four female (Sham/AB 6 week and Sham/AB 12 week groups) groups separately. Prior to two-way ANOVA, those datasets that failed to show normal distribution were logarithmically transformed.

To directly compare hypertrophy-associated alterations between the two genders, individual data of the AB groups were normalized to the mean value of the corresponding sham groups. An unpaired two-sided Student’s t-test in case of normal distribution or Mann-Whitney U test in case of non-normal distribution was used to compare the hypertrophy-associated changes in each parameter.

In case of echocardiographic measurements, two-way ANOVA with the factors “sex” and “AB” was performed to compare four groups (male/female Sham and male/female AB groups) at five different time points (baseline, week 3, week 6, week 9 and week 12). Following ANOVA, Tukey post hoc test was selected in every case to examine intergroup differences.

Spearman correlation test was performed to detect correlations between LV mass index and Tau, between collagen area and LVEDP and between collagen area and EDPVR.

A P value of <0.05 was used as a criterion for statistical difference.

5. Results

5.1. Longitudinal assessment of pressure overload-induced structural and functional alterations of the left ventricle

5.1.1. Echocardiography

From week 3 until the end of the experimental period, AWT_d, PWT_d and $LVmass_{index}$ were increased in the AB-wk18 group compared to the sham-wk18 group, indicating the development of LVH (**Fig. 7 and Fig. 8A-C**). Furthermore, at week 12, week 15 and week 18, LVEDD was also increased in the AB-wk18 group compared to the sham-wk18 group, suggesting chamber dilatation (**Fig. 8D**).

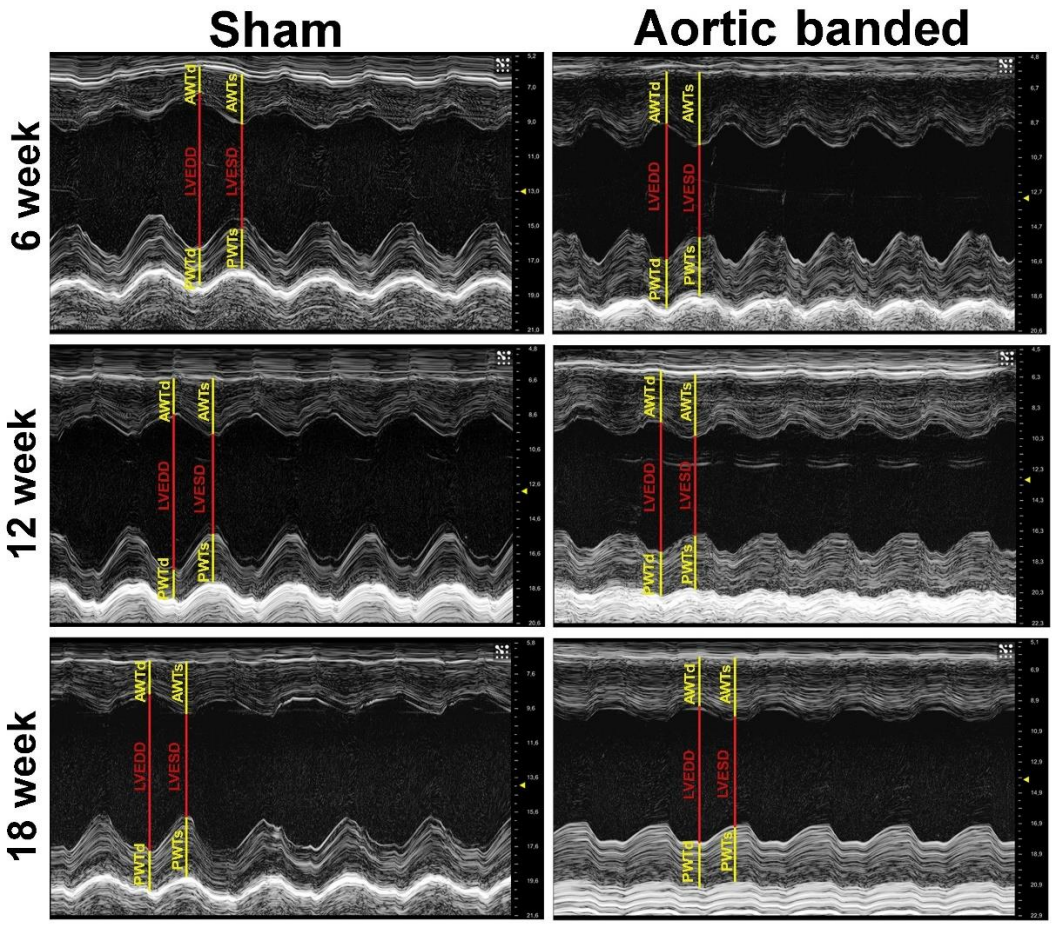

Figure 7. Representative echocardiographic recordings. Representative M-mode echocardiographic recordings at the midpapillary muscle level are shown in the sham and the aortic banded groups at week 6, 12 and 18. AWT_d: anterior wall thickness in diastole, AWT_s: anterior wall thickness in systole, LVESD: left ventricular end-systolic diameter, LVEDD: left ventricular end-diastolic diameter, PWT_d: posterior wall thickness in diastole, PWT_s: posterior wall thickness is systole.

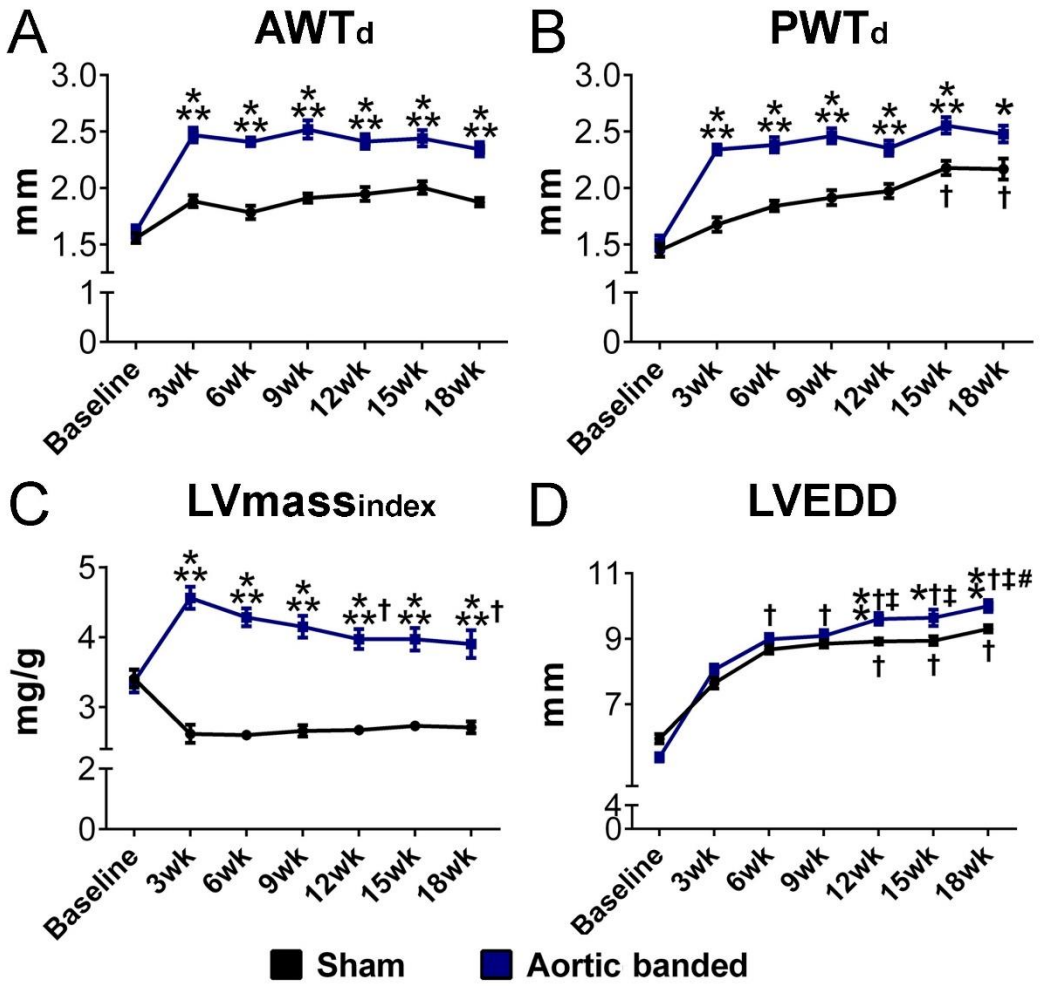

Figure 8. Echocardiographic follow-up during the development of pressure overload-induced myocardial hypertrophy. Anterior (**A**) and posterior (**B**) wall thicknesses as well as left ventricular (LV) mass index ($LVmass_{index}$) (**C**) were already increased after 3 weeks of LV pressure overload in the aortic banded groups. Furthermore, the aortic banded group was also associated with elevated LV end-diastolic diameter (LVEDD) (**D**) after 12 weeks of pressure overload. AWT_d: anterior wall thickness in diastole, PWT_d: posterior wall thickness in diastole *: P<0.05 vs. corresponding sham. **: P<0.01 vs. corresponding sham. ***: P<0.001 vs. corresponding sham. †: P<0.05 vs. week 3. ‡: P<0.05 vs. week 6. #: P<0.05 vs. week 9.

5.1.2. Pathological hypertrophy and fibrosis markers

In the AB-wk6, AB-wk12 and AB-wk18 groups, HW/TL and CD were increased compared to the corresponding sham groups (**Fig. 9**). The myocardial mRNA expression levels of β/α-MHC ratio and ANP were also elevated in the AB groups compared to their corresponding sham groups, indicating reactivation of the fetal gene program (**Fig. 10**). Furthermore, assessment of the myocardial collagen area revealed increased interstitial

fibrosis in the AB-wk12 and AB-wk18 groups compared to the sham-wk12 and sham-wk18 groups, respectively (**Fig. 11**).

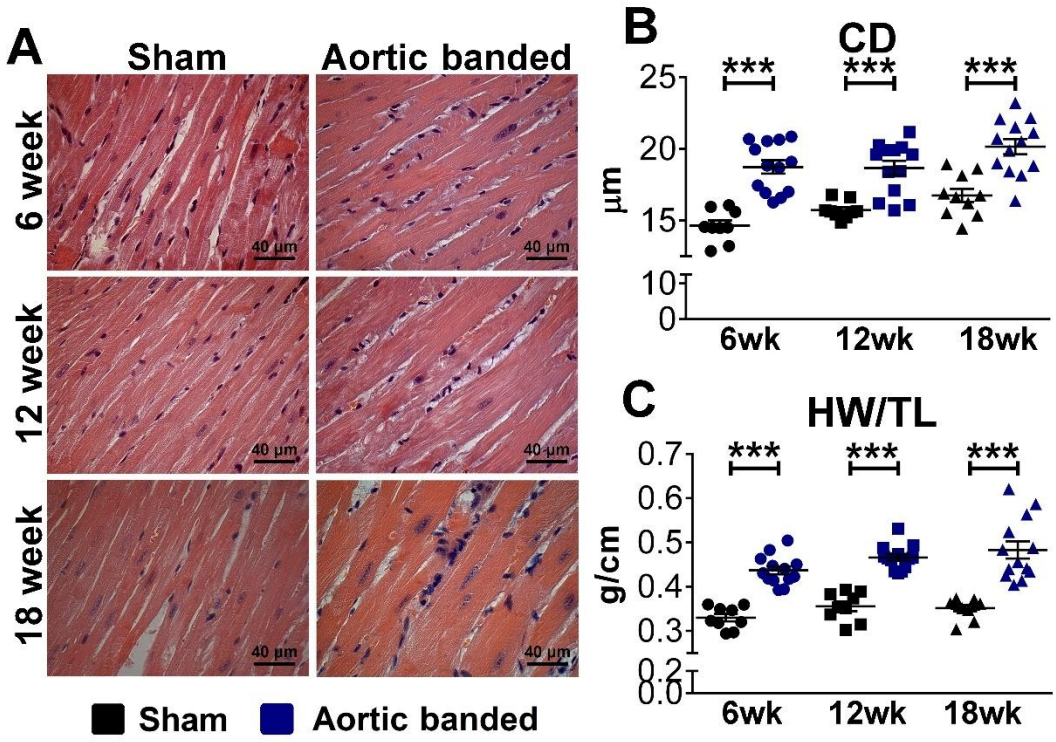

Figure 9. Macroscopic and microscopic myocardial hypertrophy markers. Representative photomicrographs (**A**) of hematoxylin and eosin staining (magnification 200x, scale bar: 40μm) are shown demonstrating enlarged cardiomyocytes in the aortic banded groups. Cardiomyocyte diameter (CD) (**B**) and heart weight-to-tibial length (HW/TL) (**C**) increased in the aortic banded groups at week 6, 12 and 18 compared to sham groups. ***: P<0.001 vs. corresponding sham.

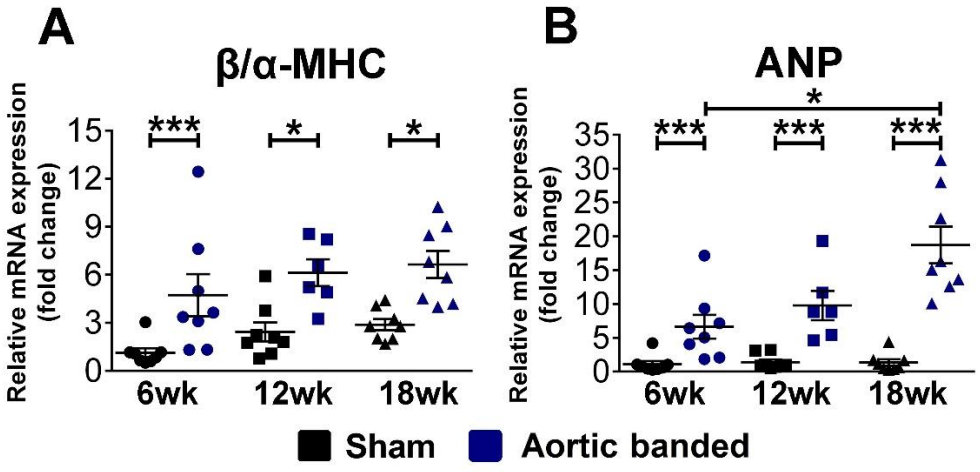

Figure 10. Fetal gene expression during pressure overload-induced myocardial hypertrophy. mRNA expression of beta-to-alpha myosin heavy chain (β/α-MHC) (**A**) and atrial natriuretic peptide (ANP) (**B**) increased in the aortic banded groups at week 6, 12 and 18 compared to the age-matched sham groups. *: P<0.05 vs. age-matched sham. ***: P<0.001 vs. age-matched sham.

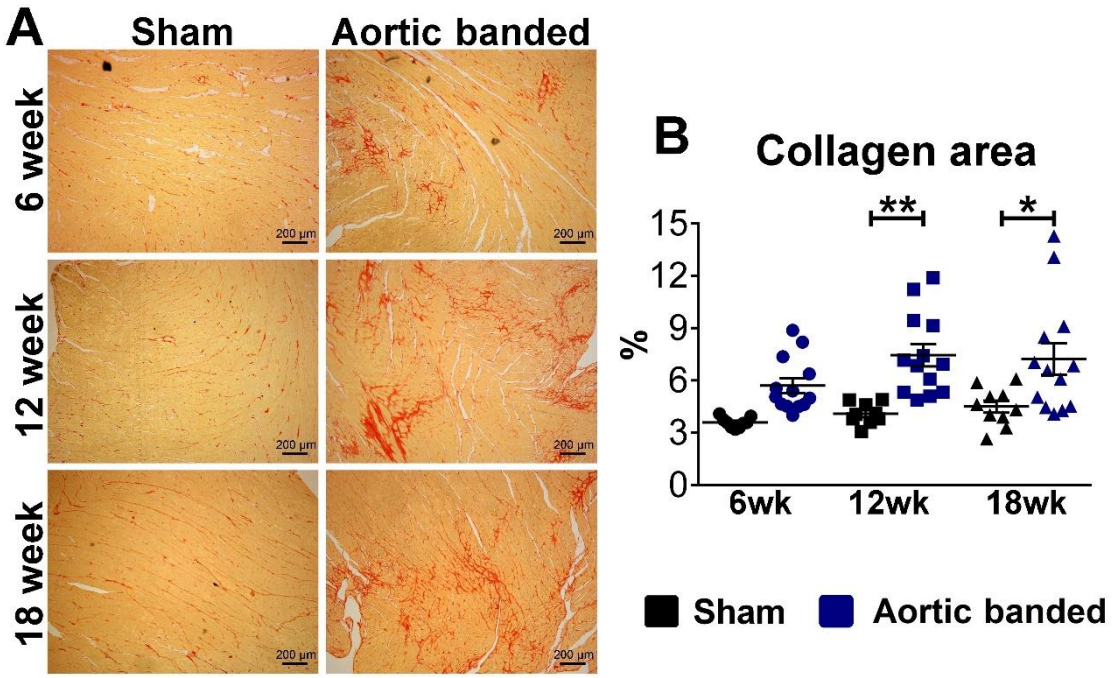

Figure 11. Interstitial fibrosis. Representative photomicrographs of picrosirius red staining (magnification 50x, scale bar: 200µm) (**A**) are shown demonstrating increased interstitial fibrosis in the aortic banded groups at week 12 and week 18. Quantification of the collagen area (**B**) confirmed increased collagen accumulation in the aortic banded groups at week 12 and 18 compared to the age-matched sham groups. *: P<0.05 vs. corresponding sham. **: P<0. 01 vs. corresponding sham.

5.1.3. Left ventricular function

5.1.3.1. Arterial loading

SBP, DBP and MAP were elevated in the AB groups compared to the corresponding sham groups, confirming the presence of increased PO proximal to the aortic constriction (**Table 4**).

5.1.3.2. Load-dependent systolic parameters

The AB-wk6 group was associated with preserved systolic performance. Accordingly, no difference could be observed in load-dependent systolic parameters (EF, SV, CO) between the AB and the sham group at week 6 (**Fig. 12, Table 4**). In contrast, in the AB-wk12 and AB-wk18 groups, EF decreased significantly, while SV and CO showed a tendency towards decreased values compared to the corresponding sham groups (**Fig. 12, Table 4**).

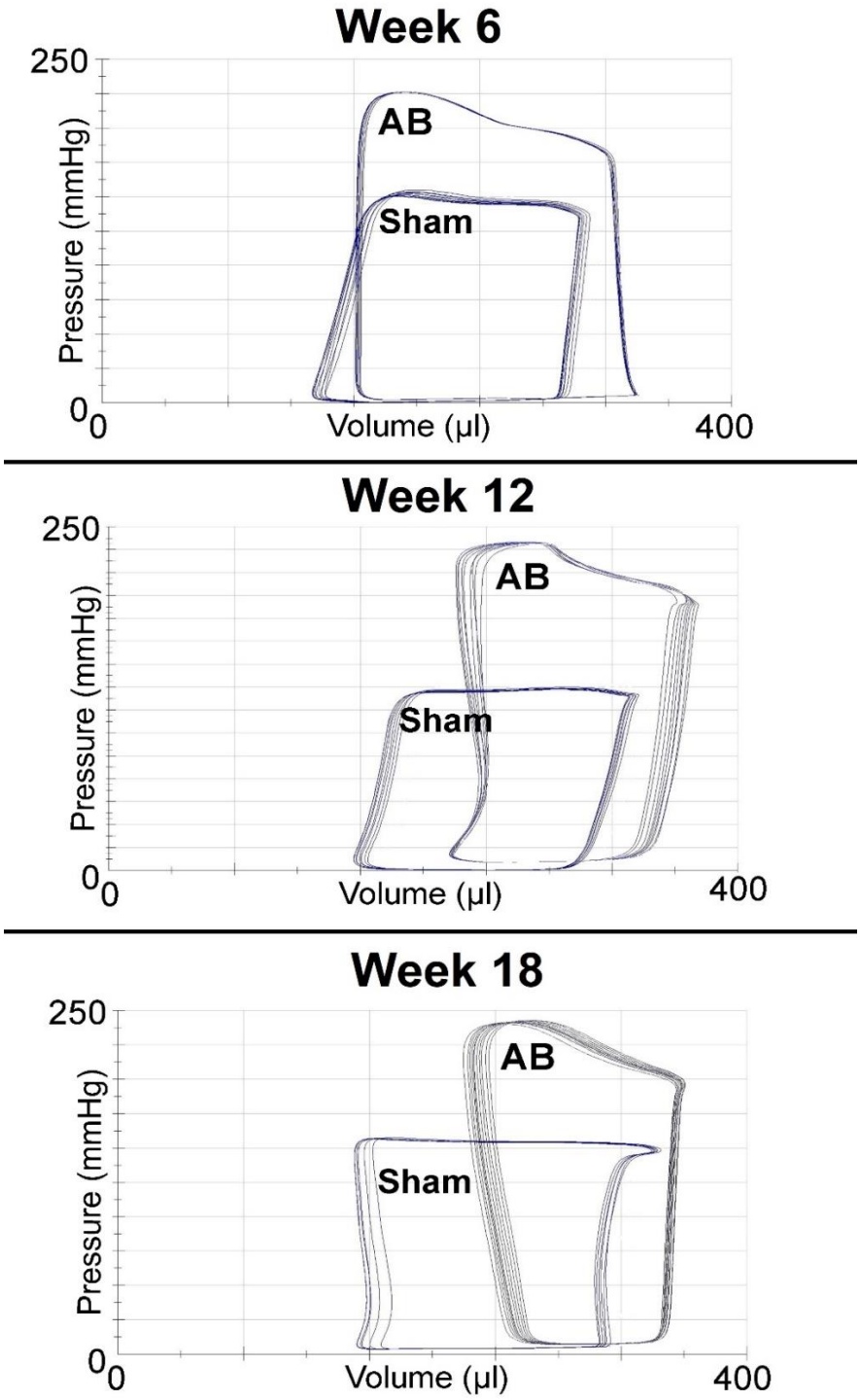

Figure 12. Representative steady-state pressure-volume (P-V) loops are shown demonstrating in vivo left ventricular (LV) function in sham and aortic banded (AB) rats at different time points. The width of the P-V loops in the AB group at week 6 does not differ from the control's width. In contrast, at week 12 and 18, the width of the loops becomes substantially smaller in the AB groups, suggesting impaired systolic performance. Furthermore, the P-V loops demonstrate a rightward shift in the AB groups at week 12 and 18, indicating chamber dilatation.

Table 4. Steady state functional parameters in aortic banded and sham-operated rats at different time points. Values are expressed as mean ± standard error of the mean. AB indicates aortic banding; SBP: systolic arterial blood pressure; DBP: diastolic arterial blood pressure; MAP: mean arterial pressure; HR: heart rate; LVEDV: LV end-diastolic volume; LVESV: LV end-systolic volume; SV: stroke volume; CO: cardiac output; EF: ejection fraction. **: P<0.01 vs. age-matched sham. ***: P<0.001 vs. age-matched sham. ##: P<0.01 vs. AB-week 6. ###: P<0.001 AB-week 6. $: P<0.05 vs. AB-week 12. $$: P<0.01 vs. AB-week 12.

	Week 6		**Week 12**		**Week 18**	
	Sham (n=9)	***AB*** (n=13)	***Sham*** (n=9)	***AB*** (n=13)	***Sham*** (n=10)	***AB*** (n=13)
SBP, mmHg	148±4	215±4***	138±5	215±5***	150±5	228±4***
DBP, mmHg	116±3	150±2***	110±4	154±4***	120±4	170±3***###$$
MAP, mmHg	127±4	172±2***	119±4	174±4***	140±4	189±3***##$
HR, beats/min	355±7	369±9	354±5	366±7	379±7	357±5
LVEDV, µl	268±16	305±14	286±23	320±20	283±18	327±14
LVESV, µl	175±15	194±12	178±17	231±11	160±11	241±11***
SV, µl	188±16	173±10	195±11	163±12	175±10	151±15
CO, ml/min	66.7±6.1	62.9±3.0	69.4±4.5	59.4±4.1	66.3±4.4	53.7±5.4
EF, %	58±3	51±2	57±2	44±2**	55±2	41±3***##

5.1.3.3. Load-independent contractility parameters

In the AB-wk6 group, ESPVR, PRSW and dP/dt_{max}-EDV increased significantly compared to the sham-wk6 group, indicating increased LV contractility (**Fig. 13-16**). This contractility augmentation diminished in the AB-wk12 and AB-wk18 groups (**Fig. 13-16**). Accordingly, the load-independent contractility parameters were not different in the AB-wk12 and AB-wk18 groups compared to sham-wk12 and sham-wk18 groups, but ESPVR and PRSW were significantly decreased compared to the AB-wk6 group (**Fig. 16**).

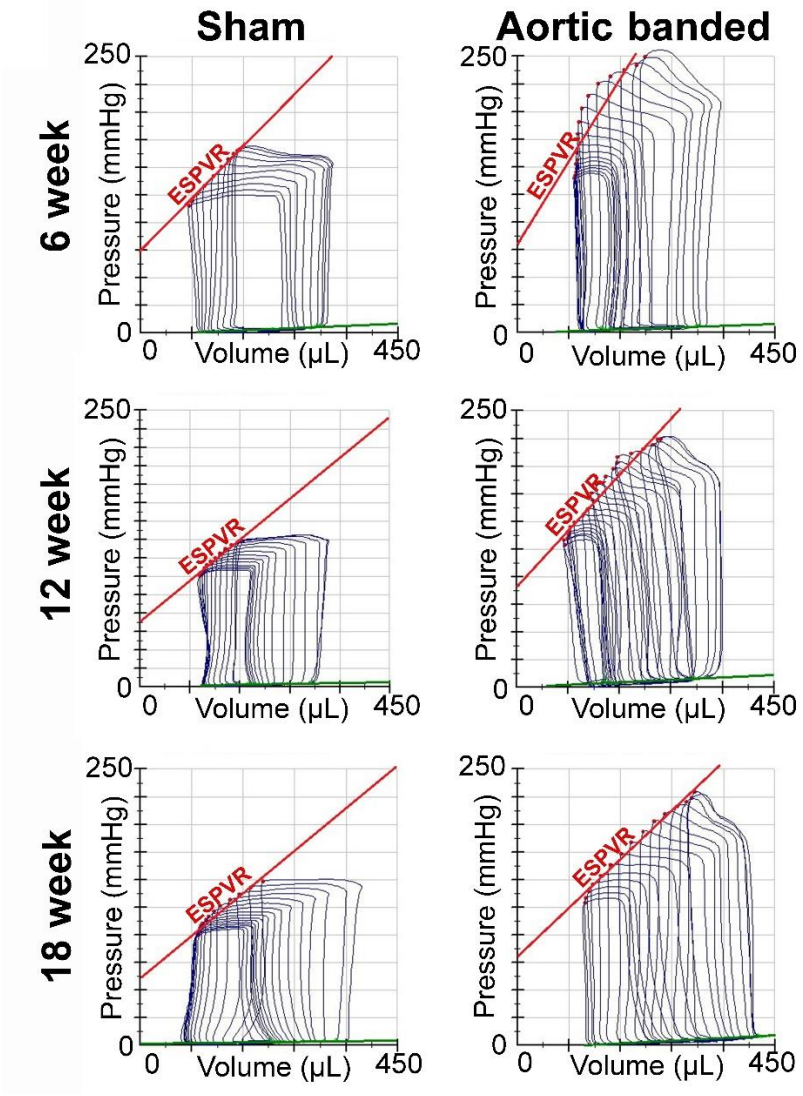

Figure 13. Representative pressure-volume loops in the aortic banded and the sham groups at different time points. Original recordings were obtained at different preloads during transient vena cava occlusion. At week 6, the slope of the end-systolic P-V relationship (ESPVR) was steeper in the aortic banded (AB) group, suggesting enhanced LV contractility. In contrast, the slope of the of the end-systolic P-V relationship (ESPVR) did not differ in the aortic banded (AB) group at week 12 and 18 from its corresponding sham group.

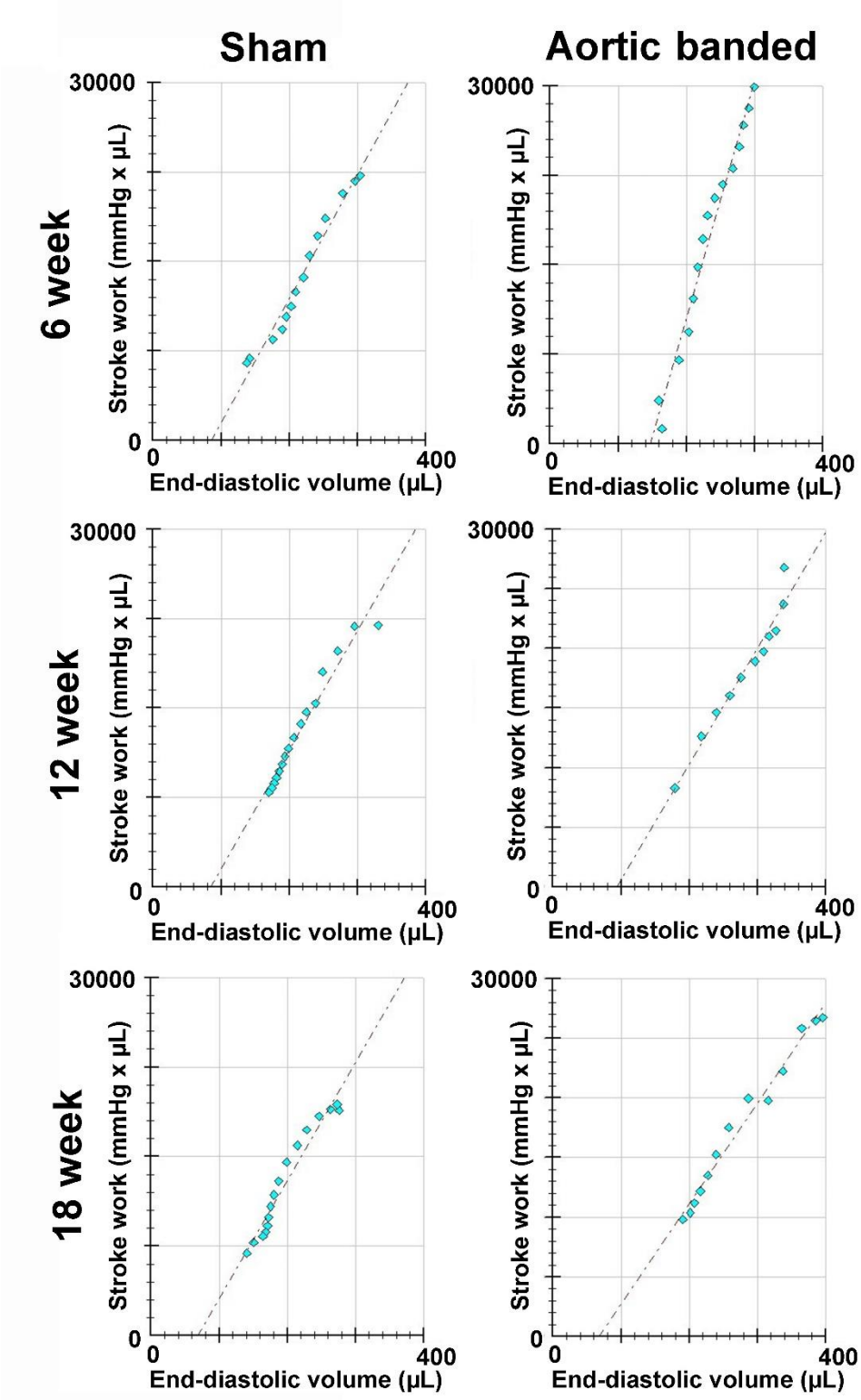

Figure 14. Alterations in preload recruitable stroke work (PRSW) during the progression of pressure overload-induced myocardial hypertrophy. PRSW indicated increased left ventricular (LV) contractility in the aortic banded (AB) group at week 6 compared to the corresponding sham group. The contractility augmentation diminished in the AB groups at week 12 and 18.

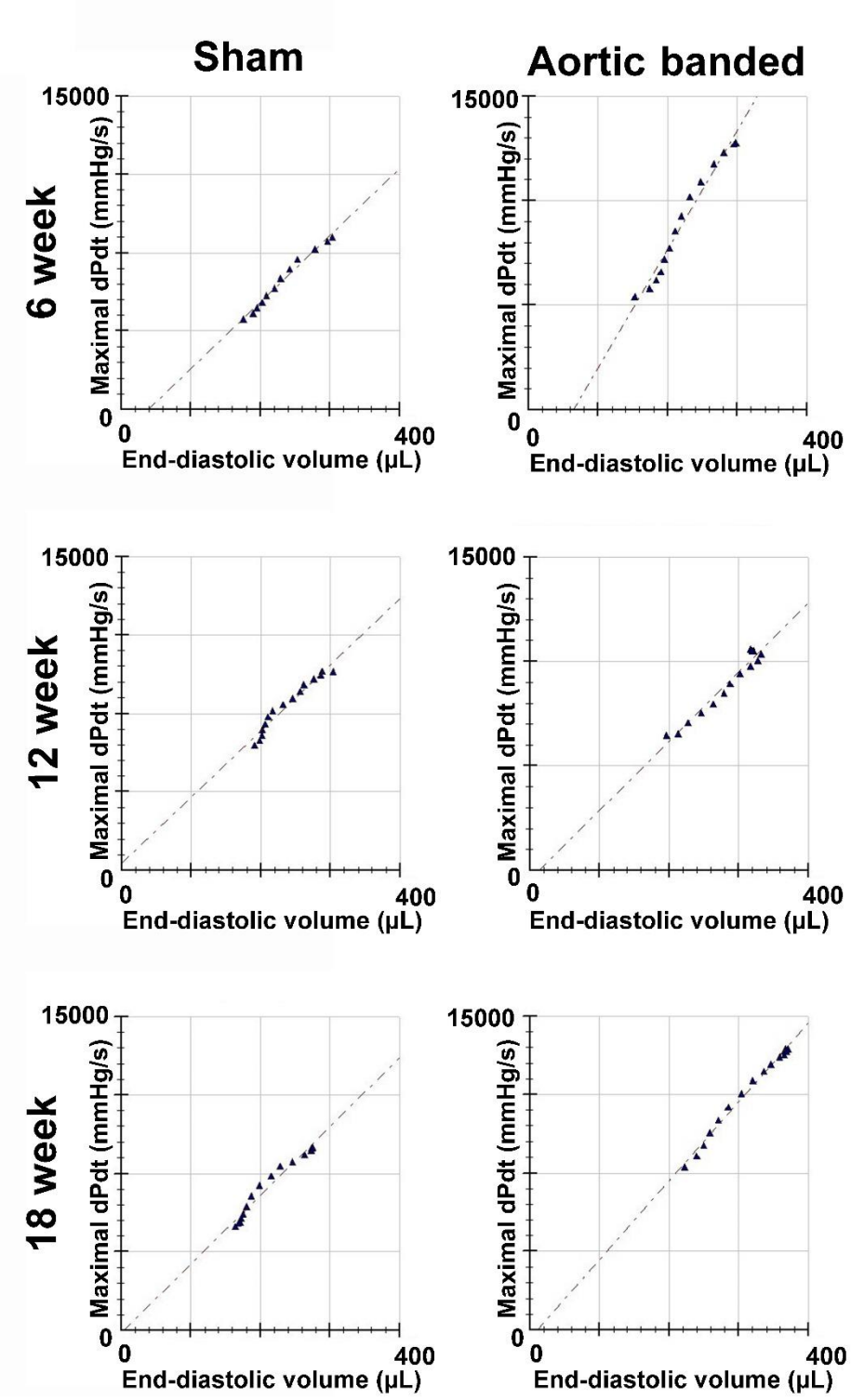

Figure 15. Alterations in the slope of the maximal systolic pressure increment (dP/dt_{max})-end diastolic volume (EDV) relationship during the progression of pressure overload-induced myocardial hypertrophy. dP/dt_{max}-EDV indicated augmented left ventricular (LV) contractility in the aortic banded (AB) group at week 6 compared to the corresponding sham group. The contractility enhancement diminished in the AB groups at week 12 and 18.

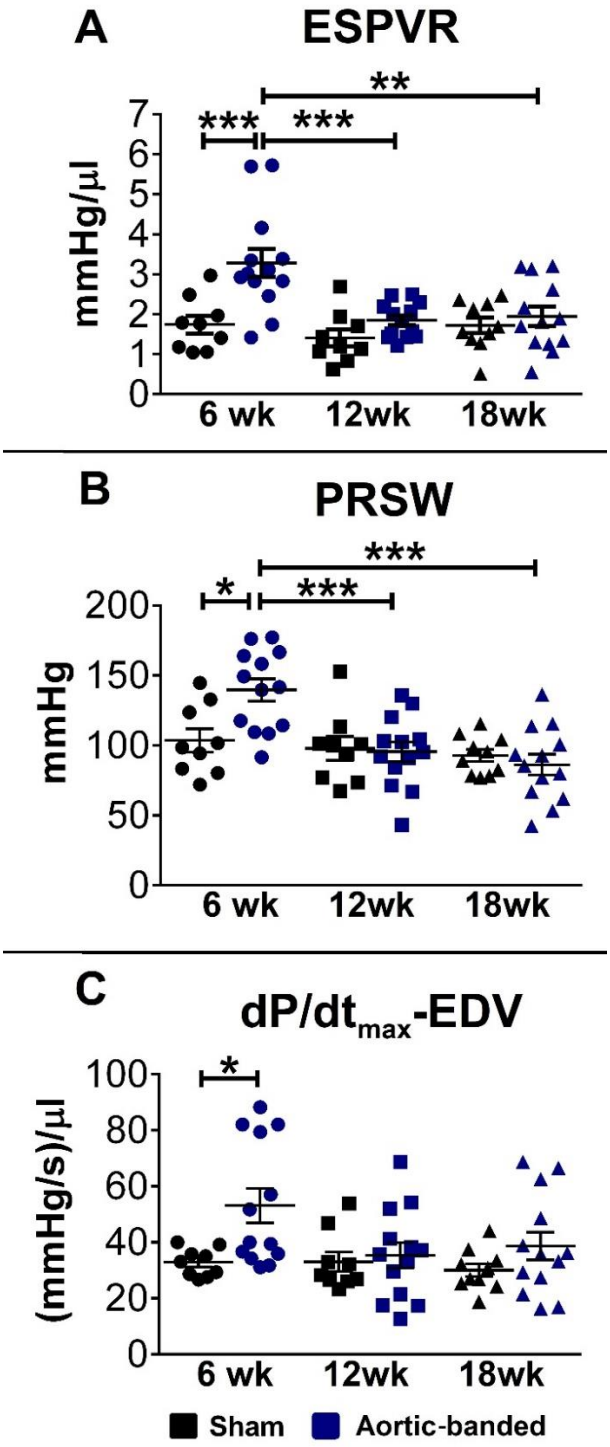

Figure 16. Left ventricular contractility parameters during the development and progression of pressure overload-induced left ventricular myocardial hypertrophy. Both the slope of the end-systolic pressure-volume relationship (ESPVR) (**A**), preload recruitable stroke work (PRSW) (**B**) and the slope of the maximal systolic pressure increment (dP/dt_{max})-end diastolic volume (EDV) relationship (**C**) were increased in the aortic banded (AB) group at week 6 compared to the corresponding sham group, suggesting enhanced left ventricular contractility. This contractility augmentation diminished in the AB groups at week 12 and 18. *: $P<0.05$. **: $P<0.01$. ***: $P<0.001$.

5.1.3.4. Ventricular-arterial coupling

In the AB-wk6 group, the enhanced LV contractility (increased ESPVR) (**Fig. 13 and Fig. 16**) counterbalanced the elevated afterload (increased Ea) (**Table 5**), therefore VAC did not differ from the corresponding sham group (**Table 5**). In contrast, in the AB-wk12 and AB-wk18 groups, the lack of compensatory LV contractility augmentation (reduced ESPVR values compared to AB-wk6) along with the elevated afterload (increased Ea) resulted in contractility-afterload mismatch. Thus, the values of VAC were significantly higher in the AB-wk12 and AB-wk18 groups compared to that of the AB-wk6 group (**Table 5**).

5.1.3.5. Diastolic parameters

Tau significantly increased in the AB-wk6, AB-wk12 and AB-wk18 groups compared to their corresponding sham groups (**Table 5**). Furthermore, the slope of EDPVR was also elevated in the AB-wk18 group compared to the sham-wk18 group (**Table 5**).

Table 5. Arterial elastance, ventriculo-arterial coupling and indices of diastolic function in aortic banded and sham-operated rats at different time points. Values are expressed as mean ± standard error of the mean. AB indicates aortic banding; E_a: arterial elastance, VAC: ventriculo-arterial coupling Tau: time constant of LV pressure decay according to the Glantz' method; EDPVR: end-diastolic pressure-volume relationship; *: P<0.05 vs. age-matched sham. **: P<0.01 vs. age-matched sham. ***: P<0.001 vs. age-matched sham. #: P<0.05 vs. AB-week 6. ##: P<0.01 vs. AB-week 6. ###: P<0.001 AB-week 6.

	Week 6		**Week 12**		**Week 18**	
	Sham (n=9)	***AB*** (n=13)	***Sham*** (n=9)	***AB*** (n=13)	***Sham*** (n=10)	***AB*** (n=13)
E_a, mmHg/µl	0.75±0.06	1.20±0.08*	0.68±0.05	1.33±0.10***	0.84±0.05	1.54±0.16***
VAC	0.50±0.08	0.45±0.06	0.54±0.06	0.76±0.08##	0.57±0.10	0.87±0.08###
Tau, ms	14.2±0.4	18.4±0.9**	12.8±0.6	19.4±0. 6***	13.0±0.3	21.7±1.2***#
EDPVR, mmHg/µl	0.038±0.005	0.038±0.007	0.028±0.004	0.042±0.006	0.014±0.003	0.032±0.004**

5.2. Investigating the effects of myocardial reverse remodeling from early- versus late-stage left ventricular hypertrophy in male rats

5.2.1. Effect of early and late debanding on echocardiographic parameters

In the AB groups, sustained PO led to continuous increment in LV mass, AWTd and PWTd **(Fig. 17-18).** Both early and late debanding resulted in significant regression of the previously increased LV mass, AWTd and PWTd (**Fig. 17-18**). To assess the extent of hypertrophy regression in the early- and in the late debanded groups, a ratio was calculated from the parameters measured at the post-debanding and the pre-debanding state. These calculated values were used to compare the effectiveness of reverse remodeling between the early and the late debanded groups. No difference was found in the extent of LV mass (**Fig. 19A**), AWTd (**Fig. 19B**) and PWTd (**Fig. 19C**) regression between the early and late debanded groups.

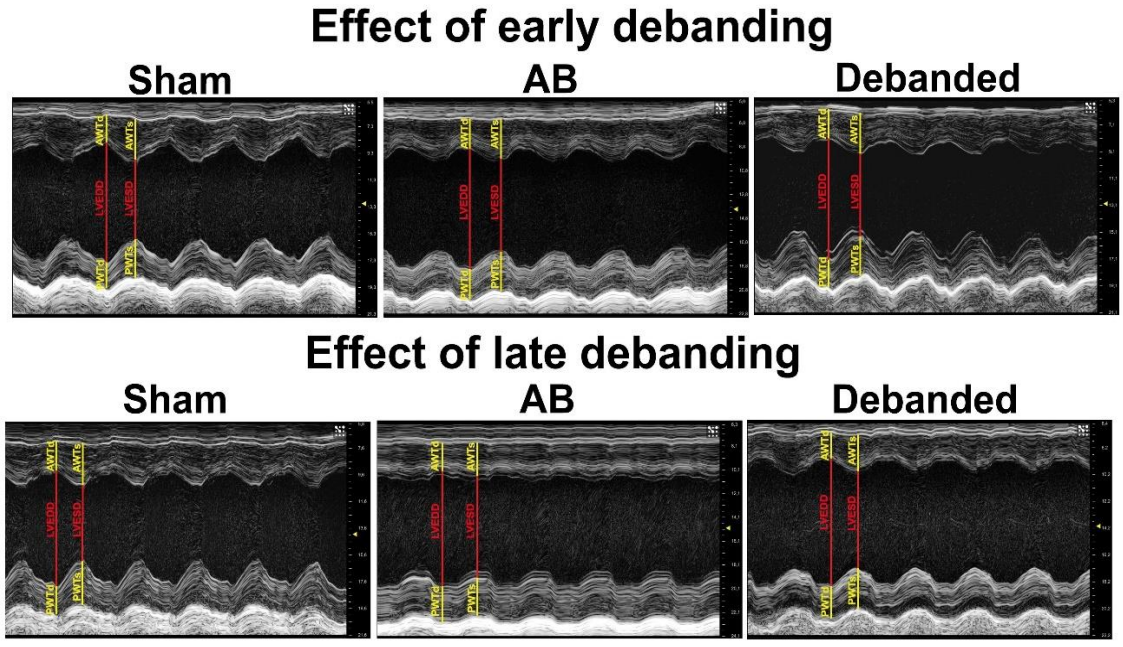

Figure 17. Representative echocardiographic images during the development of pressure overload-induced left ventricular myocardial hypertrophy and its regression after early and late debanding. Characteristic M-mode echocardiographic recordings at the midpapillary muscle level are shown at week 12 (in case of early debanding) and at week 18 (in case of late debanding) in the sham, the aortic banded (AB) and the debanded groups. Myocardial hypertrophy effectively regressed after early and late debanding as well. AWT: anterior wall thickness, PWT: posterior wall thickness, LVEDD: left ventricular (LV) end-diastolic diameter, LVESD: LV end-systolic diameter, s: systole, d: diastole.

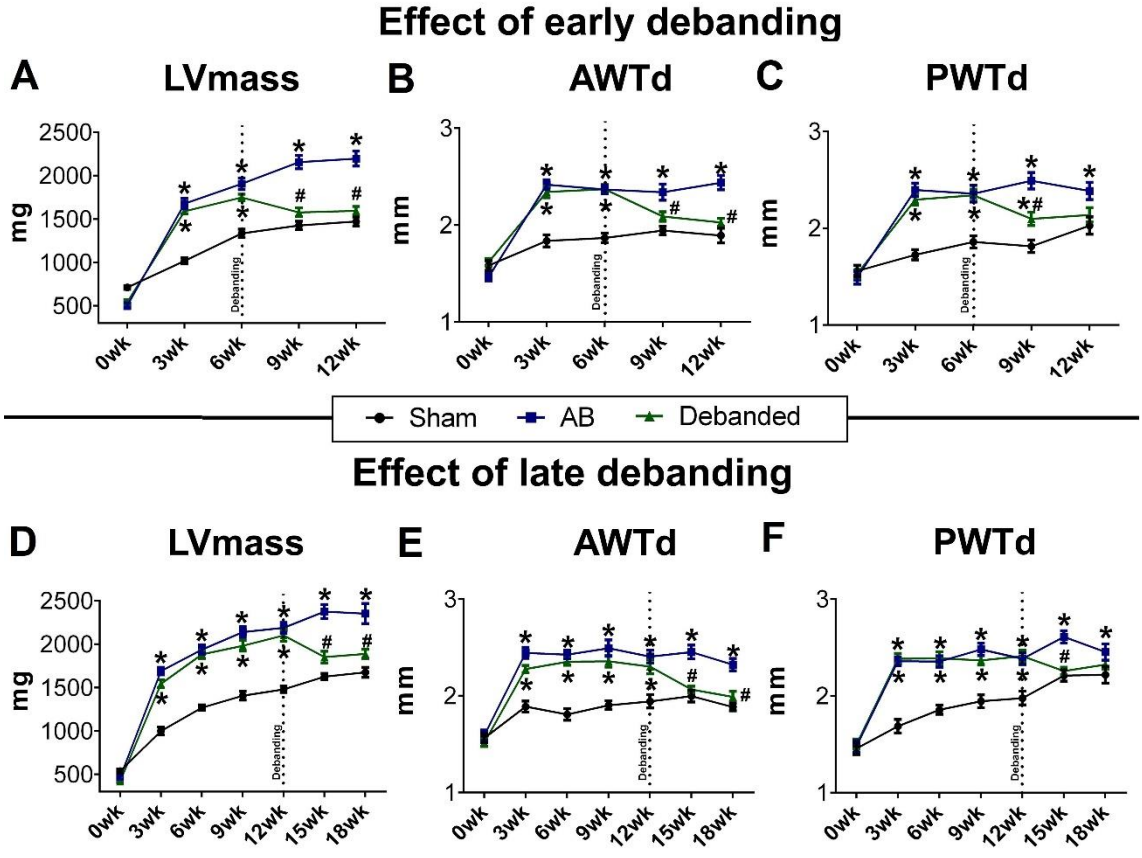

Figure 18. Echocardiographic follow-up during myocardial reverse remodeling from early- and late-stage of pathological myocardial hypertrophy. Both in the early and in the late debanded groups**,** left ventricular (LV) mass (LVmass) (**A, D**), anterior wall thickness measured in diastole (AWTd) (**B, E**) and posterior wall thickness measured in diastole (PWTd) (**C, F**) effectively regressed after pressure unloading. AB indicates aortic banded. *: P <0.05 vs. age-matched sham. #: P<0.05 vs. age-matched AB.

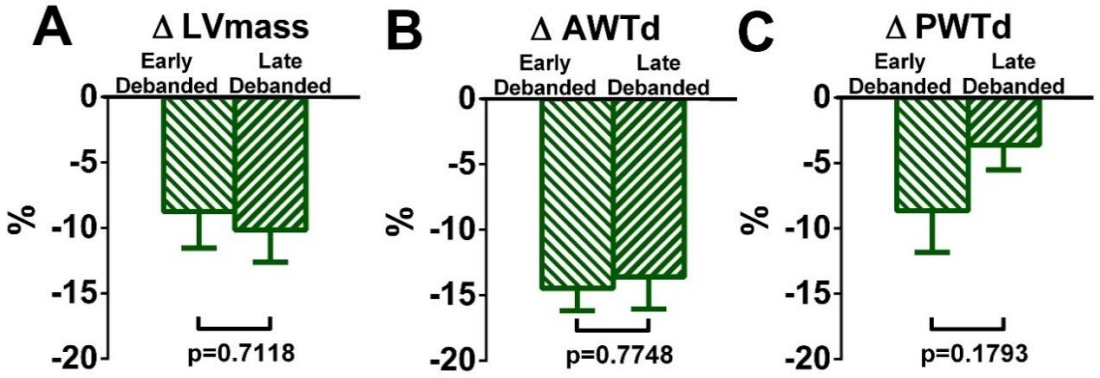

Figure 19. Direct comparison of left ventricular hypertrophy regression between the early and the late debanded groups. Left ventricular mass (LVmass) (**A**), anterior wall thickness in diastole (AWTd) (**B**) and posterior wall thickness in diastole (PWTd) (**C**) regressed to a similar extent in the early and the late debanding groups.

5.2.2. Effect of early and late debanding on pathological hypertrophy markers

In the AB groups CD, HW/TL and the expression of the fetal genes (β/α-MHC and ANP) were increased compared to the age-matched control groups (**Fig. 20-22**).

Both in the early and in the late debanded groups, CD, HW/TL and the expression of the fetal genes (β/α-MHC and ANP) were decreased compared to the age-matched AB groups (**Fig. 20A, C, Fig. 21 and Fig. 22A, C**). Regarding CD (**Fig. 20B**), HW/TL (**Fig. 20D**) and β/α-MHC (**Fig. 22B**), no differences could be detected in the extent of regression between the early- and the late debanded groups. However, the relative mRNA expression level of ANP decreased to a greater extent in the early debanded compared to the late debanded group (**Fig. 22D**).

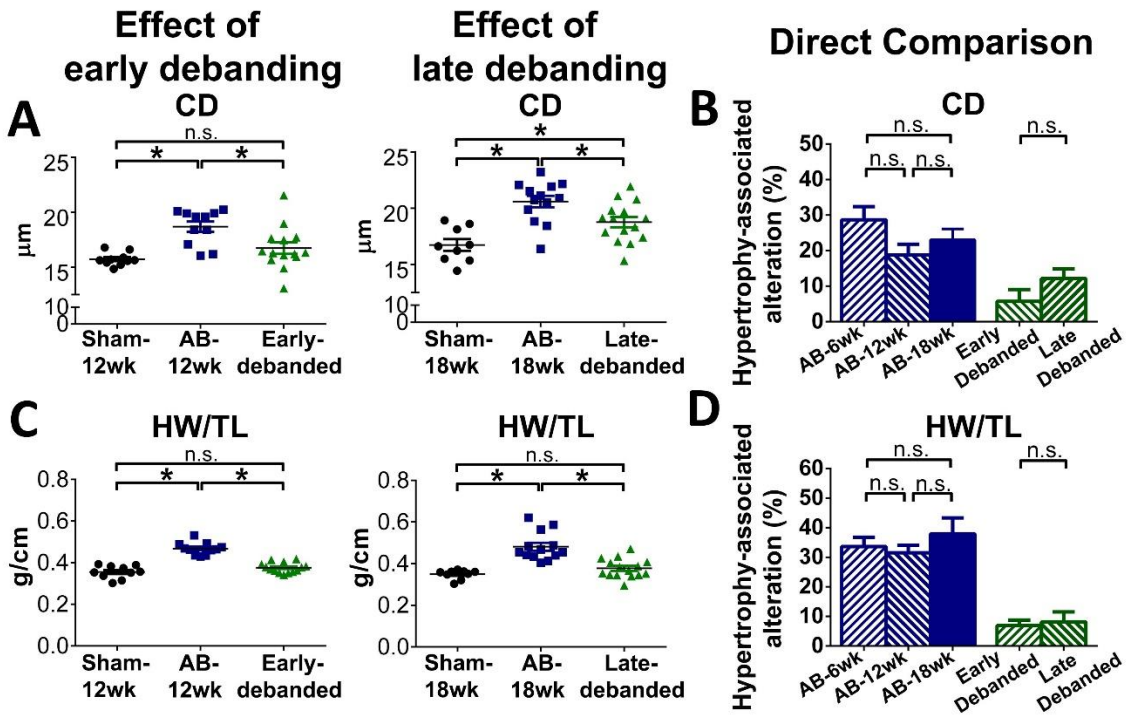

Figure 20. Effect of early and late debanding on macroscopic and microscopic myocardial hypertrophy markers.: Cardiomyocyte diameter (CD) and heart weigth-to-tibial length ratio (HW/TL) were increased in the aortic banded (AB) groups at week 12 and 18 compared to their age-matched sham groups. Both early and late debanding resulted in substantial decrement of CD and HW/TL (**A, C**). No differences could be observed in the extent of CD and HW/TL regression between the early and the late debanded groups (**B, D**). *: P<0.05.

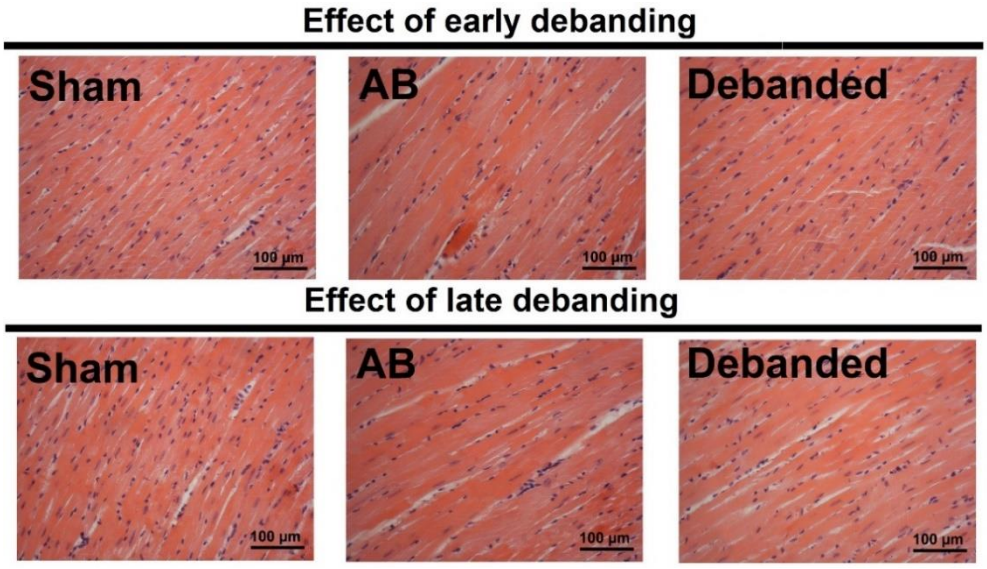

Figure 21. Representative microphotographs demonstrating enlargement of cardiomyocytes in the aortic banded (AB) groups and their regression in both the early and late debanded groups: Hematoxylin and eosin (magnification 200x, scale bar: 100µm) stained sections are shown. AB indicates aortic banding.

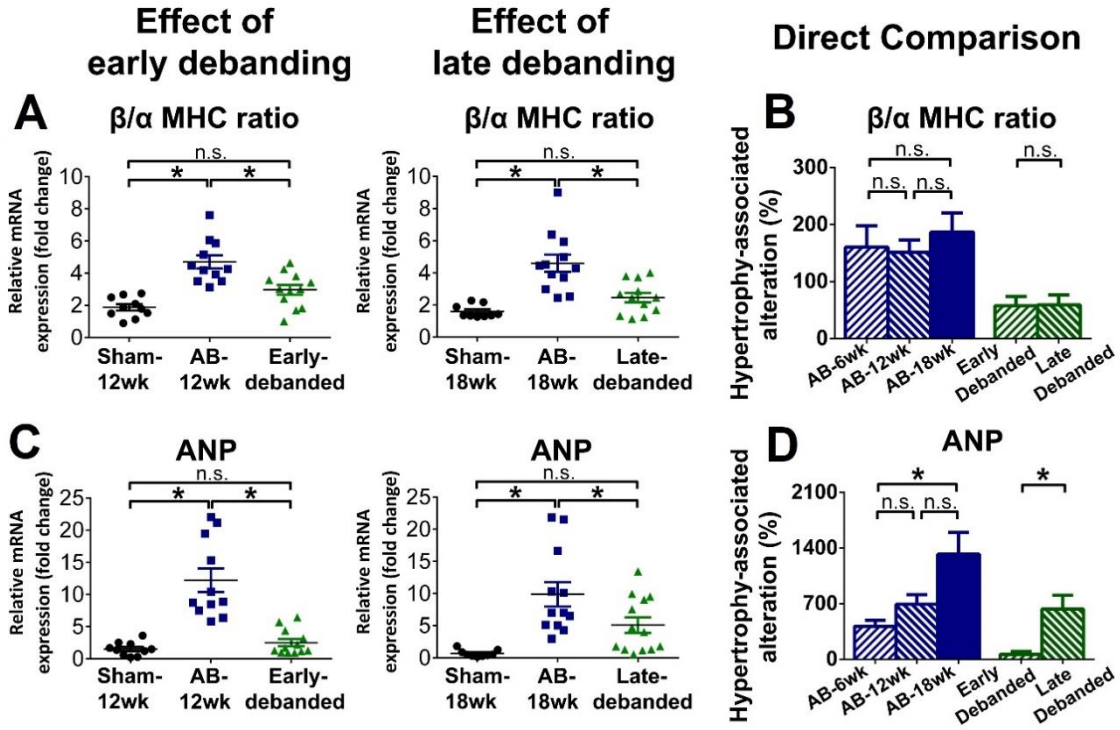

Figure 22. Fetal gene expression during pressure unloading-evoked reverse remodeling. Beta-to-alpha myosin heavy chain ratio (β/α-MHC) and atrial natriuretic peptide (ANP) were increased in the aortic banded (AB) groups at week 12 and 18 compared to the sham groups. Both early and late debanding resulted in substantial decrement of β/α-MHC and HW/TL (**A, C**). Although, β/α-MHC showed similar extent of regression in the debanded groups (**B**), ANP normalized to a greater extent in the early debanding compared to the late debanded group (**D**). *: P<0.05.

5.2.3. Effect of early and late debanding on reactive myocardial fibrosis

In the early debanded group, interstitial and perivascular fibrosis decreased compared to the age-matched AB group (**Fig. 23A, C and Fig. 24**). However, in the late debanded group, interstitial and perivascular fibrosis remained increased, and it did not differ from the age-matched AB group (**Fig. 23A, C and Fig. 24**). Accordingly, the extent of both interstitial and perivascular fibrosis showed significantly higher levels in the late debanded group compared to the early debanded group (**Fig.23B, D**).

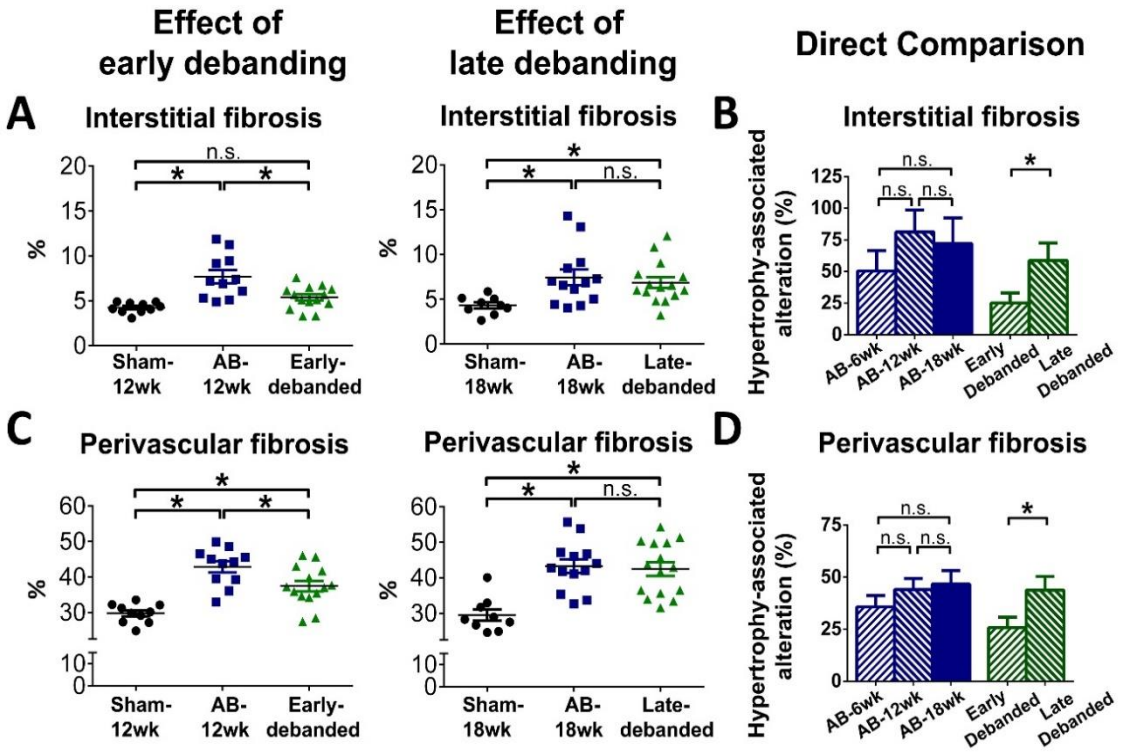

Figure 23. Regression of interstitial and perivascular fibrosis after pressure unloading at different time points. Increased interstitial and perivascular fibrosis were observed in the aortic banded (AB) groups at week 12 and 18. Regression of reactive interstitial and perivascular fibrosis could be detected only in the early debanded group, while the collagen accumulation persisted in the late debanding group (**A, C**). Accordingly, robust differences were observed in interstitial and perivascular fibrosis between the two debanded groups (**B, D**). *: P<0.05.

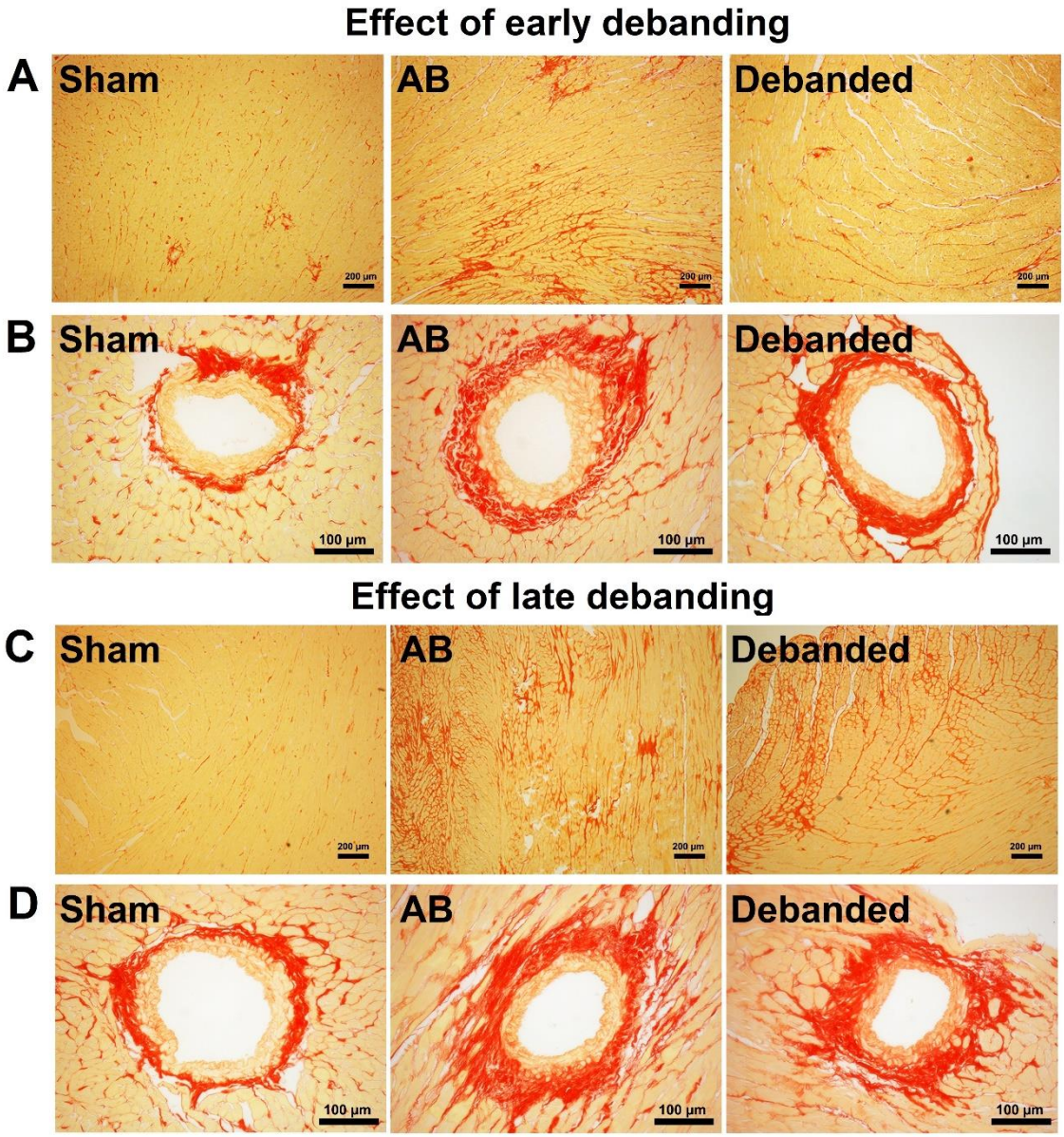

Figure 24. Representative histological photomicrographs of interstitial and perivascular fibrosis demonstrating regression of reactive fibrosis in the early debanded group and persisting collagen accumulation in the late debanded group. Representative photomicrographs of picrosirius red staining are shown demonstrating interstitial fibrosis (**A, C**) (magnification 50x, scale bar: 200µm) and perivascular fibrosis (**B, D**) (magnification 100x, scale bar: 100µm). AB: aortic banding.

In the AB groups increased mRNA levels of CTGF were detected (**Fig. 25A**). The protein level of CTGF showed a strong tendency towards increased values in the AB-wk12 group compared to the age-matched sham group. Furthermore, in the AB-wk18 groups, the protein level of CTGF was significantly increased compared to the corresponding sham group (**Fig. 25C**). The enhanced expressional (mRNA and protein)

level of CTGF was normalized in both the early and the late debanding groups (**Fig. 25A, C**). No differences could be observed in the extent of CTGF regression between the two debanded groups (**Fig. 25B, D**).

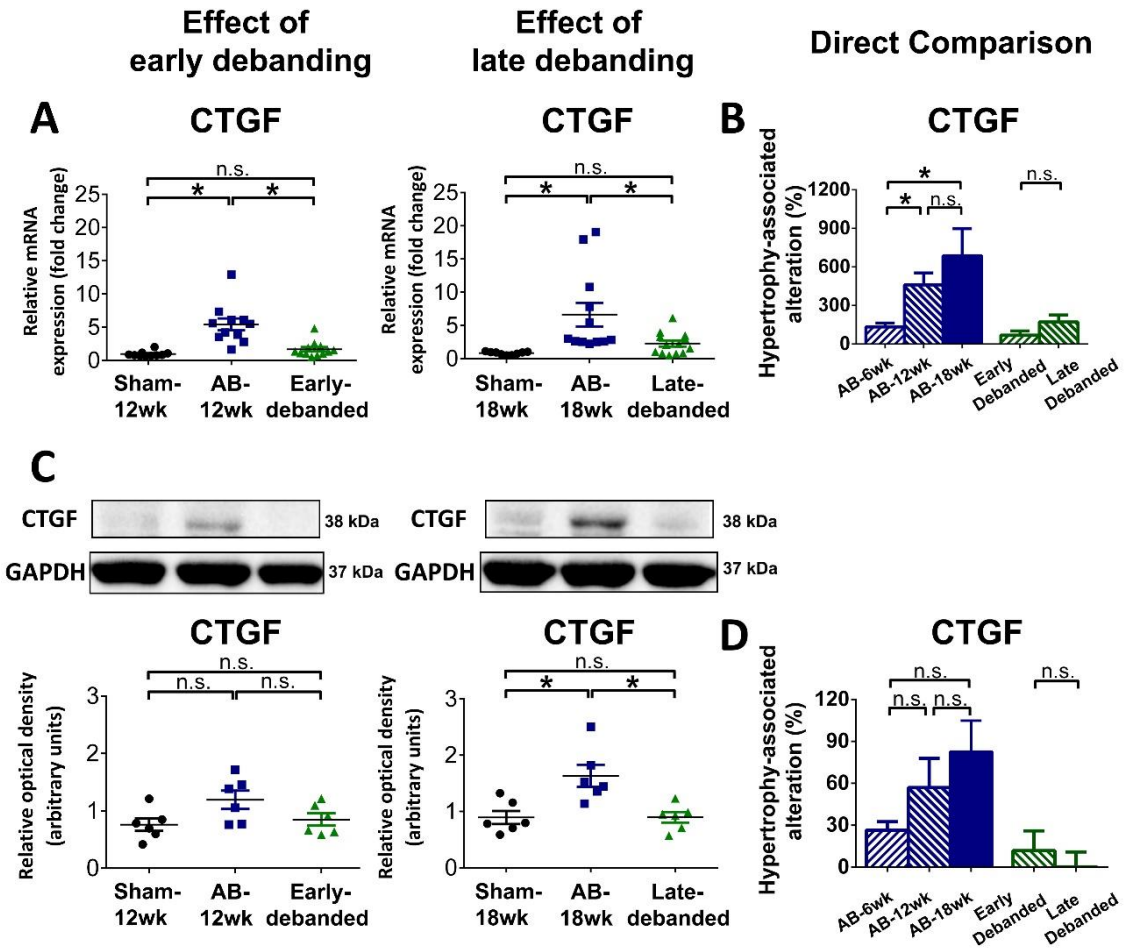

Figure 25. Effect of early and late debanding on connective tissue growth factor (CTGF) mRNA and protein expression. CTGF mRNA expression was increased in the aortic banded groups at week 12 and 18 (**A**). Furthermore, protein expression of CTGF was also significantly higher in the AB-wk18 group compared to its corresponding sham group (**C**). Both early and late debanding effectively normalized the AB-associated alterations in CTGF mRNA and protein expression (**A, C**). No differences could be observed in the extent of CTGF normalization in the early and late debanding groups (**B, D**) GAPDH: glyceraldehyde 3-phosphate dehydrogenase. *: P<0.05.

5.2.4. Effect of early and late debanding on hemodynamic parameters

5.2.4.1. Arterial loading and meridional wall stress

In the AB groups SBP, DBP, MAP and σ were increased compared to the age-matched sham groups (**Table 6**). The extent of SBP, DBP and MAP increment was equal between

the AB groups at different time points (**Table 7**). However, σ increased to a significantly greater degree in the AB-wk12 and AB-wk18 groups compared to the AB-wk6 group (**Table 7**). In the early and late debanded groups, SBP, DBP, MAP and σ were decreased compared to the age-matched AB groups (**Table 6**). The extent of afterload and wall stress reduction did not differ between the two debanded groups (**Table 7**).

5.2.4.2. Load-dependent systolic parameters

In the AB-wk12 and AB-wk18 groups, EF was significantly reduced, while SV and CO showed a tendency towards decreased values when compared to their age-matched control groups (**Table 6, Fig. 26A and Fig. 27**). Both in the early and in the late debanded groups, EF, SV and CO were increased compared to the age-matched AB groups (**Table 6, Fig. 26A and Fig. 27**). No differences were found regarding the extent of EF, SV and CO improvement between the early and late debanded groups (**Table 7, Fig.26B and Fig. 27**).

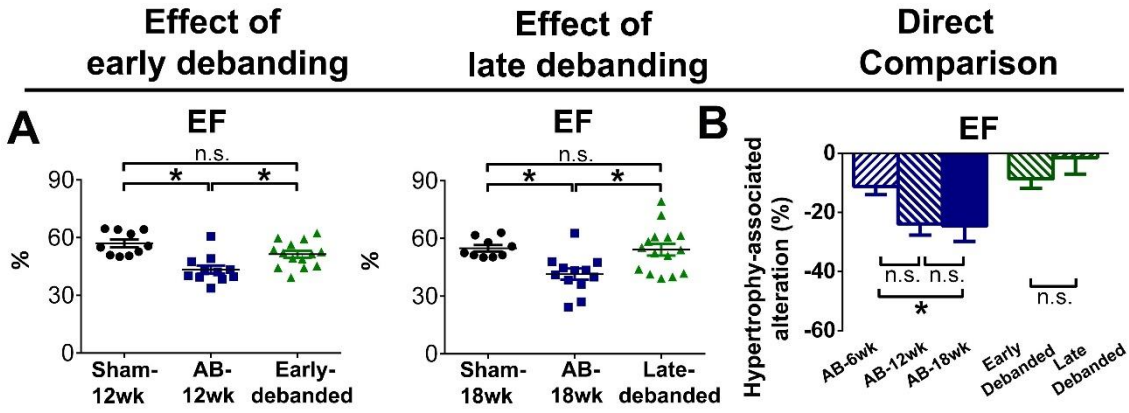

Figure 26. ***Changes in ejection fraction (EF) during the development of pathological myocardial hypertrophy and its regression by early and late debanding.*** Both the early debanding and the late debanding groups were associated with increased EF (**A**). The extent of EF improvement was similar between the two debanded groups AB indicates aortic banding. *: P<0.05.

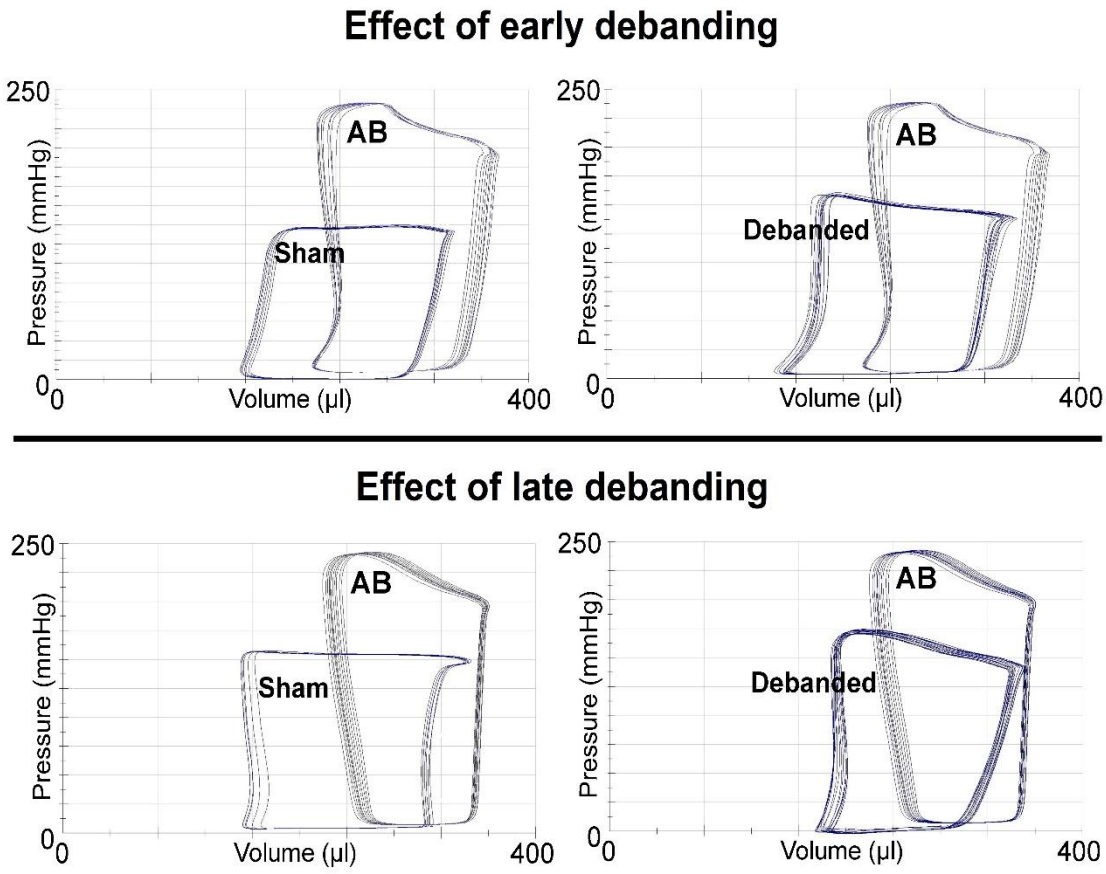

Figure 27. Representative left ventricular (LV) pressure-volume (P-V) steady-state loops demonstrating the effect of early and late debanding on left ventricular function*. In the aortic banded (AB) groups at week 12 and 18, the width of the loops was substantially smaller compared to the corresponding age-matched sham groups, suggesting impaired LV systolic function. Both early and late debanding effectively increased the width of the P-V loops, indicating that pressure unloading therapy performed either at early or late time points successfully improved LV systolic performance.*

Table 6. Hemodynamic parameters in the aortic banded (AB) groups at different time points and in the early and the late debanded groups. Values are expressed as mean ± standard error of the mean. AB indicates aortic banding; SBP: systolic arterial blood pressure; DBP: diastolic arterial blood pressure; MAP: mean arterial pressure; σ: meridional wall stress, HR: heart rate; dP/dt_{max}: maximal slope of systolic pressure increment; dP/dt_{min}: maximal slope of diastolic pressure decrement; LVEDP: left ventricular (LV) end-diastolic pressure; LVESP: LV end-systolic pressure; LVEDV: LV end-diastolic volume; LVESV: LV end-systolic volume; SV: stroke volume; CO: cardiac output. *: P<0.05 vs. age-matched Sham, #: P<0.05 vs. age-matched AB.

	12 week			**18 week**		
	Sham (n=10)	***AB*** (n=11)	***Early debanded*** (n=14)	***Sham*** (n=9)	***AB*** (n=12)	***Late debanded*** (n=15)
SBP, mmHg	139±4	214±5*****	169±3***#**	152±5	226±5*	181±4***#**
DBP, mmHg	110±3	154±5*****	127±3***#**	121±4	167±4*	134±2***#**
MAP, mmHg	120±4	174±4*****	141±3***#**	132±4	187±4*	150±3***#**
σ, kdyn/cm^2	13.9±0.3	27.8±1.6*****	18.3±1.1***#**	18.9±0.8	37.9±2.0*****	25.4±1.5***#**
HR, beats/min	356±6	365±7	357±7	381±7.5	359±4.7*****	351±5.1*****
dP/dt_{max}, mmHg/s	8291±353	10579±436*****	9467±483	9670±359	11062±505	9522±267**#**
dP/dt_{min}, mmHg/s	-9220±313	-9633±277	-9887±563	-10266±328	-8838±437*****	-8907±237*****
LVEDP, mmHg	4.0±0.4	7.1±0.9*****	5.3±0.7	5.4±0.4	7.8±1.0*****	5.8±0.4
LVESP, mmHg	133±3	202±4*****	161±4***#**	147±5	209±5*****	168±5***#**
LVEDV, µl	340±19	357±18	340±16	329±19	372±19	362±13
LVESV, µl	148±13	201±11*****	166±10	150±10	216±12*****	166±13**#**
SV, µl	192±10	156±12	174±10	178±11	156±17	196±14
CO, ml/min	68.6±4.1	56.7±4.3	61.4±3.0	68.3±4.4	55.9±5.8	68.8±5.0

Table 7. Comparison of pressure overload-induced alterations in the aortic banded groups at different time points and during myocardial reverse remodeling after early and late debanding. The values of the aortic banded (AB) and the debanded groups were normalized to the corresponding sham groups. These calculated values are expressed as mean ± standard error of the mean. SBP indicates systolic arterial blood pressure; DBP: diastolic arterial blood pressure; MAP: mean arterial pressure; Ea: arterial elastance, σ: meridional wall stress, LVEDP: left ventricular end-diastolic pressure; LVESP: LV end-systolic pressure; LVEDV: LV end-diastolic volume; LVESV: LV end-systolic volume; SV: stroke volume; CO: cardiac output. *: P<0.05 vs. age-matched Sham.

	AB			**Debanded**		
	6 wk *(n=10)*	***12 wk*** *(n=11)*	***18 wk*** *(n=12)*	***Early*** *(n=14)*	***Late*** *(n=15)*	***P value (early verus late debanded)***
ΔSBP, %	50±3	55±4	49±3	21±2	19±3	0.53
ΔDBP, %	32±2	39±4	38±3	14±3	11±2	0.38
ΔMAP, %	39±2	45±4	42±3	17±3	14±2	0.40
Δσ, %	33±11	100±12*	101±11*	31±8	36±8	0.65
ΔLVEDP, %	51±21	79±23	46±19	31±16	9±7	0.21
ΔLVESP, %	52±4	53±3	43±3	22±3	15±3	0.10
ΔLVEDV, %	7±6	5±5	13±6	1±5	10±4	0.13
ΔLVESV, %	23±8	35±7	44±8	11±7	11±8	0.98
ΔSV, %	-5±6	-19±6	-13±9	-8±5	10±8	0.07
ΔCO, %	-4±4	-17±6	-18±9	-8±5	1±7	0.31

5.2.5.3. Load-independent contractility parameters

In the AB-wk12 and AB-wk18 groups, neither ESPVR nor PRSW differed from their corresponding control groups (**Fig. 28, 29A, 30A**). Similarly, no alteration could be observed in ESPVR and PRSW after early or late debanding. (**Fig. 28, 29A, 30A**).

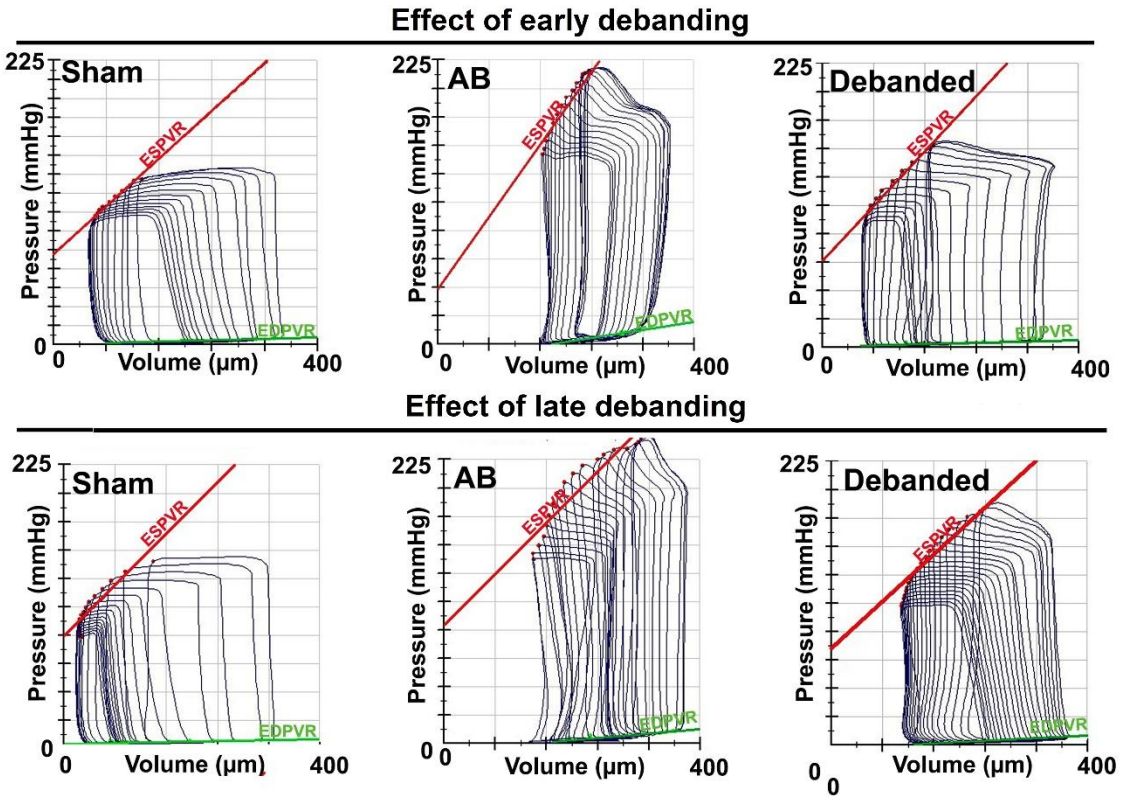

Figure 28. ***Representative pressure volume loops demonstrating characteristic alterations in the aortic banded (AB) groups and in the early and late debanded groups.*** Original recordings were obtained at different preloads during transient vena cava occlusion. The slope of end-systolic pressure volume relationship (ESPVR) did not differ among the study groups. In contrast, the slope of the end-diastolic pressure volume relationship (EDPVR) was increased in the AB groups, suggesting impaired myocardial stiffness. Increased EDPVR was normalized in the early debanded group, while it persisted in the late debanded group.

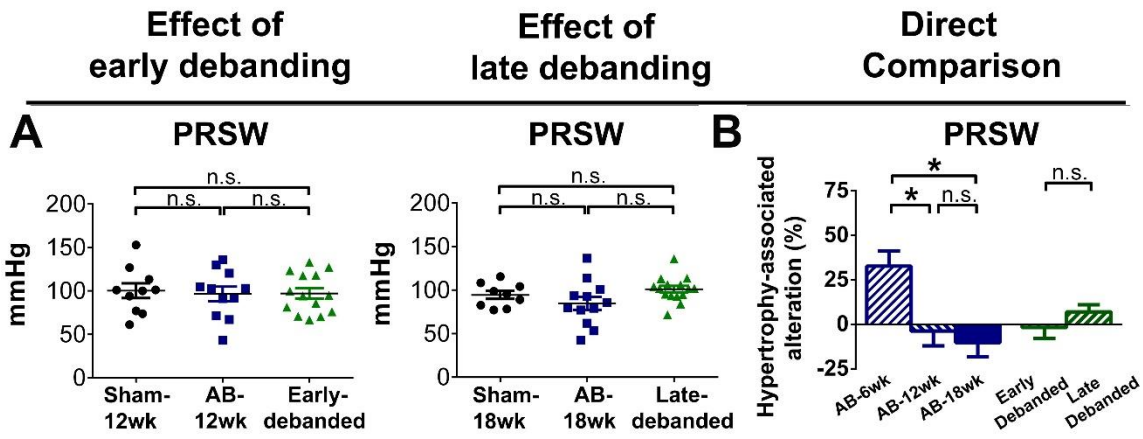

Figure 29. ***Alterations in preload recruitable stroke work (PRSW) after early and late debanding.*** PRSW did not differ in the aortic banded (AB) groups at week 12 and week 18 from the corresponding control groups (**A**). Similarly, no alterations could be detected in PRSW neither in the early nor in the late debanding groups (**A, B**). *: P<0.05.

5.2.5.4. Ventriculo-arterial coupling

In the AB-wk12 and AB-wk18 groups, ESPVR did not differ from the control groups (**Fig. 30A**). Therefore, at these time points, increased Ea (**Fig. 30C**) was not compensated by enhanced contractility, which led to impaired VAC (**Fig. 30E**). Both in the early- and in the late debanded groups, reduction of Ea efficiently normalized the relation of the LV contractility and the connecting arterial system and resulted in adequate VAC values (**Fig. 30E**). No differences could be observed in the extent of VAC normalization between the early and the late debanded groups (**Fig. 30F**).

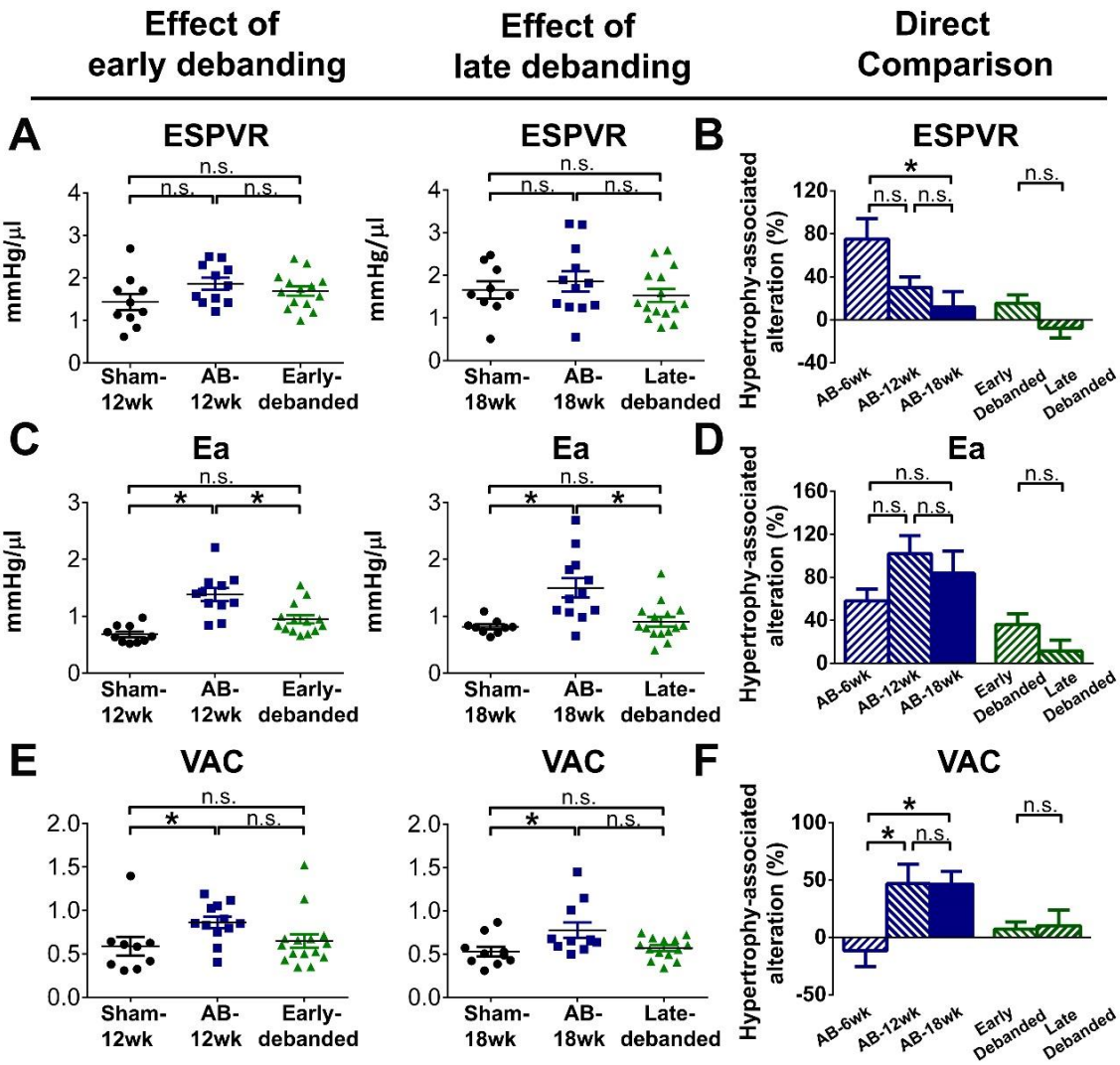

Figure 30. Ventriculo-arterial coupling (VAC) during the development of aortic banding (AB)-induced pathological myocardial hypertrophy and during its regression by early and late debanding. The slope of end-systolic pressure-volume relationship (ESPVR) did not differ among the study groups (**A-B**). In contrast arterial elastance (Ea) was significantly increased in the aortic banded (AB) groups at week 12 and 18 (**C**). Both early and late debanding effectively reduced the increased Ea (**C**). The extent of Ea normalization was similar between the two debanded groups (**D**). The lack of compensatory contractility augmentation led to impaired ventriculo-arterial coupling (VAC) in the AB groups at week 12 and 18. By decreasing Ea, both early and late debanding resulted in the normalization of VAC. No differences could be detected in the improvement of VAC between the early and the late debanded groups. *: P<0.05.

5.2.5.5. Diastolic parameters

Tau was prolonged in all the AB groups (**Fig. 31A**). Furthermore, the slope of EDPVR was also increased in AB groups at week 12 and 18 compared to sham (**Fig. 31C**). In the early debanded group, the prolonged active relaxation was effectively shortened, and Tau

did not differ from the control's level (**Fig. 31A**). In the late debanded group, Tau was also decreased compared to the age-matched AB group. However, the extent of improvement was smaller compared to the early debanded group and Tau remained significantly prolonged in the late debanded group when compared the control's level (**Fig. 31A-B**). Furthermore, in the early debanded group, LV stiffness was also decreased compared to the corresponding AB group (**Fig. 31C**). In contrast, no significant differences could be observed in EDPVR between the late debanded group and the AB-wk18 group (**Fig. 31C**). Therefore, the extent of improvement in LV stiffness was also significantly smaller in the late debanded group than that observed in the early debanded group (**Fig. 31D**).

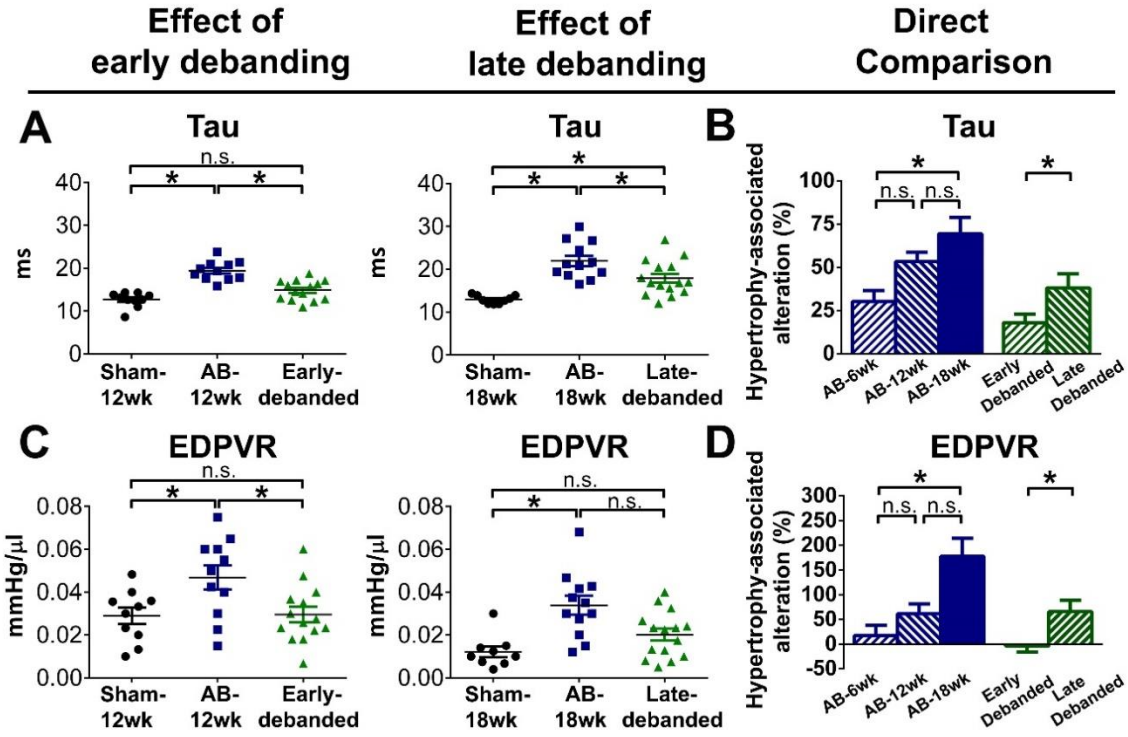

Figure 31. ***Diastolic function during the development of aortic banding (AB)-induced LVH and its regression by early and late debanding.*** Prolongation of the active relaxation time constant (Tau) and increased myocardial stiffness (assessed by the elevated slope of the end-diastolic pressure-volume relationship [EDPVR]) were detected in the AB groups at week 12 and 18 (**A, C**). Debanding the aortic constriction at an early time point effectively improved both aspects of diastolic function (**A, C**). In contrast, late debanding failed to normalize diastolic dysfunction. Accordingly, robust differences were observed between the early and the late debanding groups (**B, D**). *: P<0.05.

5.3. Investigation of sex differences during the development of pressure overload-induced left ventricular hypertrophy

5.3.1. Effect of sex on the temporal development of left ventricular hypertrophy

LV mass index was increased in both male and female AB rats from week 3 until the end of the experimental period (**Fig. 32 and Fig. 33A**). RWT revealed concentric LV geometry at week 6 in both male and female AB groups (**Fig 32 and Fig. 33C**). Concentric geometry was also observed in the female AB rats at week 12. However, at week 12, RWT substantially decreased in male rats, leading to eccentric LV geometry (**Fig. 33C**). Furthermore, reduction of EF was only observed in the male AB-wk12 group (**Fig. 33A**).

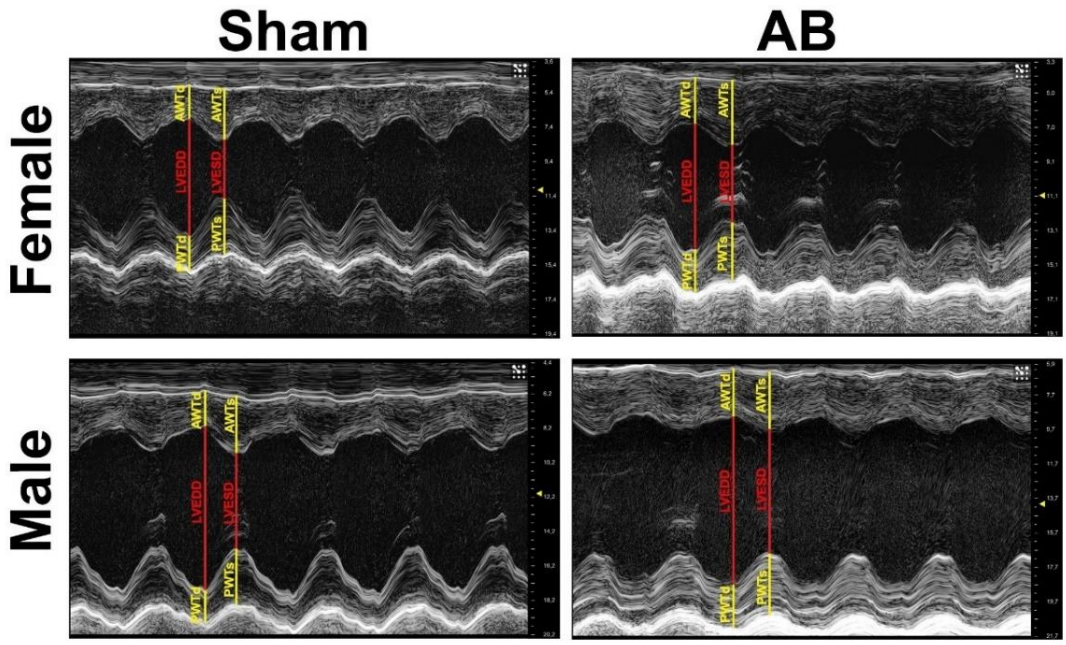

Figure 32. ***Representative echocardiographic recordings demonstrating sex-related differences in male and female aortic banded (AB) rats at week 12.*** The female AB was associated with increased left ventricular (LV) wall thicknesses, concentric geometry and maintained systolic function. In contrast the male AB was characterized by increased LV wall thicknesses, eccentric remodeling and decreased systolic function. AWT indicates anterior wall thickness, PWT: posterior wall thickness, LVEDD: left ventricular end-diastolic diameter, LVESD: left ventricular end-systolic diameter, s: systole, d: diastole.

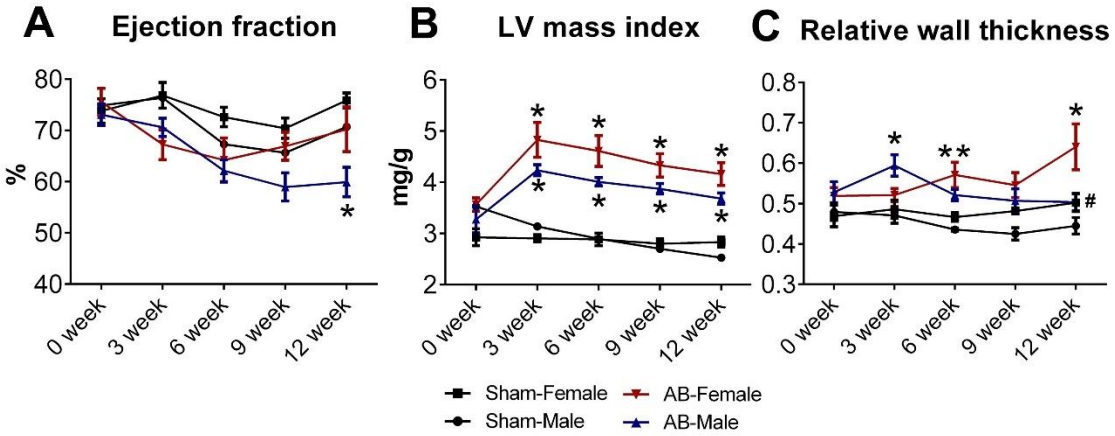

Figure 33. ***Echocardiographic follow-up during the development of pressure overload-induced myocardial hypertrophy in male and female rats.*** The female aortic banded (AB) group was associated with maintained ejection fraction (**A**), enhanced left ventricular (LV) mass index (**B**) and increased relative wall thickness (**C**) at both early (week 6) and later time points (week 12). The male AB group was also characterized by preserved ejection fraction (**A**), increased LV mass index (**B**) and increased relative wall thickness (**C**) at a relatively early time point (week 6). However, deterioration of ejection fraction (**A**) and decrement of relative wall thickness (**B**) took place in male AB rats at week 12, leading to substantial differences between the two sexes. *P < 0.05 vs. age and sex-matched sham. #: P<0.05 vs. female AB.

5.3.2. Sex differences in pathological hypertrophy and fibrosis markers

Week 6. At this early stage, HW/TL, CD, myocardial collagen area and CTGF mRNA levels were enhanced in both male and female AB rats compared to their age- and sex-matched sham groups (**Fig. 34-37**). The extent of hypertrophy and fibrosis was comparable between the two sexes at this early time point (**Table 8**).

Week 12. At this later stage, the hypertrophy and fibrosis markers were also increased in male and female AB rats compared to their sham groups (**Fig. 34-37**). However, the direct comparison of sexes revealed higher increments in HW/TL and CD in females compared to males (**Table 8**). In contrast, fibrosis showed significant progression from week 6 to week 12 only in male AB rats (**Fig. 35 and Fig. 37**). Furthermore, the extent of AB-associated increment in CTGF expression was also significantly higher in males compared to females (**Table 8**).

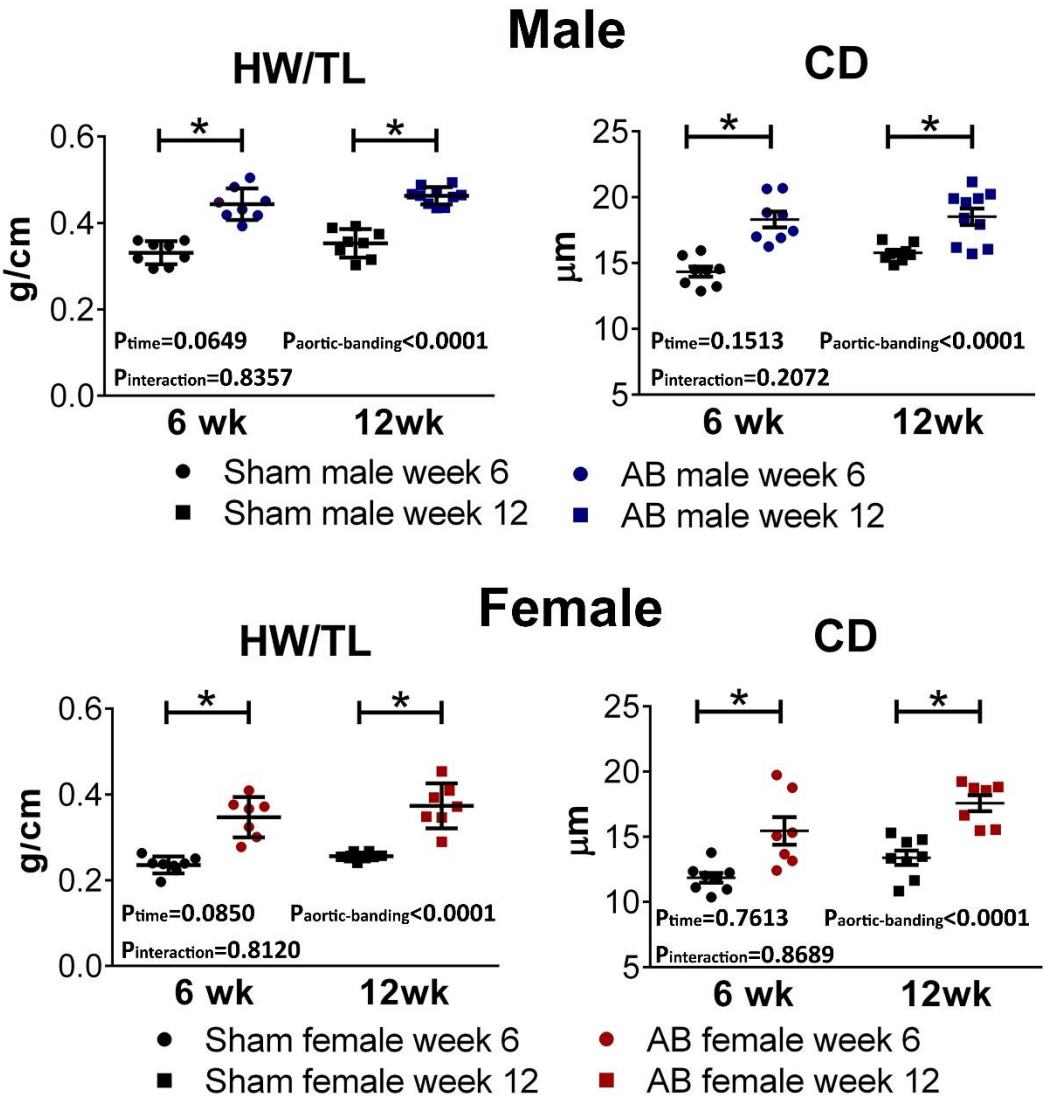

Figure 34. The effect of sex on myocardial hypertrophy markers. Heart weight-to-tibial length (HW/TL) and cardiomyocyte diameter (CD) were increased in male and female aortic banded (AB) rats at week 6 and 12 as well. *: P<0.05.

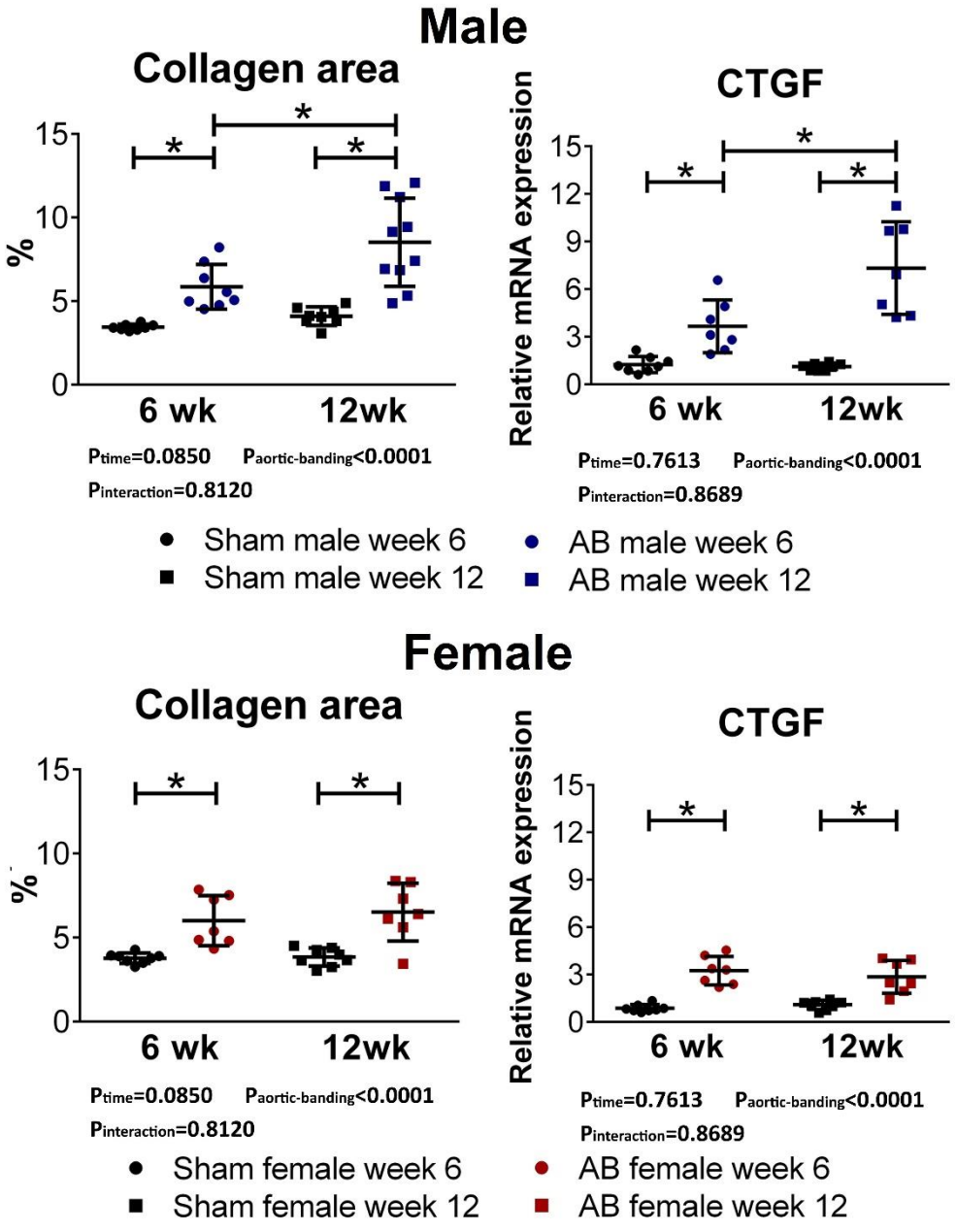

Figure 35. The effect of sex on fibrosis markers. Collagen area and mRNA level of connective tissue growth factor (CTGF) were increased in male and female aortic banded (AB) rats at week 6 and 12 as well when compared to their age-matched sham groups. Furthermore, fibrosis showed significant progression from week 6 to week 12 in male AB rats, while in female AB rats the collagen area and CTGF expression was comparable at week 6 and week 12. *: P<0.05.

Table 8. Comparison of pressure overload-induced morphological, ultrastructural and molecular alterations in the aortic banded groups in male and female rats at different time points. The values of the aortic banded groups were normalized to the corresponding sham groups. These calculated values are expressed as mean ± standard error of the mean. LV indicates left ventricle; RWT: relative wall thickness; HW/TL: heart weight-to-tibial length; CD: cardiomyocyte diameter; CTGF: connective tissue growth factor.

	6 week			**12 week**		
	Male *(n=8)*	***Female*** *(n=7)*	***P value (male vs. female)***	***Male*** *(n=10)*	***Female*** *(n=7)*	***P value (male vs. female)***
ΔLV mass index, %	49±5	47±12	0.90	46±4	47±8	0.88
ΔRWT, %	27±4	29±11	0.84	13±5	28±11	0.21
ΔHW/TL, %	34±4	47±8	0.13	31±2	46±8	<0.05
ΔCD, %	28±4	30±9	0.78	17±4	31±5	0.04
ΔFibrosis area, %	70±15	59±15	0.60	108±20	69±17	0.19
ΔCTGF, %	193±50	272±39	0.24	557±99	162±36	<0.01

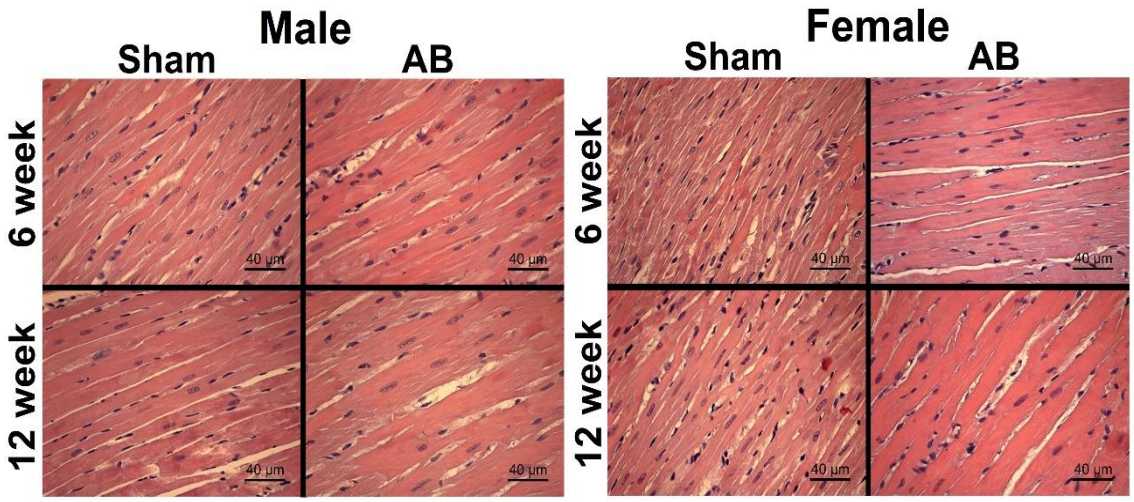

Figure 36. Representative photomicrographs demonstrating enlargement of cardiomyocytes in the aortic banded (AB) male and female groups at week 6 and 12. Hematoxylin and eosin (magnification 200x, scale bar: 40 µm)-stained sections are shown. AB indicates aortic banding.

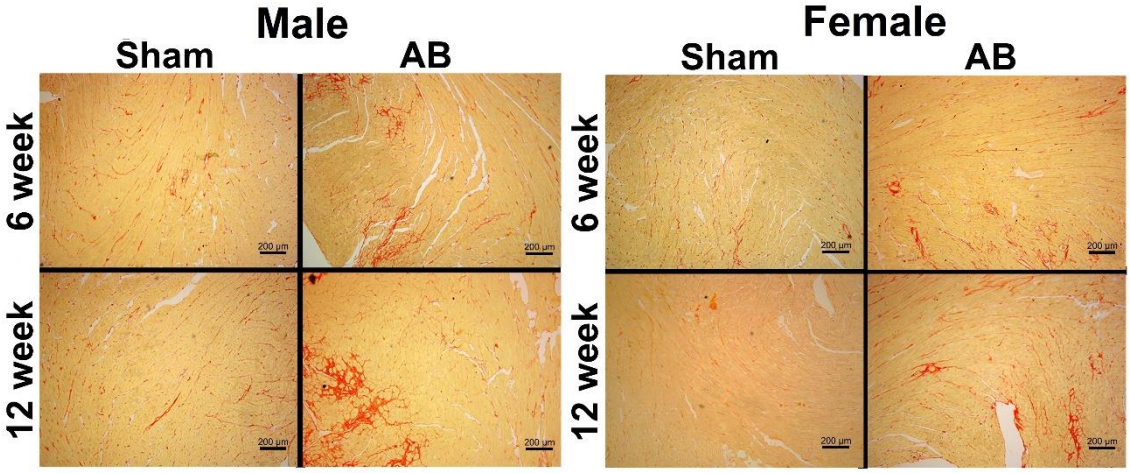

Figure 37. Representative histological photomicrographs demonstrating enhanced interstitial fibrosis in male and female aortic banded (AB) rats. Picrosirius red-stained sections (magnification 50x, scale bar: 200 µm) are shown. Collagen accumulation (indicated by the red area) was observed in both male and female AB rats at week 6. Furthermore, fibrosis was progressed to a greater extent in male but not in female AB rats at week 12.

5.3.2. Characteristic sex-related functional differences

5.3.2.1. Arterial loading

At week 6 and 12, in both male and female AB rats increased SBP, DBP and MAP confirmed the presence of increased afterload (**Table 9**).

5.3.2.2. Load-dependent systolic parameters

Week 6. After 6 weeks of sustained PO, the AB groups were associated with preserved EF in both genders (**Fig. 38 and Table 9**.) Furthermore, in female AB rats, SV and CO were slightly increased compared to the corresponding control group (**Table 9**).

Week 12. At week 12, reduced EF was confirmed in the male AB group (**Fig. 38 and Table 9**). In contrast, the values of EF did not differ from the corresponding sham group in female AB animals. The different alterations in EF resulted in significant difference between the two genders (**Table 10**). Furthermore, the parameters of SV and CO showed also a tendency towards decreased values in the male AB group, while these tendencies could not be observed among female animals (**Table 9**).

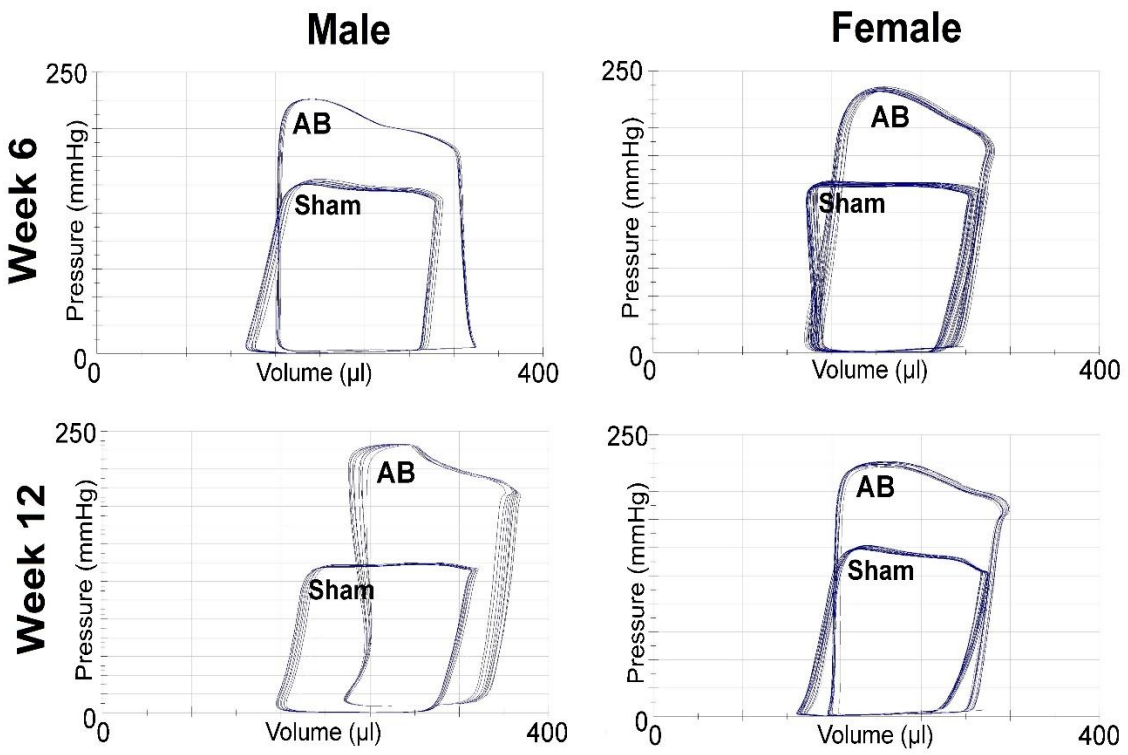

Figure 38. Representative steady-state pressure-volume (P-V) loops in male and female aortic banded and sham rats at different time points. photomicrographs demonstrating enhanced interstitial fibrosis in male and female aortic banded (AB) rats. The width of the P-V loops in the male and female AB groups at week 6 was similar to the controls', indicating preserved systolic function. In contrast, the width of the P-V loops was smaller in the male AB group compared to the male sham group at week 12, suggesting deterioration of systolic performance. In contrast to males, the width of the P-V loops in females remained at the control's level at week 12, despite of the aortic banding.

Table 9. Hemodynamic parameters in male and female rats 6 and 12 weeks after aortic banding or sham operation. Values are expressed as mean ± standard error of the mean. AB indicates aortic banding; SBP: systolic arterial blood pressure; DBP: diastolic arterial blood pressure; MAP: mean arterial pressure; HR: heart rate; dP/dt_{max}: maximal slope of systolic pressure increment; $dP/dt_{min:}$ maximal slope of diastolic pressure decrement; LVESP: left ventricular end-systolic pressure; LVEDP: LV end-diastolic pressure; LVEDV: LV end-diastolic volume; LVESV: LV end-systolic volume; SV: stroke volume; EF: ejection fraction; CO: cardiac output; Tau: time constant of LV pressure decay according to the Glantz' method; EDPVR: end-diastolic pressure-volume relationship. *: P<0.05 vs. age-matched Sham. #: P<0.05 vs. AB-wk6.

	Male				**Female**			
	6 week		**12 week**		**6 week**		**12 week**	
	Sham	***AB***	***Sham***	***AB***	***Sham***	***AB***	***Sham***	***AB***
SBP, mmHg	144±6	216±5*****	137±5	211±4*****	144±3	232±10*****	140±5	224±12*****
DBP, mmHg	112±5	150±3*****	110±4	152±5*****	112±2	167±6*****	110±5	156±7*****
MAP, mmHg	123±5	172±3*****	119±4	172±4*****	123±2	188±7*****	120±5	179±8*****
HR, beats/min	355±7	361±9	360±4	362±8	362±9	372±10	374±15	381±7
dP/dt_{max}, mmHg/s	7960±310	11080±390*****	8230±350	10670±410*****	8820±410	12040±890*****	9500±350	13240±560*****
dP/dt_{min}, mmHg/s	-8640±240	-11120±350*****	-9590±280	-9630±290#	-10640±590	-12580±650	-10720±420	-13190±1060
LVEDP, mmHg	4.0±0.7	5.7±0.6	3.7±0.4	6.4±0.9*****	3.7±0.2	4.8±0.7	3.2±0.4	3.3±0.5
LVESP, mmHg	132±3	201±6*	126±4	196±3*	139±4	202±10*	140±3	210±9*
LVEDV, µl	307±17	364±5	346±21	373±21	263±25	320±14	295±5	297±9
LVESV, µl	132±13	175±9	150±13	207±13*****	127±15	136±15	136±5	146±6
SV, µl	175±18	189±9	196±12	166±13	136±11	184±8*****	159±8	151±11
EF, %	57±4	52±2	57±2	44±2*****	54±3	58±3	54±2	51±3
CO, ml/min	63.0±7.1	68.0±3.2	70.8±4.7	59.8±4.7	48.5±3.0	68.4±4.1*****	59.1±3.2	57.7±4.7
Tau, ms	13.8±0.4	17.9±0.6*****	12.3±0.6	19.4±0.8*****	12.3±0.6	15.5±1.0*****	12.0±0.4	15.9±1.3*****
EDPVR, mmHg/ µl	0.035±0.005	0.038±0.006	0.028±0.005	0.048±0.006*	0.042±0.006	0.051±0.010	0.033±0.004	0.045±0.007

5.3.2.3. Load-independent contractility parameters

Week 6. At this early-stage, the load-independent indices of cardiac contractility (PRSW and ESPVR) were significantly increased in both male and female AB groups when compared to their control groups (**Fig. 39, Fig. 40A and Fig. 41A**). The direct comparison of the two sexes revealed no significant differences in the extent of contractility augmentation at this time point (**Fig. 40B, Fig. 41B**).

Week 12. At this later stage, a significant reduction from the 6-week state could be observed in PRSW and ESPVR among male AB rats. In contrast, in female animals, LV contractility remained increased, and PRSW and ESPVR were significantly higher when compared to the corresponding sham group (**Fig. 39, Fig. 40A and Fig. 41A**). The differences in contractility changes between male and female rats were well reflected by direct gender comparison, which showed significantly greater increments in PRSW and ESPVR in females (**Fig. 40B and Fig. 41B**).

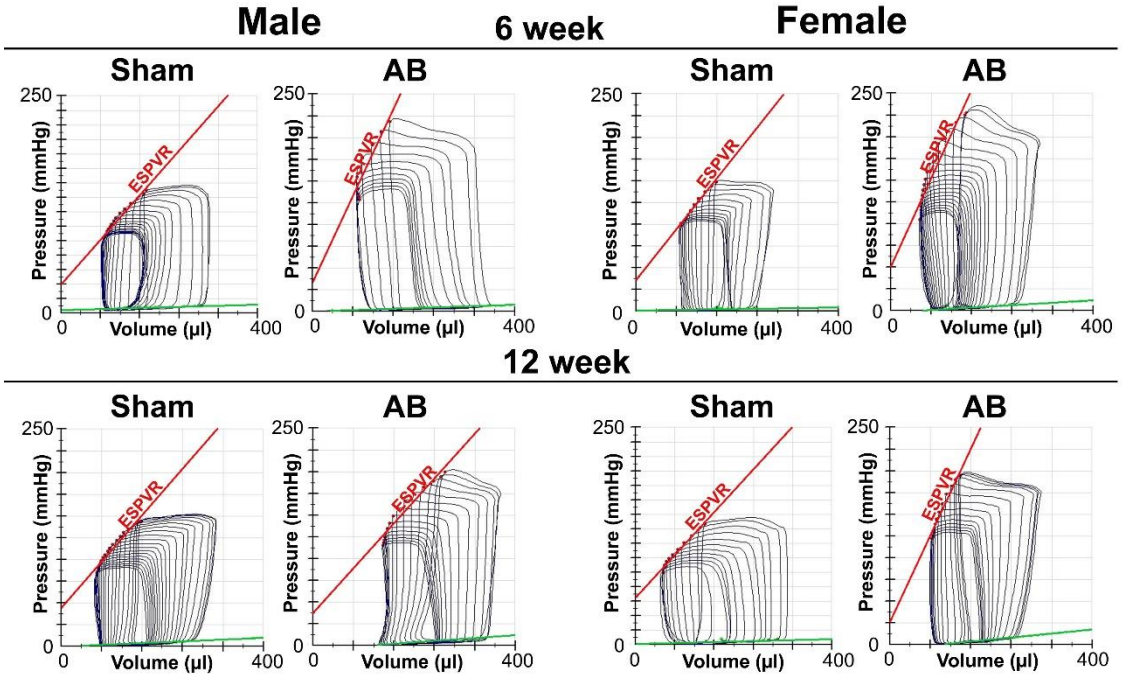

Figure 39. Representative Pressure-Volume loops demonstrating sex differences in LVH. Original recordings were obtained at different preloads during transient vena cava occlusion and show steeper slope of the end-systolic P-V relationship (ESPVR) in male and female aortic banded (AB) rats at week 6, suggesting enhanced contractility. At week 12, in the AB groups, the slope of ESPVR decreased among males but remained increased among females indicating sex differences.

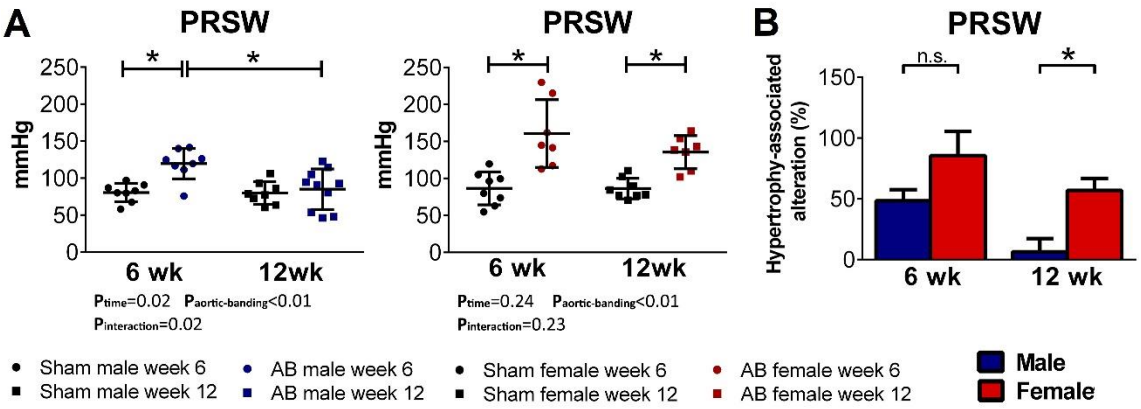

Figure 40. Alterations in preload recruitable stroke work (PRSW) in male and female aortic banded (AB) rats. PRSW was enhanced in both male and female AB rats at week 6 (**A**) compared to their corresponding sham groups. Female AB rats demonstrated increased PRSW at week 12 as well. In contrast, the augmented LV contractility (increased PRSW) reduced to the control's level in male AB rats at week 12 (**A**). Accordingly, robust differences were observed in PRSW between the two sexes at week 12 (**B**). *: P<0.05.

5.3.2.4. Ventricular-arterial coupling

Week 6. At this early stage, augmentation in ESPVR exceeded the increment in E_a, resulting in preserved VAC ratio in the AB groups in both genders. Furthermore, the robust increment of ESPVR in female animals resulted in functional overcompensation, as reflected by reduced VAC ratio (**Fig. 41E**).

Week 12. At this later stage, reduction of contractility in male AB rats led to an impairment in the VAC ratio, which showed significantly higher values in AB week 12 group when compared to AB week 6 group. On the contrary, the maintained contractility augmentation in female AB rats ensured preserved VAC ratio even after 12 weeks of PO. The sex differences in VAC appeared also during direct comparison at week 12 (**Fig. 41F**)

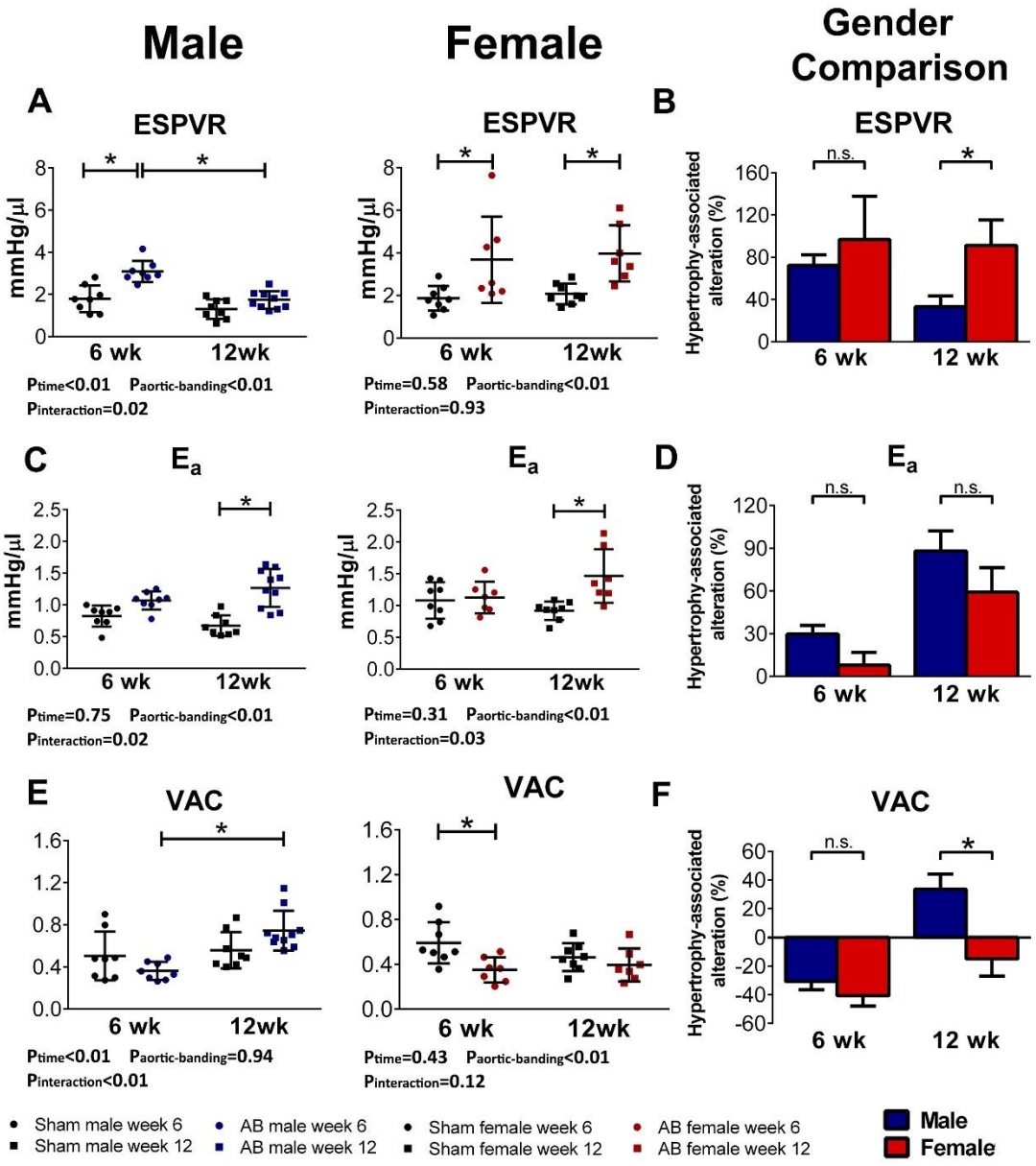

Figure 41. Sex differences in ventriculo-arterial coupling (VAC) during the development and progression of pressure overload-induced myocardial hypertrophy. The contractility augmentation (assessed by increased slope of end-systolic pressure-volume relationship [**A**]) counterbalanced the increased arterial elastance (E_a) (**C**), leading to maintained ventriculo-arterial coupling (**E**) in both male and female AB rats at week 6 and in female AB rats at week 12. In contrast, the contractility augmentation was diminished in the male AB group at week 12 (**A, B**) leading to impaired VAC ratio (**E, F**). *: P<0.05

5.3.2.5. Diastolic parameters

Week 6. The AB groups were associated with prolonged Tau in both sexes when compared to the corresponding sham groups, indicating impaired relaxation. The degree of Tau prolongation was similar between the two genders at week 6 (**Table 9-10**).

Week 12. At this stage, prolongation of Tau was also evident in both male and female AB rats. However, at this time, impairment of active relaxation occurred at a significantly greater extent in male AB rats when compared to that of female littermates (**Table 9-10**). Increment of LV mass index showed strong correlation with prolongation of Tau (r=0.53; p<0.01). Furthermore, LVEDP and the slope EDPVR were also consistently elevated in male but not in the female AB animals at week 12, leading to substantial differences between the two genders (**Table 9-10**). In addition, a significant correlation was detected between LVEDP and collagen area (r=0.30; p=0.02) and also between EDPVR and collagen area (r=0.28; p=0.03).

Table 10. Comparison of pressure overload-induced functional alterations between the two sexes The values of the aortic banded groups were normalized to the corresponding sham groups. Values are expressed as mean ± standard error of the mean. SBP: systolic arterial blood pressure; DBP: diastolic arterial blood pressure; MAP: mean arterial pressure; HR: heart rate; dP/dt_{max}: maximal slope of systolic pressure increment; $dP/dt_{min:}$ maximal slope of diastolic pressure decrement; LVEDP: LV end-diastolic pressure; LVESP: LV end-systolic pressure; LVEDV: LV end-diastolic volume; LVESV: LV end-systolic volume; SV: stroke volume; EF: ejection fraction; CO: cardiac output; Tau: time constant of LV pressure decay according to the Glantz' method; EDPVR: end-diastolic pressure-volume relationship.

	6 week			**12 week**		
	Male *(n=8)*	***Female*** *(n=7)*	***P value (male vs. female)***	***Male*** *(n=10)*	***Female*** *(n=7)*	***P value (male vs. female)***
ΔSBP, %	50±3	62±7	0.14	54±3	60±8	0.99
ΔDBP, %	34±3	49±5	0.02	38±5	42±6	0.65
ΔMAP, %	40±3	54±5	0.03	44±4	49±7	0.54
ΔHR, %	2±3	3±3	0.72	1±2	2±2	0.62
$\Delta dP/dt_{max}$, %	39±5	36±10	0.80	30±5	39±6	0.22
$\Delta dP/dt_{min}$, %	29±4	18±6	0.17	1±3	23±10	0.02
ΔLVEDP, %	44±16	31±19	0.61	73±23	5±17	<0.05
ΔLVESP, %	53±5	46±7	0.41	56±2	50±6	0.34
ΔLVEDV, %	19±2	22±5	0.59	8±6	1±3	0.38
ΔLVESV, %	33±7	7±12	0.07	38±8	8±4	0.01
ΔSV, %	8±5	35±6	<0.01	-15±7	-5±7	0.32
ΔEF, %	-9±4	7±6	0.04	-22±4	-6±5	0.02
ΔCO, %	8±5	42±8	<0.01	-16±7	-2±8	0.22
ΔTau, %	29±4	26±8	0.69	58±6	33±11	<0.05
ΔEDPVR, %	10±17	21±24	0.71	76±22	36±21	0.23

6. Discussion

The purpose of the present investigation was threefold. The first goal was to provide a detailed hemodynamic characterization of *in vivo* LV function at different stages of PO-induced LVH. The second goal was to examine the reversibility of the PO-evoked structural and functional abnormalities from early and late stage LVH. Finally, the third goal was to examine potential sex-related differences in LV structure and function during the adaptation to chronic PO.

6.1. Longitudinal assessment of pressure overload-induced structural and functional alterations of the left ventricle

In the current study, the abdominal AB rat model was utilized to induce sustained PO of the LV. Based on prior literature data (61), and on our own experiences with this particular model (47, 57, 124), the time points of week 6, 12 and 18 were chosen to detect characteristic alterations of early and late stages of PO-induced LVH, respectively.

6.1.1. Structural and molecular alterations during the development and progression of pressure overload-induced left ventricular hypertrophy

The two main ultrastructural characteristics of PO-induced LVH are cardiomyocyte hypertrophy and myocardial fibrosis (134). Previous research work has provided clear evidence that the development of cardiomyocyte hypertrophy precedes the manifestation of myocardial fibrosis during PO-evoked pathological remodeling. Hence at a relative early stage, cardiomyocyte hypertrophy and low level of myocardial fibrosis are the dominant histopathological findings, whereas at later stages cardiomyocyte hypertrophy is accompanied by progressive collagen accumulation (16).

In the current study, development of marked myocardial hypertrophy was observed in the AB group at week 6, as indicated by echocardiographic data (increased wall thicknesses and $LVmass_{index}$), post mortem measurement (increased HW/TL) and histological analysis (increased cardiomyocyte width). The pathological nature of myocardial hypertrophy was confirmed by the reactivation of the fetal gene program (enhanced β/α-MHC ratio and ANP mRNA levels) (17). Despite the development of

robust myocardial hypertrophy, interstitial fibrosis remained at a relatively low level in the AB group at week 6.

The macroscopic, microscopic and molecular hypertrophy markers were also markedly elevated in the AB groups at week 12 and 18. In addition, at these later time points, AB was also associated with chamber dilatation (increased LVEDD) and progressive accumulation of the interstitial collagen content).

6.1.2. Characterization of left ventricular systolic function and contractility during the development and progression of pathological hypertrophy

Traditionally, the echocardiography-derived load-dependent indices have been utilized to describe alterations in LV systolic function during the development of PO-induced LVH and its transition to HF (135). Calculation of these parameters have indicated that systolic function is preserved at a relatively early stage of LVH. However, as PO-induced LVH advances, systolic function becomes progressively impaired.

Nevertheless, it is important to note that the robust alterations in afterload makes the conventional load-dependent parameters inappropriate for the characterization of intrinsic LV function under sustained PO (e.g. AS, AH or abdominal AB). In contrast, the assessment of P-V loops at different preloads enables the calculation of *in vivo* LV contractility parameters independently of loading conditions. Hence, in the current study we performed P-V analysis to gain a deeper understanding of the dynamic alterations of LV contractility at different stages of PO-induced LVH.

To assess LV contractility, three load-independent gold standard parameters (ESPVR, PRSW and dP/dt_{max}-EDV) were calculated from P-V analysis data (136). All of these sensitive indices were substantially increased in the AB-wk6 group, confirming enhanced LV contractility at a relatively early stage of PO-evoked LVH. Of particular interest, calculation of VAC (the ratio of arterial afterload to LV contractility) has revealed that the augmentation of LV contractility efficiently counterbalanced the increment in arterial afterload (Ea) in the AB group at week 6. Consistent with this finding, the load-dependent parameters of LV systolic function (e.g. EF) were maintained at this early stage of PO-induced LVH.

In contrast, at more advanced stages of PO-induced LVH (in the AB-wk12 and AB-wk18 groups) the compensatory augmentation of LV contractility (increased ESPVR,

PRSW and dP/dt_{max}-EDV in the AB-wk6 group) diminished. The decompensation of the hypercontractile state combined with the persistently increased arterial afterload (Ea) resulted in a contractility-afterload mismatch (impaired VAC ratio). Therefore, at these later time points the net systolic performance became decreased, which was reflected by the reduction of load-dependent systolic parameters (e.g. EF).

Although LV systolic function decreased in the AB-wk12 and AB-wk18 groups, it is important to point it out that LV contractility did not differ from the corresponding sham groups. These hemodynamic results are of particular importance, providing evidence that increased arterial afterload and not impaired LV contractility is predominantly responsible for the systolic dysfunction in the abdominal AB rat model. Our findings are in good agreement with the reports of R. J. Hajjar, demonstrating severely reduced systolic function but normal LV contractility in the TAC model (60).

6.1.3. Characterization of LV diastolic function during the development and progression of pathological hypertrophy

Impairment of diastolic function is a hallmark of PO-induced pathological LVH. Importantly, both components of diastole, namely active relaxation and passive filling have been reported to deteriorate under sustained PO.

Active relaxation. Of particular interest is the observation that prolongation of active relaxation occurs early after PO induction. Consistent with this statement, numerous investigations have documented impaired ventricular relaxation already at early stages of PO-induced LVH (47, 66). In line with the data of previous research, we observed increased values of Tau in the AB group already at week 6. Prolongation of active relaxation was also evident in the AB-wk12 and AB-wk18 groups.

Passive filling. Passive filling is predominantly determined by the structural composition of the LV walls. One of the main pathogenic alterations that underlies the reduced LV compliance in PO-induced LVH is increased myocardial fibrosis (137). In the current investigation, neither the amount of interstitial fibrosis nor the slope of EDPVR (the P-V derived parameter of ventricular stiffness) differed in the AB-wk6 group from the control's value. In contrast, at later stages the robust increase in interstitial collagen accumulation was associated with impaired ventricular stiffness.

6.2. Investigating the effects of myocardial reverse remodeling from early- versus late-stage left ventricular hypertrophy

As described above, we have established two distinct stages of PO-induced LVH by utilizing the abdominal AB rat model for different time periods. The structural and functional alterations of the LV in the AB group at week 6 met the criteria of an early stage of PO-induced LVH. Accordingly, marked myocardial hypertrophy, relatively low levels of myocardial fibrosis, preserved systolic function and impaired active relaxation were observed in the AB-wk6 group. In contrast, at more advanced stages (at week 12 and week 18) typical signs of late-stage LVH were detected. In accordance, robust myocardial hypertrophy, severe myocardial fibrosis, impaired systolic function, prolonged active relaxation and increased myocardial stiffness were noted in the AB-wk12 and AB-wk18 groups.

Current guidelines recommend AVR/TAVI for AS patients at advanced stages, when HF symptoms are already present and/or LV systolic function is reduced (138). However, it has been increasingly recognized that HF symptoms and LV dysfunction often persist even after successful pressure unloading therapies (71). Hence, it has been suggested that performing surgeries at earlier time points might provide a greater improvement in LV function and HF symptoms compared to the current late-stage interventions. Based on this, in the next set of experiments our goal was to investigate whether removing the aortic constriction at an earlier time point could induce a reverse remodeling process to a greater extent in regard to structural, molecular and functional alterations compared to a late-stage intervention. To address these questions, the aortic constriction was removed in two subgroups of AB animals at week 6 (early debanding) or week 12 (late debanding). The reverse remodeling processes were then examined after a subsequent 6 week-long follow-up periods.

6.2.1. Regression of myocardial hypertrophy after early and late debanding

Ample evidence has accumulated supporting the notion that myocardial hypertrophy effectively regresses after pressure unloading therapy (70, 72). In concordance with earlier findings, the present study also found that removal of the aortic constriction led to substantial regression of myocardial hypertrophy from both early- and late-stage LVH. No differences could be found in the extent of hypertrophy regression between the early

and the late debanded groups either on macroscopic (LV mass, AWTd, PWTd, HW/TL), microscopic (CD) or gene expression level (β/α MHC ratio). Furthermore, the regression of myocardial hypertrophy also displayed a similar time course in the early and the late debanded groups. Accordingly, in both experimental groups, regression of myocardial mass almost reached its full extent after 3 weeks of pressure unloading. The comparable degree of hypertrophy regression in the early and late debanded groups could be explained by the fact that the same degree of afterload (ΔSBP, ΔDBP, ΔMAP, ΔEa) and meridional wall stress (Δσ) reduction was achieved in both cases.

6.2.2. Regression of reactive myocardial fibrosis after early and late debanding

Both clinical and preclinical data exist demonstrating that reactive myocardial fibrosis regresses in a significantly slower fashion after pressure unloading therapy compared to myocardial hypertrophy (72, 88). Accordingly, the first histopathological evidence for the resorption of interstitial collagen fibers is often observed only years after AVR (64, 65, 72, 74). In the current study, removing the aortic constriction at week 6 (when LVH was associated with relatively low level of interstitial fibrosis) efficiently attenuated the accumulation of reactive myocardial fibrosis (both interstitial and perivascular) in the myocardium during the 6-week-long observation period. These results are in agreement with our previous findings using this model (124, 139). On the contrary, removal of the aortic constriction at week 12 (when LVH was associated with severe reactive myocardial fibrosis) did not lead to a regression of reactive interstitial and perivascular fibrosis during the 6-week-long follow-up. In line with our findings, in a previous pre-clinical study with a similar experimental approach (comparing early and late debanding), normalization of perivascular collagen content also occurred to a greater extent in the early debanded group compared to the late debanded group (91).

Surprisingly, CTFG, which is one of the master regulators of cardiac fibrosis, showed decreased mRNA and protein expression in the late debanded group as well. This is of particular interest, as it has been previously demonstrated that inhibition of CTGF expression can induce the regression of pre-established tissue fibrosis (140). Thus, the observed robust decrease in the expression of CTGF may indicate that regression of reactive fibrosis would have also occurred in the late debanded group in case of a longer follow-up period.

6.2.3. Effect of complete versus incomplete structural reverse remodeling on left ventricular systolic and diastolic function

We would like to call the reader's attention to the fact that in the early debanded group both myocardial hypertrophy and fibrosis regressed. In contrast, in the late debanding group, only myocardial hypertrophy was normalized while myocardial fibrosis persisted six weeks after the removal of the aortic constriction. Therefore, our experimental approach allowed us to investigate the effect of complete versus incomplete structural reverse remodeling on different aspects of LV function under laboratory conditions.

6.2.3.1. Recovery of left ventricular systolic function after early and late debanding

Removal of chronic PO often induces a rapid improvement in systolic function, even before the normalization of LV structural abnormalities (especially fibrosis) is completed (70, 96). This phenomenon can be underpinned by the fact that at certain stages of PO-induced LVH, the increased arterial loading condition (due to AS, AH or AB) and not the depressed LV contractility is primarily responsible for the contractility-afterload mismatch and thus for the reduced systolic function (141). As such, it can be hypothesized that in these cases the acute relief of afterload can lead to sudden normalization of VAC and thereby increment in ejection performance. As mentioned above, at the early stage of LVH (AB-wk6 group) LV contractility was enhanced, VAC was maintained and EF was preserved. In contrast, at later stages of LVH (week 12 and week 18) the compensatory augmentation of LV contractility was diminished. Therefore, in the AB-wk12 and AB-wk18 groups impaired VAC and reduced EF were detected. However, it is important to highlight that even in the late stage groups the increased arterial afterload (Ea) and not the depressed LV contractility was the source of the observed contractility-afterload mismatch. In correspondence, reduction of Ea after pressure unloading successfully normalized the VAC ratio in the late debanded group similarly to the early debanded group. Hence, EF was also effectively recovered after late debanding.

6.2.3.2. Recovery of left ventricular diastolic function after early and late debanding

In contrast to systolic function, diastolic dysfunction has been reported to persist for years after the termination of the pathological stimulus of PO (71). This phenomenon has been explained by the fact that recovery of diastolic function might require a complete normalization of the pathological structural alterations (especially fibrosis) of the LV.

Active relaxation. Previous research data indicates that active relaxation is extremely sensitive to the alterations in afterload. This is underpinned by the fact that an acute increase in systolic peak pressure has been found to be sufficient for the prolongation of active relaxation, independently from the development of LVH (142). Furthermore, Ikonodimis et al. showed that patients undergoing AVR experienced a significant improvement in myocardial relaxation early after surgery, at a time point when regression of LV wall thicknesses had not yet occurred (79). In accordance, we also found that termination of sustained PO effectively decreased the prolonged Tau in both the early and late debanded groups. However, the extent of Tau improvement proved to be inferior in the late debanded group compared to the early debanded group. This can partly be explained by a higher persistent stretch on the single cardiomyocytes in the late debanded group, which was reflected by increased ANP expression in our investigation (143). The enhanced tension at the myofibrillar level might have originated from ultrastructural differences between the early- and the late debanded groups, since at the ventricular level, meridional wall stress was reduced to the same degree after early and late debanding. In accordance with our findings, prior investigations identified persistent interstitial fibrosis and incomplete normalization of cardiomyocyte enlargement as potential sources of increased myofibrillar tension following AVR (72). In our study CD decreased to the same extent in the early- and the late debanded groups. Therefore, it can be inferred that the persistently elevated interstitial fibrosis was mainly responsible for the increased tension on the single cardiomyocyte level and thereby for the incomplete normalization of impaired active relaxation in the late debanded group. Furthermore, it has been suggested that severe perivascular fibrosis can reduce the oxygen supply of the cardiomyocytes (40), thereby decreasing the energy production of the myocardium. Considering the fact that active relaxation is an ATP-dependent process, an indirect connection might indeed exist between increased perivascular fibrosis and impaired

ventricular relaxation in the hypertrophied LV. Correspondingly, the persistent perivascular fibrosis could have also contributed to the ineffective normalization of prolonged active relaxation in the late debanded group.

Passive filling. Passive filling, representing the second component of diastole, is predominantly determined by the structural properties of the LV. As previously mentioned, enhanced interstitial collagen accumulation is one of the most important ultrastructural alterations that increase the stiffness of the LV. Therefore, it is not surprising that previous investigations have observed improvements in myocardial compliance only years after AVR, when regression of interstitial fibrosis had already taken place (64, 65). In our study, P-V derived EDPVR values also followed the alterations in interstitial fibrosis after pressure unloading. Accordingly, in the early debanded group, the relatively low level of myocardial fibrosis was associated with normalized EDPVR values. However, the debanding surgery at the later time point failed to reduce the extent of interstitial fibrosis and in parallel could not improve the increased passive stiffness during the 6-week long follow-up period. Therefore, our hemodynamic data were in accordance with previous clinical findings, demonstrating that regression of interstitial fibrosis is inevitable for the normalization of the increased myocardial stiffness.

6.3. Sex differences during the development of pressure overload-induced left ventricular hypertrophy

Sex differences have been suggested to play an important role in the development of PO-induced LVH. Accordingly, in women with long-lasting AH or AS as well as in female rodents with AB, smaller LV dimensions (105, 106, 109), more concentric LV geometry (105-107), better systolic function (105-109), less interstitial fibrosis (109, 115), less apoptosis (101) and different regulation of genes encoding mitochondrial factors (118) were documented compared to their male counterparts with comparable mechanical overload.

Despite the above mentioned extensive clinical and experimental research, potential sex-related differences with regards to LV hemodynamics have not yet been investigated. Hence, in the current experiment we aimed to perform P-V analysis in male and female rats using our well-established abdominal AB rat model.

6.3.1. Sex differences in myocardial hypertrophy and fibrosis

Based on the findings of relevant animal models, sex differences in LVH may be attributed to the fact that following a common initial stage, progressive maladaptive remodeling occurs in male but not in female rodents (104). In accordance with prior research, we found that the early-stage of PO-induced LVH was associated with a comparable degree of myocardial hypertrophy, equal amounts of interstitial fibrosis and concentric LV geometry in both male and female AB rats. In contrast at week 12, late-stage features of LVH were identified in male but not in female AB rats. Accordingly, at week 12 the male AB group was characterized by intensified fibrotic remodeling (indicated by increased collagen area and CTGF mRNA expression compared to the 6-week state) and LV dilatation (leading to eccentric LV geometry. These findings stand in parallel with our previous experiences with the abdominal AB model (Study 1 and 2). On the other hand, the hypertrophied hearts in the female group still showed concentric geometry and a similar extent of interstitial fibrosis as observed at week 6. Furthermore, at this later time point, the relative extent of hypertrophy was greater in female versus male AB rats. These structural differences between male and female rodents at an advanced stage of PO-induced LVH are in line with the results of Douglas et al., who investigated gender-related myocardial differences in rats with 20 weeks of AB (104).

6.3.2. Sex differences in left ventricular systolic function under pressure overload

Load-dependent systolic parameters have been reported to be more preserved in female patients with chronic AS and female animals with experimentally induced LV PO compared to their male counterparts (105-107). However, potential sex-related discrepancies in load-independent LV contractility parameters during the development of PO-induced LVH have not been examined yet. As such, the present study represents the first attempt to characterize LV systolic function in male and female AB rats independently from the confounding effects of loading conditions.

Assessment of P-V loops has revealed that both male and female AB groups were associated with augmented LV contractility (ESPVR, PRSW) at week 6. Calculation of VAC confirmed that the increment in LV contractility (ESPVR) was sufficient to compensate for the enhanced afterload (E_a) in both sexes at this particular time point.

Furthermore, in female AB animals, the excessive functional adaptation to sustained PO led to increased systolic performance (reflected by higher SV, CO and decreased VAC) at this early stage of LVH. Therefore, although systolic function was maintained in both male and female AB rats, the lack of functional overcompensation in males resulted in sex-related differences already at this early time point. The finding that sex-dependent disparities in systolic function begin to manifest early after the onset of LVH is supported by a former study from Weinberg et al. (117). In their isolated heart experiment, they observed a better preserved LV contractile reserve capacity in female rats compared to male ones after 6 weeks of AB.

In good agreement with previous studies, our investigation revealed that sex-related differences in LV systolic function became more pronounced at a later stage of PO-induced LVH. Accordingly, at week 12 the contractility augmentation diminished in male AB rats, resulting in a mismatch between the LV and the connecting arterial system (impaired VAC ratio). The transition from compensated LVH to systolic HF was also reflected by the reduction of load-dependent systolic parameters (EF) in male AB rats. On the contrary, female AB rats demonstrated enhanced LV contractility (increased ESPVR and PRSW) after 12 weeks of PO. The contractility augmentation in female AB animals resulted in a maintained VAC and preserved global systolic function (EF) despite the chronically increased arterial afterload.

6.3.3. Sex differences in left ventricular diastolic function under pressure overload

Previous studies have raised the possibility that sex differences may also exist in LV diastolic function in case of PO-induced LVH (109). However, to date only a few studies have sought to assess different aspects of LV diastolic function in male and female patients or experimental animals with LVH.

Active relaxation. Detailed analysis of P-V loops provided evidence that the development of LVH was associated with prolongation of active relaxation (as assessed by the Tau, the active relaxation time constant) in both sexes. Of particular interest, impairment of ventricular relaxation was already detected at week 6, becoming even more pronounced at week 12. The PO-related changes in Tau among male rats were identical to those observed previously in our consecutive studies with the abdominal AB rat model

(in Study 1 and 2). However, the finding of impaired active relaxation in female rats with sustained PO was novel. Furthermore, we found that the severity of diastolic dysfunction was similar in the two sexes at week 6. In contrast, at week 12 we detected significantly greater prolongation of Tau in male AB rats when compared to their female littermates. Our functional results may be underpinned by previous molecular experiments, indicating sex-specific regulation of sarco/endoplasmic reticulum Ca^{2+}-ATPase during the development of LVH (117).

Passive filling. Both clinical and preclinical findings suggest that male sex is associated with a more severe deterioration of the passive diastolic properties of the LV under sustained PO. Accordingly, Villari et al. documented impaired myocardial stiffness in male but not in female patients with long-standing AS (109). Furthermore, experimental studies have observed that elevation of LVEDP accompanies the development of LVH in male animals, whereas in females LVEDP remains at physiologically low levels despite the manifestation of pathological hypertrophy. Considering that myocardial compliance (the passive expansion capability of the LV) is primarily determined by the structural composition of the ventricular wall, the characteristic sex-related discrepancies in passive filling have been predominantly attributed to the differences in ECM remodeling. In the current study, we also observed that the slope of EDVPR (marker of chamber stiffness) and LVEDP was only increased in the male AB-wk12 group. Importantly, it was also found that interstitial fibrosis occurred to a greater extent in the male AB group at week 12. Hence, the impairment of the passive diastolic properties of the LV in male AB rats may have indeed originated from maladaptive myocardial ECM remodeling. This conclusion was also strengthened by the fact that a strong correlation was discovered between fibrosis and ventricular stiffness parameters among the study groups.

6.4. Limitations

One possible limitation of the studies might be that the gradual rise of arterial blood pressure (proximal to the aortic constriction) has not been registered. However, literature data clearly indicate that in the abdominal AB rat model, a substantial increment of arterial blood pressure occurs already in the first 2 weeks after the surgical application of the constriction (144). Therefore, it can be confidently stated that the severe increment in afterload had been long persisted before the selected time points (weeks 6, week 12 and week 18) in the current studies.

Furthermore, it has to be also noted here that the AB rat model involves numerous mechanistic components that ultimately evoke the pathological remodeling of the LV. Accordingly, previous investigations have indicated that constricting the abdominal aorta at the suprarenal level not only induces PO in the proximal part of the aorta but also leads to the hypoperfusion of the kidneys with subsequent activation of the renin-angiotensin-aldosterone system (145, 146). Therefore, it cannot be ruled out that in our study, neuro-humoral factors also contributed to the development of LVH.

In study 2 a relatively short follow-up period (6 weeks) was utilized to detect the functional consequences of myocardial reverse remodeling. Therefore, further research is warranted to test whether the observed differences between the early and the late debanded groups also exist after a substantially longer period of time.

In study 3, a standard size was used to induce PO in rats. However, male animals grew to a greater body size, which raised the possibility that in male rats a relatively more severe aortic constriction developed. Therefore, to exclude the possibility of different degrees of PO in male and female rats, numerous parameters of afterload were calculated (SBP, DBP, MAP, and Ea), which showed no differences between the sexes. Accordingly, it could be hypothesized that indeed genetic and hormonal factors have mainly contributed to the observed sex-dependent differences in our model.

7. Conclusion

Ample evidence supports the notion that termination of the pathological stimulus of PO could result in a state of reverse remodeling. Nevertheless, it has been also recognized that not all the patients experience the same extent of functional and structural improvement following pressure unloading therapy. Hence, efforts have been taken to identify factors which might influence the regression of LVH. These studies have indicated that the time point of medical interventions and the sex of the patients might determine the success of the reverse remodeling process.

One of the main conclusions of our experiments is that pressure unloading therapy at both early and late time points effectively improves LV systolic function. By performing invasive P-V analysis we confirmed that increased arterial afterload and not depressed LV contractility underpins the reduced systolic performance even at advanced stages of PO-induced LVH in the abdominal AB rat model. Hence, terminating the PO at both early and late time points rapidly normalizes the relation between the contractile state of the LV and the afterload of the connecting arterial system.

In contrast to systolic function, we found that diastolic function (both active relaxation and myocardial stiffness) recovers to a greater extent in case of early debanding compared to late debanding. This finding might be explained by the fact that the early pressure unloading therapy entailed a more complete structural reverse remodeling compared to the late-stage surgery. Accordingly, regression of reactive interstitial and perivascular fibrosis was only detected in the early debanded group, while it persisted in the late debanded group. These results call attention to the fact that performing pressure unloading therapy (AVR, TAVI) at an earlier time point may be superior in regard to normalization of diastolic function.

Furthermore, the sex of the patients has been also suggested to influence the outcome of pressure unloading therapies. Here, we confirmed that the advanced stage of PO-induced LVH is associated with less myocardial fibrosis as well as less severely impaired LV active relaxation and myocardial stiffness in female compared to male AB rats. As interstitial fibrosis and diastolic dysfunction have been found to be those factors, which display less reversibility after pressure unloading, our results might indicate that women could indeed experience a more complete functional reverse remodeling from late-stage LVH.

8. Summary

PO-induced pathological LVH regresses after pressure unloading. Nevertheless, it has been recognized that in some patients, LV dysfunction and HF symptoms persist even after optimal medical therapy. Of particular interest, current guidelines recommend AVR only in case of severe AS, when HF symptoms are present and/or LV systolic function is reduced (EF<50%). In the frame of the present investigation we demonstrated that the severe stage of PO-induced LVH (that recapitulates the clinical situation of those patients who are eligible for AVR) was associated with robust myocardial hypertrophy, intensified collagen accumulation, reduced systolic function and marked diastolic dysfunction (prolonged active relaxation and impaired myocardial stiffness) in the abdominal AB rat model. Importantly, pressure unloading at this advanced stage of LVH efficiently reduced the extent of myocardial hypertrophy. Similarly, a complete recovery of LV systolic function was also observed. On the contrary myocardial fibrosis failed to regress during the 6-week long follow-up period. The incomplete regression of reactive fibrosis impeded the recovery of both the active and the passive components of diastolic function. To test, whether an earlier intervention could be more beneficial compared to late-stage surgery, we have investigated the reverse remodeling process after terminating the PO at an earlier time point (before severe ECM remodeling took place). Importantly we found that early pressure unloading resulted in a significantly greater improvement of both active relaxation and myocardial stiffness. Hence, our results call attention to the importance of early interventions in case of PO-induced LVH.

Besides the timing of pressure unloading therapies, recent studies have shed light on the notion that the sex of the patient might be another important determinant of the reverse remodeling process. This is underpinned by the fact that due to a substantially slower disease progression, early stage characteristics of LVH (with relatively low level of myocardial fibrosis) are more often observed in female patients and experimental animals compared to their male counterparts. In the current investigation we yielded evidence that PO-induced LVH in female rats was associated with better LV contractility and systolic function as well as less severely impaired active relaxation and myocardial stiffness. Considering that diastolic dysfunction displays poor reversibility, the less deteriorated active relaxation and myocardial stiffness in female animals might indicate a greater capacity for functional improvement after pressure unloading.

9. Összefoglalás

A fokozott nyomásterhelés által indukált patológiás bal kamra (BK) hipertrófia (BKH) a nyomásterhelés megszüntetése után visszaalakul. Ugyanakkor kutatások igazolják, hogy egyes betegekben a szívelégtelenség tünetei és a BK-i diszfunkció a megfelelő terápiás beavatkozások után is fennállnak. Erre magyarázatul szolgálhat, hogy a jelenleg érvényes ajánlások aorta stenosis fennállása esetében csak igen súlyos, előrehaladott állapotban (amikor a szívelégtelenség tünetei már megjelentek és/vagy a szisztolés funkció jelentősen károsodott) javasolják a műtéti beavatkozást. Jelen patkánykísérletünkben a BKH súlyos, előrehaladott stádiumát nagymértékű szívizomhipertrófia, fokozott fibrózis, csökkent szisztolés funkció és súlyosan károsodott diasztolés funkció (megnyúlt aktív relaxáció és fokozott miokardiális stiffness) jellemezte. Ebben a stádiumban végrehajtott nyomásterhelés-csökkentő terápia a szívizomhipertrófia jelentős regresszióját eredményezte. Ezzel párhuzamosan a szisztolés funkció szintén teljes mértékben helyreállt. Ugyanakkor, a BKH késői stádiumából a fokozott kollagén felhalmozódás nem mutatott csökkenést. Hemodinamikai méréseink rávilágítottak arra, hogy a perzisztáló miokardiális fibrózis gátolta a diasztolés funkció mindkét aspektusának (aktív relaxáció és passzív telődés) a javulását. Patkánymodellünkben ezért megvizsgáltuk, hogy vajon egy korábban kezdett nyomásterhelés-csökkentő terápia nagyobb mértékű funkcionális regenerációt biztosíthat a jelenleg alkalmazott késői beavatkozással szemben. Érdekes módon azt találtuk, hogy a korai terápia a diasztolés funkció szignifikánsan nagyobb mértékű javulását eredményezte a késői műtéttel szemben. Eredményeink ezért felhívják a figyelmet a korai beavatkozások szükségességére fokozott nyomásterhelés indukálta BKH esetén.

Az elmúlt években világossá vált, a női nem szintén fontos befolyásoló hatással bírhat a BKH visszaalakulására. Ennek hátterében az áll, hogy nők esetében a fokozott nyomásterhelés hatására eltérő változások játszódnak le a szívizomban. Ezt igazolja, hogy női betegekben kisebb mértékű fibrózist és kedvezőbb BK-i geometriát írtak le férfi beteghez képest. Jelen kísérletünkben megfigyeltük, hogy nőstény patkányokban a BKH késői stádiumára jobb BK-i kontraktilitás és szisztolés teljesítőképesség valamint kevésbé károsodott aktív relaxáció és falmerevség volt jellemző. A diasztolés funkció kisebb mértékű károsodása felveti a lehetőségét, hogy nőkben a nyomásterhelés-csökkentő terápia valóban teljesebb funkcionális regenerációt idézhet elő.

10. Bibliography

1. Ziaeian B, Fonarow GC. (2016) Epidemiology and aetiology of heart failure. Nat Rev Cardiol, 13:368-378.

2. Ponikowski P, Voors AA, Anker SD, Bueno H, Cleland JGF, Coats AJS, Falk V, Gonzalez-Juanatey JR, Harjola VP, Jankowska EA, Jessup M, Linde C, Nihoyannopoulos P, Parissis JT, Pieske B, Riley JP, Rosano GMC, Ruilope LM, Ruschitzka F, Rutten FH, van der Meer P, Group ESCSD. (2016) 2016 esc guidelines for the diagnosis and treatment of acute and chronic heart failure: The task force for the diagnosis and treatment of acute and chronic heart failure of the european society of cardiology (esc)developed with the special contribution of the heart failure association (hfa) of the esc. Eur Heart J, 37:2129-2200.

3. Ponikowski P, Anker SD, AlHabib KF, Cowie MR, Force TL, Hu S, Jaarsma T, Krum H, Rastogi V, Rohde LE, Samal UC, Shimokawa H, Budi Siswanto B, Sliwa K, Filippatos G. (2014) Heart failure: Preventing disease and death worldwide. ESC Heart Fail, 1:4-25.

4. Savarese G, Lund LH. (2017) Global public health burden of heart failure. Card Fail Rev, 3:7-11.

5. Braunwald E. (2013) Heart failure. JACC Heart Fail, 1:1-20.

6. Treibel TA, Kozor R, Schofield R, Benedetti G, Fontana M, Bhuva AN, Sheikh A, Lopez B, Gonzalez A, Manisty C, Lloyd G, Kellman P, Diez J, Moon JC. (2018) Reverse myocardial remodeling following valve replacement in patients with aortic stenosis. J Am Coll Cardiol, 71:860-871.

7. Leon MB, Smith CR, Mack M, Miller DC, Moses JW, Svensson LG, Tuzcu EM, Webb JG, Fontana GP, Makkar RR, Brown DL, Block PC, Guyton RA, Pichard AD, Bavaria JE, Herrmann HC, Douglas PS, Petersen JL, Akin JJ, Anderson WN, Wang D, Pocock S, Investigators PT. (2010) Transcatheter aortic-valve

implantation for aortic stenosis in patients who cannot undergo surgery. N Engl J Med, 363:1597-1607.

8. Williams B, Mancia G, Spiering W, Agabiti Rosei E, Azizi M, Burnier M, Clement DL, Coca A, de Simone G, Dominiczak A, Kahan T, Mahfoud F, Redon J, Ruilope L, Zanchetti A, Kerins M, Kjeldsen SE, Kreutz R, Laurent S, Lip GYH, McManus R, Narkiewicz K, Ruschitzka F, Schmieder RE, Shlyakhto E, Tsioufis C, Aboyans V, Desormais I, Authors/Task Force M. (2018) 2018 esc/esh guidelines for the management of arterial hypertension: The task force for the management of arterial hypertension of the european society of cardiology and the european society of hypertension: The task force for the management of arterial hypertension of the european society of cardiology and the european society of hypertension. J Hypertens, 36:1953-2041.

9. Collaboration NCDRF. (2017) Worldwide trends in blood pressure from 1975 to 2015: A pooled analysis of 1479 population-based measurement studies with 19.1 million participants. Lancet, 389:37-55.

10. Benjamin EJ, Muntner P, Alonso A, Bittencourt MS, Callaway CW, Carson AP, Chamberlain AM, Chang AR, Cheng S, Das SR, Delling FN, Djousse L, Elkind MSV, Ferguson JF, Fornage M, Jordan LC, Khan SS, Kissela BM, Knutson KL, Kwan TW, Lackland DT, Lewis TT, Lichtman JH, Longenecker CT, Loop MS, Lutsey PL, Martin SS, Matsushita K, Moran AE, Mussolino ME, O'Flaherty M, Pandey A, Perak AM, Rosamond WD, Roth GA, Sampson UKA, Satou GM, Schroeder EB, Shah SH, Spartano NL, Stokes A, Tirschwell DL, Tsao CW, Turakhia MP, VanWagner LB, Wilkins JT, Wong SS, Virani SS, American Heart Association Council on E, Prevention Statistics C, Stroke Statistics S. (2019) Heart disease and stroke statistics-2019 update: A report from the american heart association. Circulation, 139:e56-e66.

11. Iung B, Vahanian A. (2011) Epidemiology of valvular heart disease in the adult. Nat Rev Cardiol, 8:162-172.

12. Iung B, Baron G, Butchart EG, Delahaye F, Gohlke-Barwolf C, Levang OW, Tornos P, Vanoverschelde JL, Vermeer F, Boersma E, Ravaud P, Vahanian A. (2003) A prospective survey of patients with valvular heart disease in europe: The euro heart survey on valvular heart disease. Eur Heart J, 24:1231-1243.

13. Osnabrugge RL, Mylotte D, Head SJ, Van Mieghem NM, Nkomo VT, LeReun CM, Bogers AJ, Piazza N, Kappetein AP. (2013) Aortic stenosis in the elderly: Disease prevalence and number of candidates for transcatheter aortic valve replacement: A meta-analysis and modeling study. J Am Coll Cardiol, 62:1002-1012.

14. Eveborn GW, Schirmer H, Heggelund G, Lunde P, Rasmussen K. (2013) The evolving epidemiology of valvular aortic stenosis. The tromso study. Heart, 99:396-400.

15. Schwartzkopff B, Motz W, Frenzel H, Vogt M, Knauer S, Strauer BE. (1993) Structural and functional alterations of the intramyocardial coronary arterioles in patients with arterial hypertension. Circulation, 88:993-1003.

16. Weber KT, Janicki JS, Pick R, Capasso J, Anversa P. (1990) Myocardial fibrosis and pathologic hypertrophy in the rat with renovascular hypertension. Am J Cardiol, 65:1G-7G.

17. McMullen JR, Jennings GL. (2007) Differences between pathological and physiological cardiac hypertrophy: Novel therapeutic strategies to treat heart failure. Clin Exp Pharmacol Physiol, 34:255-262.

18. Cooper Gt, Kent RL, Uboh CE, Thompson EW, Marino TA. (1985) Hemodynamic versus adrenergic control of cat right ventricular hypertrophy. J Clin Invest, 75:1403-1414.

19. Nadruz W. (2015) Myocardial remodeling in hypertension. J Hum Hypertens, 29:1-6.

20. Ruwhof C, van der Laarse A. (2000) Mechanical stress-induced cardiac hypertrophy: Mechanisms and signal transduction pathways. Cardiovasc Res, 47:23-37.

21. Bernardo BC, Weeks KL, Pretorius L, McMullen JR. (2010) Molecular distinction between physiological and pathological cardiac hypertrophy: Experimental findings and therapeutic strategies. Pharmacol Ther, 128:191-227.

22. Lorell BH, Carabello BA. (2000) Left ventricular hypertrophy: Pathogenesis, detection, and prognosis. Circulation, 102:470-479.

23. Souders CA, Borg TK, Banerjee I, Baudino TA. (2012) Pressure overload induces early morphological changes in the heart. Am J Pathol, 181:1226-1235.

24. Esposito G, Rapacciuolo A, Naga Prasad SV, Takaoka H, Thomas SA, Koch WJ, Rockman HA. (2002) Genetic alterations that inhibit in vivo pressure-overload hypertrophy prevent cardiac dysfunction despite increased wall stress. Circulation, 105:85-92.

25. Levy D, Garrison RJ, Savage DD, Kannel WB, Castelli WP. (1990) Prognostic implications of echocardiographically determined left ventricular mass in the framingham heart study. N Engl J Med, 322:1561-1566.

26. Gorgulu S, Norgaz T, Nurkalem Z, Ergelen M, Eksik A, Genc A, Zencirci AE. (2010) Comparison of left ventricular contractility in pressure and volume overload: A strain rate study in the clinical model of aortic stenosis and regurgitation. Echocardiography, 27:798-802.

27. You J, Wu J, Zhang Q, Ye Y, Wang S, Huang J, Liu H, Wang X, Zhang W, Bu L, Li J, Lin L, Ge J, Zou Y. (2018) Differential cardiac hypertrophy and signaling pathways in pressure versus volume overload. Am J Physiol Heart Circ Physiol, 314:H552-H562.

28. Brilla CG, Weber KT. (1992) Reactive and reparative myocardial fibrosis in arterial hypertension in the rat. Cardiovasc Res, 26:671-677.

29. Kong P, Christia P, Frangogiannis NG. (2014) The pathogenesis of cardiac fibrosis. Cell Mol Life Sci, 71:549-574.

30. Weidemann F, Herrmann S, Stork S, Niemann M, Frantz S, Lange V, Beer M, Gattenlohner S, Voelker W, Ertl G, Strotmann JM. (2009) Impact of myocardial fibrosis in patients with symptomatic severe aortic stenosis. Circulation, 120:577-584.

31. Creemers EE, Pinto YM. (2011) Molecular mechanisms that control interstitial fibrosis in the pressure-overloaded heart. Cardiovasc Res, 89:265-272.

32. Moorjani N, Ahmad M, Catarino P, Brittin R, Trabzuni D, Al-Mohanna F, Narula N, Narula J, Westaby S. (2006) Activation of apoptotic caspase cascade during the transition to pressure overload-induced heart failure. J Am Coll Cardiol, 48:1451-1458.

33. Piek A, de Boer RA, Sillje HH. (2016) The fibrosis-cell death axis in heart failure. Heart Fail Rev, 21:199-211.

34. Carver W, Nagpal ML, Nachtigal M, Borg TK, Terracio L. (1991) Collagen expression in mechanically stimulated cardiac fibroblasts. Circ Res, 69:116-122.

35. Bishop JE, Lindahl G. (1999) Regulation of cardiovascular collagen synthesis by mechanical load. Cardiovasc Res, 42:27-44.

36. Wang J, Chen H, Seth A, McCulloch CA. (2003) Mechanical force regulation of myofibroblast differentiation in cardiac fibroblasts. Am J Physiol Heart Circ Physiol, 285:H1871-1881.

37. Spinale FG. (2007) Myocardial matrix remodeling and the matrix metalloproteinases: Influence on cardiac form and function. Physiol Rev, 87:1285-1342.

38. Iwanaga Y, Aoyama T, Kihara Y, Onozawa Y, Yoneda T, Sasayama S. (2002) Excessive activation of matrix metalloproteinases coincides with left ventricular remodeling during transition from hypertrophy to heart failure in hypertensive rats. J Am Coll Cardiol, 39:1384-1391.

39. Toischer K, Rokita AG, Unsold B, Zhu W, Kararigas G, Sossalla S, Reuter SP, Becker A, Teucher N, Seidler T, Grebe C, Preuss L, Gupta SN, Schmidt K, Lehnart SE, Kruger M, Linke WA, Backs J, Regitz-Zagrosek V, Schafer K, Field LJ, Maier LS, Hasenfuss G. (2010) Differential cardiac remodeling in preload versus afterload. Circulation, 122:993-1003.

40. Kai H, Kuwahara F, Tokuda K, Imaizumi T. (2005) Diastolic dysfunction in hypertensive hearts: Roles of perivascular inflammation and reactive myocardial fibrosis. Hypertens Res, 28:483-490.

41. Swynghedauw B. (1999) Molecular mechanisms of myocardial remodeling. Physiol Rev, 79:215-262.

42. Barry SP, Davidson SM, Townsend PA. (2008) Molecular regulation of cardiac hypertrophy. Int J Biochem Cell Biol, 40:2023-2039.

43. Rajabi M, Kassiotis C, Razeghi P, Taegtmeyer H. (2007) Return to the fetal gene program protects the stressed heart: A strong hypothesis. Heart Fail Rev, 12:331-343.

44. Reiser PJ, Portman MA, Ning XH, Schomisch Moravec C. (2001) Human cardiac myosin heavy chain isoforms in fetal and failing adult atria and ventricles. Am J Physiol Heart Circ Physiol, 280:H1814-1820.

45. Nakao K, Minobe W, Roden R, Bristow MR, Leinwand LA. (1997) Myosin heavy chain gene expression in human heart failure. J Clin Invest, 100:2362-2370.

46. Taegtmeyer H, Sen S, Vela D. (2010) Return to the fetal gene program: A suggested metabolic link to gene expression in the heart. Ann N Y Acad Sci, 1188:191-198.

47. Nemeth BT, Matyas C, Olah A, Lux A, Hidi L, Ruppert M, Kellermayer D, Kokeny G, Szabo G, Merkely B, Radovits T. (2016) Cinaciguat prevents the development of pathologic hypertrophy in a rat model of left ventricular pressure overload. Sci Rep, 6:37166.

48. Nishikimi T, Maeda N, Matsuoka H. (2006) The role of natriuretic peptides in cardioprotection. Cardiovasc Res, 69:318-328.

49. Tsuchimochi H, Kurimoto F, Ieki K, Koyama H, Takaku F, Kawana M, Kimata S, Yazaki Y. (1988) Atrial natriuretic peptide distribution in fetal and failed adult human hearts. Circulation, 78:920-927.

50. Cameron VA, Ellmers LJ. (2003) Minireview: Natriuretic peptides during development of the fetal heart and circulation. Endocrinology, 144:2191-2194.

51. Gardner DG. (2003) Natriuretic peptides: Markers or modulators of cardiac hypertrophy? Trends Endocrinol Metab, 14:411-416.

52. Pacher P, Nagayama T, Mukhopadhyay P, Batkai S, Kass DA. (2008) Measurement of cardiac function using pressure-volume conductance catheter technique in mice and rats. Nat Protoc, 3:1422-1434.

53. Burkhoff D, Mirsky I, Suga H. (2005) Assessment of systolic and diastolic ventricular properties via pressure-volume analysis: A guide for clinical, translational, and basic researchers. Am J Physiol Heart Circ Physiol, 289:H501-512.

54. Zhu H, Tannous P, Johnstone JL, Kong Y, Shelton JM, Richardson JA, Le V, Levine B, Rothermel BA, Hill JA. (2007) Cardiac autophagy is a maladaptive response to hemodynamic stress. J Clin Invest, 117:1782-1793.

55. Marzak H, Ayme-Dietrich E, Lawson R, Mokni W, Combe R, Becker J, Fertak LE, Champy MF, Monassier L. (2014) Old spontaneously hypertensive rats gather together typical features of human chronic left-ventricular dysfunction with preserved ejection fraction. J Hypertens, 32:1307-1316.

56. Alyono D, Ring WS, Crumbley AJ, Schneider JR, O'Connor MJ, Parrish D, Bache RJ, Anderson RW. (1984) Global left ventricular contractility in three models of hypertrophy evaluated with emax. J Surg Res, 37:48-54.

57. Olah A, Nemeth BT, Matyas C, Hidi L, Lux A, Ruppert M, Kellermayer D, Sayour AA, Szabo L, Torok M, Meltzer A, Geller L, Merkely B, Radovits T. (2016) Physiological and pathological left ventricular hypertrophy of comparable degree is associated with characteristic differences of in vivo hemodynamics. Am J Physiol Heart Circ Physiol, 310:H587-597.

58. Asanoi H, Sasayama S, Kameyama T. (1989) Ventriculoarterial coupling in normal and failing heart in humans. Circ Res, 65:483-493.

59. Kass DA, Kelly RP. (1992) Ventriculo-arterial coupling: Concepts, assumptions, and applications. Ann Biomed Eng, 20:41-62.

60. Chemaly ER, Chaanine AH, Sakata S, Hajjar RJ. (2012) Stroke volume-to-wall stress ratio as a load-adjusted and stiffness-adjusted indicator of ventricular systolic performance in chronic loading. J Appl Physiol (1985), 113:1267-1284.

61. Ku HC, Su MJ. (2014) Dpp4 deficiency preserved cardiac function in abdominal aortic banding rats. PLoS One, 9:e85634.

62. Inoko M, Kihara Y, Morii I, Fujiwara H, Sasayama S. (1994) Transition from compensatory hypertrophy to dilated, failing left ventricles in dahl salt-sensitive rats. Am J Physiol, 267:H2471-2482.

63. Villari B, Hess OM, Kaufmann P, Krogmann ON, Grimm J, Krayenbuehl HP. (1992) Effect of aortic valve stenosis (pressure overload) and regurgitation (volume overload) on left ventricular systolic and diastolic function. Am J Cardiol, 69:927-934.

64. Villari B, Vassalli G, Monrad ES, Chiariello M, Turina M, Hess OM. (1995) Normalization of diastolic dysfunction in aortic stenosis late after valve replacement. Circulation, 91:2353-2358.

65. Villari B, Vassalli G, Betocchi S, Briguori C, Chiariello M, Hess OM. (1996) Normalization of left ventricular nonuniformity late after valve replacement for aortic stenosis. Am J Cardiol, 78:66-71.

66. Hamdani N, Bishu KG, von Frieling-Salewsky M, Redfield MM, Linke WA. (2013) Deranged myofilament phosphorylation and function in experimental heart failure with preserved ejection fraction. Cardiovasc Res, 97:464-471.

67. Takimoto E, Champion HC, Li M, Belardi D, Ren S, Rodriguez ER, Bedja D, Gabrielson KL, Wang Y, Kass DA. (2005) Chronic inhibition of cyclic gmp phosphodiesterase 5a prevents and reverses cardiac hypertrophy. Nat Med, 11:214-222.

68. Ruppert M, Korkmaz-Icoz S, Li S, Brlecic P, Nemeth BT, Olah A, Horvath EM, Veres G, Pleger S, Grabe N, Merkely B, Karck M, Radovits T, Szabo G. (2018) Comparison of the reverse-remodeling effect of pharmacological soluble guanylate cyclase activation with pressure unloading in pathological myocardial left ventricular hypertrophy. Front Physiol, 9:1869.

69. Koitabashi N, Kass DA. (2011) Reverse remodeling in heart failure--mechanisms and therapeutic opportunities. Nat Rev Cardiol, 9:147-157.

70. Gao XM, Kiriazis H, Moore XL, Feng XH, Sheppard K, Dart A, Du XJ. (2005) Regression of pressure overload-induced left ventricular hypertrophy in mice. Am J Physiol Heart Circ Physiol, 288:H2702-2707.

71. Gjertsson P, Caidahl K, Bech-Hanssen O. (2005) Left ventricular diastolic dysfunction late after aortic valve replacement in patients with aortic stenosis. Am J Cardiol, 96:722-727.

72. Krayenbuehl HP, Hess OM, Monrad ES, Schneider J, Mall G, Turina M. (1989) Left ventricular myocardial structure in aortic valve disease before, intermediate, and late after aortic valve replacement. Circulation, 79:744-755.

73. Monrad ES, Hess OM, Murakami T, Nonogi H, Corin WJ, Krayenbuehl HP. (1988) Time course of regression of left ventricular hypertrophy after aortic valve replacement. Circulation, 77:1345-1355.

74. Hess OM, Ritter M, Schneider J, Grimm J, Turina M, Krayenbuehl HP. (1984) Diastolic stiffness and myocardial structure in aortic valve disease before and after valve replacement. Circulation, 69:855-865.

75. Flett AS, Sado DM, Quarta G, Mirabel M, Pellerin D, Herrey AS, Hausenloy DJ, Ariti C, Yap J, Kolvekar S, Taylor AM, Moon JC. (2012) Diffuse myocardial fibrosis in severe aortic stenosis: An equilibrium contrast cardiovascular magnetic resonance study. Eur Heart J Cardiovasc Imaging, 13:819-826.

76. Dobson LE, Fairbairn TA, Musa TA, Uddin A, Mundie CA, Swoboda PP, Ripley DP, McDiarmid AK, Erhayiem B, Garg P, Malkin CJ, Blackman DJ, Sharples LD, Plein S, Greenwood JP. (2016) Sex-related differences in left ventricular remodeling in severe aortic stenosis and reverse remodeling after aortic valve replacement: A cardiovascular magnetic resonance study. Am Heart J, 175:101-111.

77. Dobson LE, Musa TA, Uddin A, Fairbairn TA, Swoboda PP, Erhayiem B, Foley J, Garg P, Haaf P, Fent GJ, Malkin CJ, Blackman DJ, Plein S, Greenwood JP. (2016) Acute reverse remodelling after transcatheter aortic valve implantation: A link between myocardial fibrosis and left ventricular mass regression. Can J Cardiol, 32:1411-1418.

78. Christakis GT, Joyner CD, Morgan CD, Fremes SE, Buth KJ, Sever JY, Rao V, Panagiotopoulos KP, Murphy PM, Goldman BS. (1996) Left ventricular mass regression early after aortic valve replacement. Ann Thorac Surg, 62:1084-1089.

79. Ikonomidis I, Tsoukas A, Parthenakis F, Gournizakis A, Kassimatis A, Rallidis L, Nihoyannopoulos P. (2001) Four year follow up of aortic valve replacement for isolated aortic stenosis: A link between reduction in pressure overload, regression of left ventricular hypertrophy, and diastolic function. Heart, 86:309-316.

80. Bjornstad JL, Skrbic B, Sjaastad I, Bjornstad S, Christensen G, Tonnessen T. (2012) A mouse model of reverse cardiac remodelling following banding-debanding of the ascending aorta. Acta Physiol (Oxf), 205:92-102.

81. Bjornstad JL, Sjaastad I, Nygard S, Hasic A, Ahmed MS, Attramadal H, Finsen AV, Christensen G, Tonnessen T. (2011) Collagen isoform shift during the early phase of reverse left ventricular remodelling after relief of pressure overload. Eur Heart J, 32:236-245.

82. Weinheimer CJ, Kovacs A, Evans S, Matkovich SJ, Barger PM, Mann DL. (2018) Load-dependent changes in left ventricular structure and function in a pathophysiologically relevant murine model of reversible heart failure. Circ Heart Fail, 11:e004351.

83. Walther T, Schubert A, Falk V, Binner C, Kanev A, Bleiziffer S, Walther C, Doll N, Autschbach R, Mohr FW. (2001) Regression of left ventricular hypertrophy after surgical therapy for aortic stenosis is associated with changes in extracellular matrix gene expression. Circulation, 104:I54-58.

84. Mewton N, Liu CY, Croisille P, Bluemke D, Lima JA. (2011) Assessment of myocardial fibrosis with cardiovascular magnetic resonance. J Am Coll Cardiol, 57:891-903.

85. Everett RJ, Tastet L, Clavel MA, Chin CWL, Capoulade R, Vassiliou VS, Kwiecinski J, Gomez M, van Beek EJR, White AC, Prasad SK, Larose E, Tuck C, Semple S, Newby DE, Pibarot P, Dweck MR. (2018) Progression of hypertrophy and myocardial fibrosis in aortic stenosis: A multicenter cardiac magnetic resonance study. Circ Cardiovasc Imaging, 11:e007451.

86. Messroghli DR, Nordmeyer S, Dietrich T, Dirsch O, Kaschina E, Savvatis K, D Oh-I, Klein C, Berger F, Kuehne T. (2011) Assessment of diffuse myocardial

fibrosis in rats using small-animal look-locker inversion recovery t1 mapping. Circ Cardiovasc Imaging, 4:636-640.

87. Weber KT, Sun Y, Gerling IC, Guntaka RV. (2017) Regression of established cardiac fibrosis in hypertensive heart disease. Am J Hypertens, 30:1049-1052.

88. Miranda-Silva D, Goncalves-Rodrigues P, Almeida-Coelho J, Hamdani N, Lima T, Conceicao G, Sousa-Mendes C, Claudia M, Gonzalez A, Diez J, Linke WA, Leite-Moreira A, Falcao-Pires I. (2019) Characterization of biventricular alterations in myocardial (reverse) remodelling in aortic banding-induced chronic pressure overload. Sci Rep, 9:2956.

89. Cho JS, Cho EJ, Lee J, Choi HD, Park KC, Lee KH, Yang KJ, Park MW, Park GM, Her SH, Kim CJ. (2014) Myocardial mechanics in a rat model with banding and debanding of the ascending aorta. J Cardiovasc Ultrasound, 22:189-195.

90. Liu J, Drak D, Krishnan A, Chen SY, Canniffe C, Bao S, Denyer G, Celermajer DS. (2017) Left ventricular fibrosis and systolic hypertension persist in a repaired aortic coarctation model. Ann Thorac Surg, 104:942-949.

91. Ito N, Isoyama S, Takahashi T, Takishima T. (1993) Coronary dilator reserve and morphological changes after relief of pressure-overload in rats. J Mol Cell Cardiol, 25:3-14.

92. Andersen NM, Stansfield WE, Tang RH, Rojas M, Patterson C, Selzman CH. (2012) Recovery from decompensated heart failure is associated with a distinct, phase-dependent gene expression profile. J Surg Res, 178:72-80.

93. Yang DK, Choi BY, Lee YH, Kim YG, Cho MC, Hong SE, Kim DH, Hajjar RJ, Park WJ. (2007) Gene profiling during regression of pressure overload-induced cardiac hypertrophy. Physiol Genomics, 30:1-7.

94. Vizzardi E, D'Aloia A, Fiorina C, Bugatti S, Parrinello G, De Carlo M, Giannini C, Di Bello V, Petronio AS, Curello S, Ettori F, Dei Cas L. (2012) Early regression of left ventricular mass associated with diastolic improvement after transcatheter aortic valve implantation. J Am Soc Echocardiogr, 25:1091-1098.

95. Poulsen SH, Sogaard P, Nielsen-Kudsk JE, Egeblad H. (2007) Recovery of left ventricular systolic longitudinal strain after valve replacement in aortic stenosis and relation to natriuretic peptides. J Am Soc Echocardiogr, 20:877-884.

96. Biederman RW, Magovern JA, Grant SB, Williams RB, Yamrozik JA, Vido DA, Rathi VK, Rayarao G, Caruppannan K, Doyle M. (2011) Lv reverse remodeling imparted by aortic valve replacement for severe aortic stenosis; is it durable? A cardiovascular mri study sponsored by the american heart association. J Cardiothorac Surg, 6:53.

97. Regitz-Zagrosek V, Oertelt-Prigione S, Seeland U, Hetzer R. (2010) Sex and gender differences in myocardial hypertrophy and heart failure. Circ J, 74:1265-1273.

98. Regitz-Zagrosek V, Kararigas G. (2017) Mechanistic pathways of sex differences in cardiovascular disease. Physiol Rev, 97:1-37.

99. Brower GL, Gardner JD, Janicki JS. (2003) Gender mediated cardiac protection from adverse ventricular remodeling is abolished by ovariectomy. Mol Cell Biochem, 251:89-95.

100. Iorga A, Li J, Sharma S, Umar S, Bopassa JC, Nadadur RD, Centala A, Ren S, Saito T, Toro L, Wang Y, Stefani E, Eghbali M. (2016) Rescue of pressure overload-induced heart failure by estrogen therapy. J Am Heart Assoc, 5

101. Fliegner D, Schubert C, Penkalla A, Witt H, Kararigas G, Dworatzek E, Staub E, Martus P, Ruiz Noppinger P, Kintscher U, Gustafsson JA, Regitz-Zagrosek V. (2010) Female sex and estrogen receptor-beta attenuate cardiac remodeling and

apoptosis in pressure overload. Am J Physiol Regul Integr Comp Physiol, 298:R1597-1606.

102. Skavdahl M, Steenbergen C, Clark J, Myers P, Demianenko T, Mao L, Rockman HA, Korach KS, Murphy E. (2005) Estrogen receptor-beta mediates male-female differences in the development of pressure overload hypertrophy. Am J Physiol Heart Circ Physiol, 288:H469-476.

103. Babiker FA, Lips D, Meyer R, Delvaux E, Zandberg P, Janssen B, van Eys G, Grohe C, Doevendans PA. (2006) Estrogen receptor beta protects the murine heart against left ventricular hypertrophy. Arterioscler Thromb Vasc Biol, 26:1524-1530.

104. Douglas PS, Katz SE, Weinberg EO, Chen MH, Bishop SP, Lorell BH. (1998) Hypertrophic remodeling: Gender differences in the early response to left ventricular pressure overload. J Am Coll Cardiol, 32:1118-1125.

105. Carroll JD, Carroll EP, Feldman T, Ward DM, Lang RM, McGaughey D, Karp RB. (1992) Sex-associated differences in left ventricular function in aortic stenosis of the elderly. Circulation, 86:1099-1107.

106. Aurigemma GP, Silver KH, McLaughlin M, Mauser J, Gaasch WH. (1994) Impact of chamber geometry and gender on left ventricular systolic function in patients > 60 years of age with aortic stenosis. Am J Cardiol, 74:794-798.

107. Douglas PS, Otto CM, Mickel MC, Labovitz A, Reid CL, Davis KB. (1995) Gender differences in left ventricle geometry and function in patients undergoing balloon dilatation of the aortic valve for isolated aortic stenosis. Nhlbi balloon valvuloplasty registry. Br Heart J, 73:548-554.

108. Gerdts E, Okin PM, de Simone G, Cramariuc D, Wachtell K, Boman K, Devereux RB. (2008) Gender differences in left ventricular structure and function during

antihypertensive treatment: The losartan intervention for endpoint reduction in hypertension study. Hypertension, 51:1109-1114.

109. Villari B, Campbell SE, Schneider J, Vassalli G, Chiariello M, Hess OM. (1995) Sex-dependent differences in left ventricular function and structure in chronic pressure overload. Eur Heart J, 16:1410-1419.

110. Olivetti G, Giordano G, Corradi D, Melissari M, Lagrasta C, Gambert SR, Anversa P. (1995) Gender differences and aging: Effects on the human heart. J Am Coll Cardiol, 26:1068-1079.

111. Petrov G, Regitz-Zagrosek V, Lehmkuhl E, Krabatsch T, Dunkel A, Dandel M, Dworatzek E, Mahmoodzadeh S, Schubert C, Becher E, Hampl H, Hetzer R. (2010) Regression of myocardial hypertrophy after aortic valve replacement: Faster in women? Circulation, 122:S23-28.

112. Satoh M, Matter CM, Ogita H, Takeshita K, Wang CY, Dorn GW, 2nd, Liao JK. (2007) Inhibition of apoptosis-regulated signaling kinase-1 and prevention of congestive heart failure by estrogen. Circulation, 115:3197-3204.

113. Stangl V, Baldenhofer G, Knebel F, Zhang K, Sanad W, Spethmann S, Grubitzsch H, Sander M, Wernecke KD, Baumann G, Stangl K, Laule M. (2012) Impact of gender on three-month outcome and left ventricular remodeling after transfemoral transcatheter aortic valve implantation. Am J Cardiol, 110:884-890.

114. Okin PM, Gerdts E, Kjeldsen SE, Julius S, Edelman JM, Dahlof B, Devereux RB, Losartan Intervention for Endpoint Reduction in Hypertension Study I. (2008) Gender differences in regression of electrocardiographic left ventricular hypertrophy during antihypertensive therapy. Hypertension, 52:100-106.

115. Kararigas G, Dworatzek E, Petrov G, Summer H, Schulze TM, Baczko I, Knosalla C, Golz S, Hetzer R, Regitz-Zagrosek V. (2014) Sex-dependent regulation of

fibrosis and inflammation in human left ventricular remodelling under pressure overload. Eur J Heart Fail, 16:1160-1167.

116. Treibel TA, Kozor R, Fontana M, Torlasco C, Reant P, Badiani S, Espinoza M, Yap J, Diez J, Hughes AD, Lloyd G, Moon JC. (2018) Sex dimorphism in the myocardial response to aortic stenosis. JACC Cardiovasc Imaging, 11:962-973.

117. Weinberg EO, Thienelt CD, Katz SE, Bartunek J, Tajima M, Rohrbach S, Douglas PS, Lorell BH. (1999) Gender differences in molecular remodeling in pressure overload hypertrophy. J Am Coll Cardiol, 34:264-273.

118. Witt H, Schubert C, Jaekel J, Fliegner D, Penkalla A, Tiemann K, Stypmann J, Roepcke S, Brokat S, Mahmoodzadeh S, Brozova E, Davidson MM, Ruiz Noppinger P, Grohe C, Regitz-Zagrosek V. (2008) Sex-specific pathways in early cardiac response to pressure overload in mice. J Mol Med (Berl), 86:1013-1024.

119. Aurigemma GP, Gaasch WH. (1995) Gender differences in older patients with pressure-overload hypertrophy of the left ventricle. Cardiology, 86:310-317.

120. Houser SR, Margulies KB, Murphy AM, Spinale FG, Francis GS, Prabhu SD, Rockman HA, Kass DA, Molkentin JD, Sussman MA, Koch WJ, American Heart Association Council on Basic Cardiovascular Sciences CoCC, Council on Functional G, Translational B. (2012) Animal models of heart failure: A scientific statement from the american heart association. Circ Res, 111:131-150.

121. Kalk P, Godes M, Relle K, Rothkegel C, Hucke A, Stasch JP, Hocher B. (2006) No-independent activation of soluble guanylate cyclase prevents disease progression in rats with 5/6 nephrectomy. Br J Pharmacol, 148:853-859.

122. Patten RD, Hall-Porter MR. (2009) Small animal models of heart failure: Development of novel therapies, past and present. Circ Heart Fail, 2:138-144.

123. Langheinrich M, Lee MA, Bohm M, Pinto YM, Ganten D, Paul M. (1996) The hypertensive ren-2 transgenic rat tgr (mren2)27 in hypertension research. Characteristics and functional aspects. Am J Hypertens, 9:506-512.

124. Ruppert M, Korkmaz-Icoz S, Li S, Nemeth BT, Hegedus P, Brlecic P, Matyas C, Zorn M, Merkely B, Karck M, Radovits T, Szabo G. (2016) Myocardial reverse remodeling after pressure unloading is associated with maintained cardiac mechanoenergetics in a rat model of left ventricular hypertrophy. Am J Physiol Heart Circ Physiol, 311:H592-603.

125. Chen J, Chemaly ER, Liang LF, LaRocca TJ, Yaniz-Galende E, Hajjar RJ. (2011) A new model of congestive heart failure in rats. Am J Physiol Heart Circ Physiol, 301:H994-1003.

126. Korkmaz-Icoz S, Brlecic P, Ruppert M, Radovits T, Karck M, Szabo G. (2018) Mechanical pressure unloading therapy reverses thoracic aortic structural and functional changes in a hypertensive rat model. J Hypertens, 36:2350-2361.

127. Dadson K, Kovacevic V, Rengasamy P, Kim GH, Boo S, Li RK, George I, Schulze PC, Hinz B, Sweeney G. (2016) Cellular, structural and functional cardiac remodelling following pressure overload and unloading. Int J Cardiol, 216:32-42.

128. Szardien S, Nef HM, Voss S, Troidl C, Liebetrau C, Hoffmann J, Rauch M, Mayer K, Kimmich K, Rolf A, Rixe J, Troidl K, Kojonazarov B, Schermuly RT, Kostin S, Elsasser A, Hamm CW, Mollmann H. (2012) Regression of cardiac hypertrophy by granulocyte colony-stimulating factor-stimulated interleukin-1beta synthesis. Eur Heart J, 33:595-605.

129. Kilkenny C, Browne WJ, Cuthill IC, Emerson M, Altman DG. (2010) Improving bioscience research reporting: The arrive guidelines for reporting animal research. PLoS Biol, 8:e1000412.

130. Devereux RB, Alonso DR, Lutas EM, Gottlieb GJ, Campo E, Sachs I, Reichek N. (1986) Echocardiographic assessment of left ventricular hypertrophy: Comparison to necropsy findings. Am J Cardiol, 57:450-458.

131. Sunagawa K, Maughan WL, Burkhoff D, Sagawa K. (1983) Left ventricular interaction with arterial load studied in isolated canine ventricle. Am J Physiol, 245:H773-780.

132. Yamamoto K. (2010) The time constant of left ventricular relaxation: Extrication from load dependence and overestimation of functional abnormality. Circ Heart Fail, 3:178-180.

133. Kass DA, Beyar R, Lankford E, Heard M, Maughan WL, Sagawa K. (1989) Influence of contractile state on curvilinearity of in situ end-systolic pressure-volume relations. Circulation, 79:167-178.

134. Yarbrough WM, Mukherjee R, Ikonomidis JS, Zile MR, Spinale FG. (2012) Myocardial remodeling with aortic stenosis and after aortic valve replacement: Mechanisms and future prognostic implications. J Thorac Cardiovasc Surg, 143:656-664.

135. Litwin SE, Katz SE, Weinberg EO, Lorell BH, Aurigemma GP, Douglas PS. (1995) Serial echocardiographic-doppler assessment of left ventricular geometry and function in rats with pressure-overload hypertrophy. Chronic angiotensin-converting enzyme inhibition attenuates the transition to heart failure. Circulation, 91:2642-2654.

136. Kass DA. (1995) Clinical ventricular pathophysiology: A pressure-volume view.In: *Ventricular Function*, edited by Wartlier DC. Baltimore: Williams & Wilkins.

137. Conrad CH, Brooks WW, Hayes JA, Sen S, Robinson KG, Bing OH. (1995) Myocardial fibrosis and stiffness with hypertrophy and heart failure in the spontaneously hypertensive rat. Circulation, 91:161-170.

138. Baumgartner H, Falk V, Bax JJ, De Bonis M, Hamm C, Holm PJ, Iung B, Lancellotti P, Lansac E, Rodriguez Munoz D, Rosenhek R, Sjogren J, Tornos Mas P, Vahanian A, Walther T, Wendler O, Windecker S, Zamorano JL, Group ESCSD. (2017) 2017 esc/eacts guidelines for the management of valvular heart disease. Eur Heart J, 38:2739-2791.

139. Ruppert M, Korkmaz-Icoz S, Li S, Merkely B, Karck M, Radovits T, Szabo G. (2017) Reverse electrical remodeling following pressure unloading in a rat model of hypertension-induced left ventricular myocardial hypertrophy. Hypertens Res, 40:637-645.

140. Lipson KE, Wong C, Teng Y, Spong S. (2012) Ctgf is a central mediator of tissue remodeling and fibrosis and its inhibition can reverse the process of fibrosis. Fibrogenesis Tissue Repair, 5:S24.

141. Huber D, Grimm J, Koch R, Krayenbuehl HP. (1981) Determinants of ejection performance in aortic stenosis. Circulation, 64:126-134.

142. Gaasch WH, Blaustein AS, Andrias CW, Donahue RP, Avitall B. (1980) Myocardial relaxation. Ii. Hemodynamic determinants of rate of left ventricular isovolumic pressure decline. Am J Physiol, 239:H1-6.

143. Sadoshima J, Jahn L, Takahashi T, Kulik TJ, Izumo S. (1992) Molecular characterization of the stretch-induced adaptation of cultured cardiac cells. An in vitro model of load-induced cardiac hypertrophy. J Biol Chem, 267:10551-10560.

144. Masuyama H, Tsuruda T, Sekita Y, Hatakeyama K, Imamura T, Kato J, Asada Y, Stasch JP, Kitamura K. (2009) Pressure-independent effects of pharmacological

stimulation of soluble guanylate cyclase on fibrosis in pressure-overloaded rat heart. Hypertens Res, 32:597-603.

145. Baker KM, Chernin MI, Wixson SK, Aceto JF. (1990) Renin-angiotensin system involvement in pressure-overload cardiac hypertrophy in rats. Am J Physiol, 259:H324-332.

146. Massart PE, Donckier J, Kyselovic J, Godfraind T, Heyndrickx GR, Wibo M. (1999) Carvedilol and lacidipine prevent cardiac hypertrophy and endothelin-1 gene overexpression after aortic banding. Hypertension, 34:1197-1201.

11. Bibliography of the candidate's publications

11.1. Publications related to the dissertation

I. **Ruppert M***, Bódi B*, Korkmaz-Icöz S, Loganathan S, Jiang W, Lehmann L, Oláh A, Barta BA, Sayour AA, Merkely B, Karck M, Papp Z, Szabó G, Radovits T. (2019) Myofilament Ca^{2+} sensitivity correlates with left ventricular contractility during the progression of pressure overload-induced left ventricular myocardial hypertrophy in rats. J Mol Cell Cardiol, 129:208-218.
IF: 5.055
*: equal contribution

II. **Ruppert M**, Korkmaz-Icöz S, Loganathan S, Jiang W, Oláh A, Sayour AA, Barta BA, Karime C, Merkely B, Karck M, Radovits T, Szabó G. (2019) Incomplete structural reverse remodeling from late-stage left ventricular hypertrophy impedes the recovery of diastolic but not systolic dysfunction in rats. J Hypertens, 37:1200-1212.
IF: 4.209

III. **Ruppert M**, Korkmaz-Icöz S, Loganathan S, Jiang W, Lehmann L, Oláh A, Sayour AA, Barta BA, Merkely B, Karck M, Radovits T, Szabó G. (2018) Pressure-volume analysis reveals characteristic sex-related differences in cardiac function in a rat model of aortic banding-induced myocardial hypertrophy. Am J Physiol Heart Circ Physiol, 315:H502-H511.
IF: 4.048

IV. **Ruppert M**, Bódi B, Nagy D, Korkmaz-Icöz S, Loganathan S, Oláh A, Barta BA, Sayour AA, Benke K, Karck M, Merkely B, Papp Z, Szabó G, Radovits T. (2019) A miofilamentáris rendszer Ca^{2+}-érzékenysége korrellál a bal kamrai kontraktilitással a fokozott nyomásterhelés által előidézett patológiás szívizom-hipertrófia patkánymodelljében. Cardiol Hung, 49: 88-99. (Magyar nyelvű másodközlés).

11.2. Publications not related to the dissertation

I. Loganathan S, Guo Y, Jiang W, Radovits T, **Ruppert M**, Sayour AA, Brune M, Brlecic P, Gude P, Georgevici AI, Yard B, Karck M, Korkmaz-Icöz S, Szabó G. (2019) N-octanoyl dopamine is superior to dopamine in protecting graft contractile function when administered to the heart transplant recipients from brain-dead donors. Pharmacol Res. 150:104503.
IF: 5.574

II. Oláh A, Mátyás C, Kellermayer D, **Ruppert M**, Barta BA, Sayour AA, Török M, Koncsos G, Giricz Z, Ferdinandy P, Merkely B, Radovits T. (2019) Sex differences in morphological and functional aspects of exercise-induced cardiac hypertrophy in a rat model. Front Physiol, 10:889.
IF: 3.201

III. Sayour AA, Korkmaz-Icöz S, Loganathan S, **Ruppert M**, Sayour VN, Oláh A, Benke K, Brune M, Benkő R, Horváth EM, Karck M, Merkely B, Radovits T, Szabó G. (2019) Acute canagliflozin treatment protects against in vivo myocardial ischemia-reperfusion injury in non-diabetic male rats and enhances endothelium-dependent vasorelaxation. J Transl Med, 17:127.
IF: 4.098

IV. Oláh A, **Ruppert M**, Orbán TI, Apáti A, Sarkadi B, Merkely B, Radovits T. (2019) Hemodynamic characterization of a transgenic rat strain stably expressing the calcium sensor protein gcamp2. Am J Physiol Heart Circ Physiol, 316:H1224-H1228.
IF: 4.048

V. Korkmaz-Icöz S, Li S, Hüttner R, **Ruppert M**, Radovits T, Loganathan S, Sayour AA, Brlecic P, Lasitschka F, Karck M, Szabó G. (2019) Hypothermic perfusion of donor heart with a preservation solution supplemented by mesenchymal stem cells. J Heart Lung Transplant, 38:315-326.
IF: 8.578

VI. Oláh A, Kovács A, Lux A, Tokodi M, Braun S, Lakatos BK, Mátyás C, Kellermayer D, **Ruppert M**, Sayour AA, Barta BA, Merkely B, Radovits T. (2019) Characterization of the dynamic changes in left ventricular morphology and function induced by exercise training and detraining. Int J Cardiol, 277:178-185.
IF: 3.471

VII. **Ruppert M**, Korkmaz-Icöz S, Li S, Brlecic P, Németh BT, Oláh A, Horváth EM, Veres G, Pleger S, Grabe N, Merkely B, Karck M, Radovits T, Szabó G. (2018) Comparison of the reverse-remodeling effect of pharmacological soluble guanylate cyclase activation with pressure unloading in pathological myocardial left ventricular hypertrophy. Front Physiol, 9:1869.
IF: 3.201

VIII. Korkmaz-Icöz S, Brlecic P, **Ruppert M**, Radovits T, Karck M, Szabó G. (2018) Mechanical pressure unloading therapy reverses thoracic aortic structural and functional changes in a hypertensive rat model. J Hypertens, 36:2350-2361.
IF: 4.209

IX. Korkmaz-Icöz S, Li S, Loganathan S, Radovits T, **Ruppert M**, Brlecic P, Sayour AA, Veres G, Fleming T, Brune M, Most P, Karck M, Szabó G. (2018) Impairment of the akt pathway in transplanted type 1 diabetic hearts is associated with post-transplant graft injury. Interact Cardiovasc Thorac Surg, 27:884-894.
IF: 1.931

X. Mátyás C, Kovács A, Németh BT, Oláh A, Braun S, Tokodi M, Barta BA, Benke K, **Ruppert M**, Lakatos BK, Merkely B, Radovits T. (2018) Comparison of speckle-tracking echocardiography with invasive hemodynamics for the detection of characteristic cardiac dysfunction in type-1 and type-2 diabetic rat models. Cardiovasc Diabetol, 17:13.
IF: 5.948

XI. Korkmaz-Icöz S, Szczesny B, Marcatti M, Li S, **Ruppert M**, Lasitschka F, Loganathan S, Szabó C, Szabó G. (2018) Olaparib protects cardiomyocytes against oxidative stress and improves graft contractility during the early phase after heart transplantation in rats. Br J Pharmacol, 175:246-261.
IF: 6.583

XII. Benke K, Mátyás C, Sayour AA, Oláh A, Németh BT, **Ruppert M**, Szabó G, Kokeny G, Horváth EM, Hartyanszky I, Szabolcs Z, Merkely B, Radovits T. (2017) Pharmacological preconditioning with gemfibrozil preserves cardiac function after heart transplantation. Sci Rep, 7:14232.
IF: 4.122

XIII. Benke K, Sayour AA, Mátyás C, Ágg B, Németh BT, Oláh A, **Ruppert M**, Hartyanszky I, Szabolcs Z, Radovits T, Merkely B, Szabó G. (2017) Heterotopic abdominal rat heart transplantation as a model to investigate volume dependency of myocardial remodeling. Transplantation, 101:498-505.
IF: 3.960

XIV. Li S, Korkmaz-Icöz S, Radovits T, **Ruppert M**, Spindler R, Loganathan S, Hegedűs P, Brlecic P, Theisinger B, Theisinger S, Hoger S, Brune M, Lasitschka F, Karck M, Yard B, Szabó G. (2017) Donor preconditioning after the onset of brain death with dopamine derivate n-octanoyl dopamine improves early posttransplant graft function in the rat. Am J Transplant, 17:1802-1812.
IF: 6.493

XV. Korkmaz-Icöz S, Radovits T, Loganathan S, Li S, **Ruppert M**, Benke K, Brlecic P, Szabó C, Karck M, Szabó G. (2017) Prolonging hypothermic ischaemic cardiac and vascular storage by inhibiting the activation of the nuclear enzyme poly(adenosine diphosphate-ribose) polymerase. Eur J Cardiothorac Surg, 51:829-835.
IF: 3.504

XVI. **Ruppert M**, Korkmaz-Icöz S, Li S, Merkely B, Karck M, Radovits T, Szabó G. (2017) Reverse electrical remodeling following pressure unloading in a rat model of hypertension-induced left ventricular myocardial hypertrophy. Hypertens Res, 40:637-645.
IF: 3.439

XVII. Mátyás C, Németh BT, Oláh A, Török M, **Ruppert M**, Kellermayer D, Barta BA, Szabó G, Kökény G, Horváth EM, Bódi B, Papp Z, Merkely B, Radovits T. (2017) Prevention of the development of heart failure with preserved ejection fraction by the phosphodiesterase-5a inhibitor vardenafil in rats with type 2 diabetes. Eur J Heart Fail, 19:326-336.
IF: 10.683

XVIII. Oláh A, Kellermayer D, Matyas C, Németh BT, Lux A, Szabó L, Török M, **Ruppert M**, Meltzer A, Sayour AA, Benke K, Hartyánszky I, Merkely B, Radovits T. (2017) Complete reversion of cardiac functional adaptation induced by exercise training. Med Sci Sports Exerc, 49:420-429.
IF: 4.291

XIX. Németh BT, Mátyás C, Oláh A, Lux A, Hidi L, **Ruppert M**, Kellermayer D, Kökény G, Szabó G, Merkely B, Radovits T. (2016) Cinaciguat prevents the development of pathologic hypertrophy in a rat model of left ventricular pressure overload. Sci Rep, 6:37166.
IF: 4.259

XX. Korkmaz-Icöz S, Lehner A, Li S, Vater A, Radovits T, Brune M, **Ruppert M**, Sun X, Brlecic P, Zorn M, Karck M, Szabó G. (2016) Left ventricular pressure-volume measurements and myocardial gene expression profile in type 2 diabetic goto-kakizaki rats. Am J Physiol Heart Circ Physiol, 311:H958-H971.
IF: 3.348

XXI. **Ruppert M**, Korkmaz-Icöz S, Li S, Németh BT, Hegedűs P, Brlecic P, Mátyás C, Zorn M, Merkely B, Karck M, Radovits T, Szabó G. (2016) Myocardial reverse remodeling after pressure unloading is associated with maintained cardiac mechanoenergetics in a rat model of left ventricular hypertrophy. Am J Physiol Heart Circ Physiol, 311:H592-603.
IF: 3.348

XXII. Korkmaz-Icöz S, Al Said S, Radovits T, Li S, Brune M, Hegedus P, Atmanli A, **Ruppert M**, Brlecic P, Lehmann LH, Lahrmann B, Grabe N, Yoshikawa Y, Yasui H, Most P, Karck M, Szabó G. (2016) Oral treatment with a zinc complex of acetylsalicylic acid prevents diabetic cardiomyopathy in a rat model of type-2 diabetes: Activation of the akt pathway. Cardiovasc Diabetol, 15:75.
IF: 4.752

XXIII. Oláh A, Németh BT, Mátyás C, Hidi L, Lux A, **Ruppert M**, Kellermayer D, Sayour AA, Szabó L, Török M, Meltzer A, Geller L, Merkely B, Radovits T. (2016) Physiological and pathological left ventricular hypertrophy of comparable degree is associated with characteristic differences of in vivo hemodynamics. Am J Physiol Heart Circ Physiol, 310:H587-597.
IF: 3.348

XXIV. Korkmaz-Icöz S, Atmanli A, Radovits T, Li S, Hegedűs P, **Ruppert M**, Brlecic P, Yoshikawa Y, Yasui H, Karck M, Szabó G. (2016) Administration of zinc complex of acetylsalicylic acid after the onset of myocardial injury protects the heart by upregulation of antioxidant enzymes. J Physiol Sci, 66:113-125.
IF: 2.075

XXV. Mátyás C, Németh BT, Oláh A, Hidi L, Birtalan E, Kellermayer D, **Ruppert M**, Korkmaz-Icöz S, Kökény G, Horváth EM, Szabó G, Merkely B, Radovits T. (2015) The soluble guanylate cyclase activator cinaciguat prevents cardiac dysfunction in a rat model of type-1 diabetes mellitus. Cardiovasc Diabetol, 14:145.

IF: 4.534

XXVI. Korkmaz-Icöz S, Lehner A, Li S, Vater A, Radovits T, Hegedűs P, **Ruppert M**, Brlecic P, Zorn M, Karck M, Szabó G. (2015) Mild type 2 diabetes mellitus reduces the susceptibility of the heart to ischemia/reperfusion injury: Identification of underlying gene expression changes. J Diabetes Res, 2015:396414.
IF: 2.431

XXVII. Kovács A, Oláh A, Lux A, Mátyás C, Németh BT, Kellermayer D, **Ruppert M**, Török M, Szabó L, Meltzer A, Assabiny A, Birtalan E, Merkely B, Radovits T. (2015) Strain and strain rate by speckle-tracking echocardiography correlate with pressure-volume loop-derived contractility indices in a rat model of athlete's heart. Am J Physiol Heart Circ Physiol, 308:H743-748.
IF: 3.324

XXVIII. Oláh A, Németh BT, Mátyás C, Horváth EM, Hidi L, Birtalan E, Kellermayer D, **Ruppert M**, Merkely G, Szabó G, Merkely B, Radovits T. (2015) Cardiac effects of acute exhaustive exercise in a rat model. Int J Cardiol, 182:258-266.
IF: 4.638

XXIX. Korkmaz-Icöz S, Vater A, Li S, Lehner A, Radovits T, Hegedűs P, **Ruppert M**, Brlecic P, Zorn M, Karck M, Szabó G. (2015) Mild type 2 diabetes mellitus improves remote endothelial dysfunction after acute myocardial infarction. J Diabetes Complications, 29:1253-1260.
IF: 2.955

XXX. **Ruppert M**, Barta BA, Korkmaz-Icöz S, Li S, Oláh A, Mátyás Cs, Németh BT, Benke K, Sayour AA, Karck M, Merkely B, Radovits T, Szabó G. (2018) A hipertrófiás myocardium reverz elektromos remodellációjának vizsgálata patkánymodellben. Cardiol Hung, 48: 118-128. (Magyar nyelvű másodközlés).

XXXI. Oláh A, Sayour AA, Németh BT, Mátyás Cs, Hidi L, Lux Á, **Ruppert M**, Kellermayer D, Szabó L, Török M, Meltzer A, Gellér L, Merkely B, Radovits T. (2018) A hasonló fokú fiziológiás és patológiás balkamra-hipertrófia különböző in vivo hemodinamikai következményekhez vezet. Cardiol Hung, 48: 20-30. (Magyar nyelvű másodközlés).

XXXII. Németh BT, Mátyás Cs, Oláh A, Lux Á, Hidi L, **Ruppert M**, Kellermayer D, Kökény G, Szabó G, Merkely B, Radovits T. (2017) A cinaciguat megelőzi a patológiás szívizom-hipertrófia kialakulását bal kamrai nyomás-túlterhelés patkánymodelljén. Cardiol Hung, 47:183-194. (Magyar nyelvű másodközlés).

XXXIII. Mátyás Cs, Barta BA, Németh BT, Oláh A, Hidi L, Birtalan E, Kellermayer D, **Ruppert M**, Korkmaz-Icöz S, Kökény G, Horváth EM, Szabó G, Merkely B, Radovits T. (2017) A szolubilis guanilát cikláz aktivátor cinaciguat megelőzi a kardiális diszfunkció kialakulását 1-es típusú cukorbetegség patkánymodelljében. Cardiol Hung, 47:34-45. (Magyar nyelvű másodközlés).

XXXIV. Benke K, Sayour AA, Ágg B, Radovits T, Szilveszter B, Odler B, Németh BT, Pólos M, Oláh A, Mátyás C, **Ruppert M**, Hartyánszky I, Maurovich-Horvat P, Merkely B, Szabolcs Z. (2016) Génpolimorfizmusok, mint rizikófaktorok a Marfan-szindróma kardiovaszkuláris manifesztációinak előrejelzésében. Cardiol Hung, 46:76-81. (Magyar nyelvű másodközlés).

XXXV. Oláh A, Németh BT, Mátyás C, Horváth EM, Hidi L, Birtalan E, Kellermayer D, **Ruppert M**, Gellér L, Szabó G, Merkely B, Radovits T. (2016) Az egyszeri, kimerítő fizikai terhelés kardiális hatásainak vizsgálata patkánymodellen. Cardiol Hung, 46:1-9. (Magyar nyelvű másodközlés).

XXXVI. Oláh A, Lux Á, Németh BT, Hidi L, Birtalan E, Kellermayer D, Mátyás C, **Ruppert M**, Merkely G, Szabó G, Merkely B, Radovits T. (2013) A sportszív részletes hemodinamikai jellemzése bal kamrai nyomás-térfogat analízis segítségével. Cardiol Hung, 43:224-232. (Magyar nyelvű másodközlés).

12. Acknowledgements

First of all, I would like to express my sincere gratitude to my tutor, Dr. Tamás Radovits, whose guidance helped me all the time in the past years. He introduced me to the world of experimental cardiovascular research. He placed trust in me from the first day I joined his research group and his continuous support accompanied me all the time during my Ph.D. study. His inquiring attitude to scientific questions coupled with his immense knowledge and patience will always stand as an example to follow for me.

I would like to thank Prof. Béla Merkely for his instructions and recommendations during my scientific work. His special interest in research and his great knowledge in cardiovascular sciences always motivated me. Besides, it must be noted that by providing excellent technical support he made it possible for all of us to conduct experiment research at the highest level.

I thank Dr. Violetta Kékesi for her continuous and tireless work. Without her great efforts, the cardiovascular PhD program could not have been successful.

My sincere thanks also goes to Prof. Dr. Gábor Szabó, Dr. Sevil Korkmaz-Icöz and the whole experimental cardiac surgery laboratory in Heidelberg for providing me the opportunity to join their research team.

I thank my current and previous colleagues at the experimental research lab, namely Henriett Biró, Dóra Juhász, Edina Urbán, Kincső Anett Gulyás, Benjamin Prokaj and Gábor Fritz for their professional technical support. I am also very grateful to my fellow labmates, particularly to Dr. Attila Oláh, Dr. Csaba Mátyás, Dr. Balázs Tamás Németh, Dr. Kálmán Benke, Dr. Alex Ali Sayour, Dr. Dalma Kellermayer and Bálint András Barta for helping each other and sharing valuable scientific conversations.

I thank to Prof. Dr. Zoltán Papp, Beáta Bódi for the opportunity to build a fruitful cooperation between our groups.

Finally, I would like to express my deepest gratitude to my family. It has to be stated that without the continuous background support from my parents, my wife and my brothers, this thesis could not have been accomplished.